Salmonella-induced cholesterol accumulation in infected macrophages suppresses autophagy via mTORC1 activation

Holly March Torsilieri

Flemington, New Jersey

Bachelor of Science, The College of New Jersey, 2018

A Dissertation presented to the Graduate Faculty
of the University of Virginia in Candidacy for the Degree of
Doctor of Philosophy

Department of Microbiology, Immunology, and Cancer Biology

University of Virginia

May 2025

Abstract:

Salmonella enterica serovar Typhimurium is a Gram-negative bacillus that infects the host intestinal epithelium and resident macrophages. Many intracellular pathogens induce an autophagic response in host cells but have evolved mechanisms to subvert that response. Autophagy is closely linked to cellular cholesterol levels; mTORC1 senses increased cholesterol in lysosomal membranes, leading to its hyperactivity and suppression of autophagy. Previous studies indicate that *Salmonella* infection induces dramatic accumulation of cholesterol in macrophages, a fraction of which localizes to *Salmonella* containing vacuoles (SCVs). We previously reported that the bacterial effector protein SseJ triggers cholesterol accumulation through a signaling cascade involving FAK and Akt, however the importance of cholesterol accumulation to bacterial survival has remained unknown. Here we show that mTORC1 is recruited to SCVs and is hyperactivated in a cholesterol-dependent manner. If cholesterol accumulation is prevented pharmacologically or through mutation of *sseJ*, autophagy is induced and bacterial survival is attenuated. Notably, the host lipid transfer protein OSBP is also recruited to SCVs and its activity is necessary for both cholesterol transfer to SCVs and mTORC1 activation during infection. We propose that *S.* Typhimurium induces cholesterol accumulation through SseJ to activate mTORC1, preventing autophagic clearance of bacteria. We also conducted the first known lipid mass spectrometry analysis of *S.* Typhimurium infected macrophages. We found that *S.* Typhimurium manipulates macrophage lipid homeostasis via the SPI-2 effector SseJ, which is necessary for the increase in lysophosphatidylcholine and cholesterol ester species found in infected macrophages. This lipid remodeling likely facilitates bacterial persistence by promoting an anti-inflammatory M2 polarization state, which is advantageous for long-term *Salmonella* survival. Our findings provide novel insights into the interplay between *S.* Typhimurium and macrophage lipid homeostasis, highlighting lipidomic reprogramming as a mechanism for bacterial survival and immune modulation.

Table of Contents

List of Figures and Tables:

List of Abbreviations:

25-HC	25-Hydroxycholesterol
ABCA1	ATP-Binding Cassette Subfamily A Member 1
ABCG1	ATP-Binding Cassette Subfamily G Member 1
ACAT	Acyl coenzyme A:cholesterol acyltransferase
ADP	Adenosine Diphosphate
AKT	Protein Kinase B
AMPK	AMP-activated protein kinase
ANOVA	Analysis of Variance
ARNO	Arf-nucleotide binding site opener
ATG12	Autophagy Related Protein 12
ATG13	Autophagy Related Protein 13
ATG14L	Autophagy Related Protein 14 Like
ATG16L1	Autophagy Related Protein 16 Like 1
ATG5	Autophagy Related Protein 5
ATG9	Autophagy Related Protein 9
ATP	Adenosine Triphosphate
ATP6V0C	ATPase H+ Transporting V0 Subunit C
BMDMs	Bone Marrow Derived Macrophages
BODIPY	Boron-dipyrromethene
CD36	Cluster of Differentiation 36
CDC	Centers for Disease Control
Cer	Ceramide
CFU	Colony Forming Units

ChE	Cholesterol Ester
COPII	Coat Protein Complex II
D4H	Domain 4 of Perfringolysin O released by *Clostridium perfringens*
DMEM	Dulbecco's Modified Eagle Medium
DMSO	Dimethyl Sulfoxide
DTT	Dithiothreitol
EDTA	Ethylenediaminetetraacetic Acid
EEA1	Early Endosome Antigen 1
EGFP	Enhanced Green Fluorescent Protein
ER	Endoplasmic Reticulum
ESCRT	Endosomal Sorting Complexes Required for Transport
FAK	Focal Adhesion Kinase
Fc	Fragment Crystallizable
FFAT	two Phenylalanines in an Acidic Tract
FOXO3	Forkhead box O3
GEF	Guanine Exchange Factor
GFP	Green Fluorescent Protein
GRAMD1	GRAM Domain-Containing Protein 1
HDL	High-Density Lipoprotein
HEK293	Human Embryonic Kidney 293
HMGCR	3-Hydroxy-3-Methyl-Glutaryl-CoA-Reductase
HPLC	High-Performance Liquid Chromatography
HRP	Horseradish Peroxidase
IL-1β	Interleukin-1β

IL-8	Interleukin-8
IL-10	Interleukin-10
IL-13	Interleukin-13
IL-18	Interleukin-18
IL-4	Interleukin-4
IL-6	Interleukin-6
iBMDMs	Immortalized Bone Marrow Derived Macrophages
LAMP1	Lysosomal-Associated Membrane Protein 1
LAMP2	Lysosomal-Associated Membrane Protein 2
LC3B	Microtubule-Associated Protein 1 Light Chain 3B
LDL	Low-Density Lipoprotein
LDLR	Low-Density Lipoprotein Receptor
LPC	Lysophosphatidylcholine
LPS	Lipopolysaccharide
LXR	Liver X Receptor
MCS	Membrane Contact Site
M-CSF	Macrophage Colony Stimulating Factor
MDR	Multidrug Resistant
MHC-II	Major Histocompatibility Complex II
MOI	Multiplicity Of Infection
MPR	Mannose-6-Phosphate Receptor
MS	Mass Spectrometry
mTOR	Mechanistic Target of Rapamycin
Mtorc1	mTOR Complex 1
NADPH	Nicotinamide Adenine Dinucleotide Phosphate

NDP52	Nuclear Dot Protein 52 kDa
NF-κB	Nuclear Factor Kappa-light-chain-enhancer of activated B cells
NPC1	Niemann-Pick Disease, Type C1
NPC2	Niemann-Pick Disease, Type C2
ORP4	OSBP Related Protein 4
OSBP	Oxysterol Binding Protein 1
p70 S6K	p70 S6 Kinase
PAS	Phagophore Assembly Site
PAMP	Pathogen Associated Molecular Pattern
PBS	Phosphate Buffered Saline
PC	Phosphatidylcholine
PCR	Polymerase Chain Reaction
PE	Phosphatidylethanolamine
PFA	Paraformaldehyde
PI3KC	Phosphoinositide 3-Kinase C
PI3P	Phosphatidylinositol-3-Phosphate
PI4P	Phosphatidylinositol-4-Phosphate
PM	Plasma Membrane
PVDF	Polyvinylidene Difluoride
qPCR	Quantitative PCR
ROI	Region Of Interest
RFP	Red Fluorescent Protein
RNA	Ribonucleic Acid
ROS	Reactive Oxygen Species
RPMI	Roswell Park Memorial Institute media

SCAP	SREBP2 Cleavage Activating Protein
SCV	*Salmonella* Containing Vacuole
SIF	*Salmonella* Induced Filament
SLC38A9	Solute Carrier Family 38 Member 9
SM	Sphingomyelin
SPI	*Salmonella* Pathogenicity Island
SREBP2	Sterol Regulatory Binding Protein 2
St	*Salmonella enterica* serovar Typhimurium
STAT3	Signal Transducer and Activator of Transcription 3
T3SS	Type III Secretion System
TAL1	T-cell Acute Lymphocytic Leukemia Protein 1
TG	Triglycerides
TGFβ	Transforming Growth Factor β
TGN	Trans Golgi Network
TLR	Toll Like Receptor
TNFα	Tumor Necrosis Factor α
TSC2	Tuberous Sclerosis Complex 2
ULK1	Unc-51-Like Autophagy-Activating Kinase 1
VAMP	Vesicle-Associated Membrane Protein
VAP	VAMP Associated Protein
VPS15	Vacuolar Protein Sorting 15
VPS34	Vacuolar Protein Sorting 34
vATPase	Vacuolar ATPase
WT	Wild Type

Acknowledgments:

To my advisor, Dr. James Casanova: Thank you for your unwavering mentorship, support, and encouragement throughout my PhD journey. Your breadth of knowledge and passion for science is inspiring and contagious. Your dedication to my growth as a scientist and researcher is much appreciated. Thank you for always being patient and generous with your time, offering supportive feedback, and believing in my potential. Your mentorship has left a profound impact, and I am proud to have been a member of the Casanova lab.

To my thesis committee, Drs. Alison Criss, Hervé Agaisse, Bimal Desai, and Melissa Kendall: Thank you for encouraging and challenging me to be the best scientist I can. Thank you for the thoughtful insights, technical expertise, and advice. Your time, effort, and guidance have enabled me to achieve this accomplishment.

To my family: Thank you for a lifetime of love and support. You have always encouraged me to follow my dreams and listened patiently while I explained esoteric facts about bacteria. Thank you for your love, encouragement, and kindness over these years.

To my fiancé, Brad: Thank you for loving me and being there when the road got rocky. Thank you for your helpful insights and showing me the big picture when I got lost in the details. Your tireless encouragement, love, and joy for life have been a constant in these past years, and I am grateful for your partnership in my life.

Chapter 1:

Introduction

Introduction

Salmonella enterica: A global pathogen

Salmonella enterica is a Gram-negative, motile bacillus in the Enterobacteriaceae family. It is broadly divided into six subspecies that contain over 2,600 serovars, defined by their somatic and flagellar antigens (Gal-Mor et al., 2014). *Salmonellae* species are facultative intracellular and anaerobic pathogens, capable of colonizing diverse environments, including the intestines of humans and animals (Ibarra and Steele-Mortimer, 2009). *Salmonella* is typically transmitted through the fecal-oral route of infection, via contaminated food or water, making it a ubiquitous pathogen in developing communities. The ability of *Salmonella* to colonize host cells and evade the immune response make it a potent agent of disease worldwide.

Salmonella causes three major human diseases: non-invasive, non-typhoidal salmonellosis, invasive non-typhoidal salmonellosis (iNTS), and typhoid fever. Non-invasive, non-typhoidal salmonellosis is an acute gastroenteritis disease typically caused by *S. enterica* subsp. *enterica* serovar Typhimurium. *S.* Typhimurium infection is characterized by abdominal pain, vomiting, and diarrhea, with symptom onset typically occurring 6-72 hours after consumption of contaminated food or water. Salmonellosis is often mild and self-limiting and will resolve in a timely manner without treatment. Despite the resolution of symptoms, non-typhoidal *Salmonella* can persist in the intestinal tract for weeks, contributing to community infection (Kurtz et al., 2017). Non-typhoidal *Salmonella* continues to be a major cause of diarrheal disease worldwide, with 1 in 4 cases caused by a strain of *Salmonella* and an estimated 550 million cases per year (World Health Organization, 2019).

Like non-invasive salmonellosis, iNTS is commonly associated with *S.* Typhimurium, however new pathogenic clades have emerged in sub-Saharan African that are adapted to cause invasive disease in humans (Van Puyvelde et al., 2023). iNTS presents as a febrile, systemic illness with an absence of diarrhea and vomiting, a marked departure from the presentation of non-invasive salmonellosis (Brent et al., 2006; Gordon et al., 2002). Diagnosis and treatment are often occluded by clinical overlap with other febrile diseases including pneumonia and malaria (Morpeth et al., 2009). The global burden of iNTS is estimated to be over 3.4 million cases annually with a fatality rate over 20% (Ao et al., 2015). Comorbidities common in the areas where iNTS is prevalent, such as malaria or malnutrition, contribute to the high mortality linked with iNTS cases (Feasey et al., 2012). To date, iNTS contributes to the most bacterial bloodstream infections isolated from both adults and children with fever in sub-Saharan Africa (Feasey et al., 2012). No vaccines exist against non-typhoidal *Salmonella* strains, partly due to the wide variance in strains and a lack of knowledge regarding protective antigens against these strains.

The strain *S. enterica* subsp. *enterica* serovar Typhi causes typhoid fever in humans and is responsible for over 9 million cases and 110,000 deaths annually worldwide (Gal-Mor et al., 2014; World Health Organization, 2019). *S.* Typhi is restricted to human infection, but the strain *S.* Typhimurium causes a typhoid fever-like disease in mouse, making it an appropriate model for the human disease (Gal-Mor et al., 2014). Typhoid fever is considered endemic in developing countries, particularly in sub-Saharan Africa and Asia (World Health Organization, 2019). *S.* Typhi can survive and replicate in host phagocytes, leading to dissemination to secondary sites of infection such as the spleen, liver, and lymph nodes. Symptoms of typhoid fever include fever, diarrhea, and lethargy,

but left untreated can escalate to septicemia, encephalitis, and intestinal hemorrhage. An estimated 5% of infected individuals will become chronic carriers of *S.* Typhi as the bacteria continue to survive in a non-symptomatic state in the gallbladder and liver (Gunn et al., 2014). One of the principal differences between *S.* Typhi and non-typhoidal strains is the polysaccharide capsular antigen, Vi, a virulence factor that allows the bacteria to survive the acidic stomach environment as well as obstruct neutrophil chemotaxis and complement-mediated killing (Parry et al., 2002; Wilson et al., 2010; Wingdi et al., 2014). Of rising concern is the rapidly increasing rate of multidrug-resistant (MDR) and extensively drug-resistant (XDR) strains of *S.* Typhi. Approximately 75% of *S.* Typhi isolates in Africa are resistant to chloramphenicol, ampicillin, and trimethoprim-sulfamethoxazole, which were previously considered first-line antibiotics for *S*. Typhi infection (Marchello et al., 2020). Antibiotic resistance has also been detected in non-typhoidal strains, with the Centers for Disease Control (CDC) estimating that 16% of non-typhoidal *Salmonella* strains are resistant to at least one essential antibiotic (Centers for Disease Control, 2019). Due to this threat of antibiotic resistance, antibiotic treatment is discouraged except in the most severe cases.

Currently, three types of vaccines exist for *S.* Typhi: the oral live attenuated vaccine (Ty21a); the Vi capsular polysaccharide vaccine; and typhoid conjugate vaccines (TCVs). Ty21a is a highly attenuated strain of *S*. Typhi and reports efficacy of 43% for 1-5 years post-vaccination (Batool et al., 2024). However, due to the high number of bacteria required for sufficient immunity via oral dose, its use is not recommended for children under the age of 5, a critical population for typhoid prevention. The injectable Vi capsular polysaccharide subunit vaccine exhibits higher levels of efficacy (65%) but requires repeat dosing every 3 years and is poorly immunogenic in children under the

age of 2 (Guzman et al., 2006; Lin et al., 2001). The TCV injectable vaccine is a recent development that conjugates the Vi polysaccharide to a carrier protein (usually tetanus toxoid) for improved delivery and immune response. The majority of TCVs are not available worldwide or are still under pre-qualification from the World Health Organization, but preliminary studies indicate improved efficacy (80%) 2 years after immunization (Batool et al., 2024). While these vaccines provide some level of protection against *S.* Typhi, there is still a significant need for accessible preventions against both typhoidal and non-typhoidal *Salmonella* infections.

S. Typhimurium invasion strategies

S. Typhimurium is transmitted through the fecal-oral route of infection, during which the bacteria colonize the small intestine. Upon reaching the distal ileum, *S.* Typhimurium can invade the epithelial layer in a variety of methods (Figure 1-1). The intestinal Peyer's patches contain microfold cells (M cells) that continuously sample the contents of gut lumen and engage in selective endocytosis of antigens, which are transported from the lumen to an associated macrophage in the lamina propria (Jepson and Clark, 2001). *Salmonella* exploits this mechanism and infects M cells, leading to their destruction and sloughing of the epithelium (Jones et al., 1994). This damage can lead to unrestricted bacterial invasion of the epithelial layer. Similarly, *S.* Typhimurium can be captured by dendritic cells that sample the gut lumen. Finally, *S.* Typhimurium can directly penetrate epithelial cells through virulence factors that induce membrane ruffling and bacterial uptake (Niess and Reinecker, 2006).

Prior research suggests that *S.* Typhimurium capture by M cells may represent a major method of infection *in vivo*. M cells reside in Peyer's patches in the follicle-associated epithelium, and are characterized by few, irregular microvilli and a basolateral pocket that acts as a harbor for associated macrophages (Kerneis et al., 1997). M cells feature lower levels of mucus and IgA, making them accessible to luminal bacteria (Frey et al., 1996). The irregular microvilli and exposed apical membrane may also provide a more hospitable target for bacterial infection. *S.* Typhimurium selectively invades M cells following infection of murine gut loops, and human typhoid fever frequently presents with ulcerations of the Peyer's patches, suggesting that *Salmonella* may preferentially infect M cells *in vivo* (Jones et al., 1994; Everest et al., 2001).

Direct invasion of an epithelial cell requires intricate coordination of virulence factors, bacterial components, and regulatory systems. The high osmolarity and anaerobic environment of the gut lumen induces expression of flagella, adhesins, and the *Salmonella* Pathogenicity Island 1 (SPI-1), which encodes a Type Three Secretion System (T3SS) and its associated effectors (Bajaj et al., 1996; Chilcott et al., 2000). The epithelial layer is protected by a thick layer of mucus and antimicrobial proteins, designed to reduce bacterial penetration. *S.* Typhimurium uses flagella and near-surface swimming to navigate this mucosal layer and gain access to exposed epithelial cells (Furter et al., 2019). Attachment to the cell is mediated by the adhesin SiiE, which binds to glycans on the surface protein Mucin1 (Li et al., 2019a). The SPI-1 T3SS also docks at the invasion site, furthering attachment.

Once docked, the SPI-1 T3SS secretes effectors that trigger a wave of actin polymerization, leading to membrane ruffling and bacterial uptake. This is mainly driven by the SPI-1 effectors SopB, SopE, and SopE2 which stimulate actin nucleation factors. SopE and SopE2 mimic host cell guanine exchange factors (GEFs) to trigger the activation of Rac1, a Rho GTPase that activates the WAVE regulatory complex (WRC) to generate membrane ruffling (Hardt et al., 1998; Friebel et al., 2001; Eden et al., 2002; Shi et al., 2005). Rac1 alone is not sufficient to activate the WRC but requires direct binding from an Arf family GTPase (Koronakis et al., 2011). SopB, a SPI-1 lipid phosphatase, mediates phosphatidylinositol-3-phosphate (PI3P) generation at infection foci, leading to the recruitment of host GEF ARNO (Arf-nucleotide binding site opener) (Mallo et al., 2008). ARNO then activates Arf1, which can coordinate with Rac1 to activate WRC and drive actin assembly (Humphreys et al., 2012). Once internalized, *S.* Typhimurium SPI-1 effector SopD promotes recruitment of Dynamin-2 to drive scission of the plasma membrane (PM) and generate a specialized phagosome, the *Salmonella* Containing Vacuole (SCV) (Boddy et al., 2021). Through this intricate manipulation of host factors, *Salmonella* stimulates membrane ruffling to allow uptake and results in a specialized compartment for intracellular survival.

The SCV: A replicative niche

A newly formed phagosome is highly acidic due to the activity of the vacuolar ATPase (vATPase). The phagosome is further fortified by the delivery of lysosomal hydrolases and antimicrobial peptides to form a highly bactericidal compartment. To escape phagosomal killing, *S.* Typhimurium has evolved an arsenal of evasion mechanisms that allow it to survive within the phagosome and modify it into a replicative niche.

The maturation of the SCV closely resembles endosomal maturation. Within 30 minutes of formation, the SCV rapidly acquires early endosomal markers including EEA1 (Early Endosome Antigen 1) and Rab5. During intermediate maturation, these markers are replaced by late endosomal/lysosomal markers including Rab7, vATPase, and lysosome-associated membrane proteins (LAMPs) (Steele-Mortimer, 2008; Rathman et al., 1997). This intermediate phase is accompanied by a decrease in SCV pH and relocation to the perinuclear region (Rathman et al., 1997; Szeto et al., 2008). Deviating from lysosomal maturation, the SCV excludes cathepsins and mannose-6-phosphate receptors (MPRs) (Garcia-del Portillo and Finlay, 1995). The SCV further avoids fusion with terminal lysosomes through the activity of SopB. After invasion SopB relocalizes from the PM to the SCV, where it alters the membrane surface charge by targeting PI(4,5)P2 and phosphatidylserine (PS) (Bakowski et al., 2010). These phospholipids are crucial to the recruitment of Rabs that promote phagosome-lysosome fusion, thus by altering the SCV membrane surface charge and Rab targeting, *S.* Typhimurium can evade fusion of the SCV with lysosomes. In the late stage of SCV maturation (4-6 hours post infection), expression of the SPI-1 T3SS is downregulated and expression of the SPI-2 T3SS is initiated. The low pH of the vacuole induces regulatory changes in the PhoP/PhoQ two-component systems, leading to suppression of SPI-1 and upregulation of SPI-2. SPI-2 encodes over 30 effector proteins and the injection machinery of the T3SS. The SPI-2 effectors are broadly associated with enabling replication, integrity of the SCV, and survival (Figueira and Holden, 2012).

Like many of the *S.* Typhimurium effectors, the SPI-2 effector SifA has multiple roles. During maturation of the SCV, SifA sequesters Rab9, inhibiting the recruitment of MPR to the SCV and preventing delivery of lysosomal enzymes (McGourty et al., 2012). SifA

also plays a crucial role in the generation of *Salmonella*-induced filaments (SIFs), which form complex, tubular structures throughout the cells, originating from the SCV (Knuff and Finlay, 2017). Nascent SIFs begin as single-membrane tubules, but double-membraned SIFs have also been observed (Knuff and Finley, 2017). The lumen of SIFs often contains endosomal material, supporting a model where SIFs are generated through the recruitment and fusion of host membranes with the SCV. SIFs interact directly with the host endosomal system, gaining markers of LAMPs, vATPase, Rab7, and cholesterol (Drecktrah et al., 2008; Knuff and Finley, 2017). These interactions grant *S.* Typhimurium access to nutrients for replication, as the SIF network remains connected to the SCV.

Although maintenance of the vacuole is important to protect *S.* Typhimurium from cytosolic host defense, a subset of bacteria escapes from the vacuole. In epithelial cells, this vacuolar escape can lead to hyper-replication in the cytosol, which can lead to extrusion of heavily infected epithelial cells (Knodler et al., 2010). These hyper-replicating bacteria are dissimilar to vacuolar bacteria in that they express SPI-1 at high levels and are flagellated (Knodler et al., 2010). In contrast, replication is dependent on the SPI-2 T3SS within the SCV (Hensel et al., 1995). This bimodal lifestyle may represent a strategy to release invasive bacteria throughout the epithelial layer via extrusion of dying cells (Knodler et al., 2010).

After infection of the epithelial layer and maturation of the SCV, *S.* Typhimurium proceeds to the basolateral side of the epithelium where it is released by exocytosis (Muller et al., 2012). Here, the bacteria gain access to the lamina propria, which is rich in

resident phagocytes including macrophages. In the case of M cell or dendritic cell capture, the result is the same, with bacteria delivered to the macrophage rich space. Survival in an aggressive cell type such as a macrophage provides certain challenges to an intracellular pathogen. Intracellular pathogen associated molecular patterns (PAMPs) can signal Toll-like receptors (TLRs) and Nod-like receptors (NLRs) that will activate inflammasomes to restrict bacterial spread. *S.* Typhimurium evades these receptors by downregulating or changing its lifestyle to avoid detection. For instance, *S.* Typhimurium downregulates production of flagellin once within a cell to avoid detection by NLRC and subsequent pyroptosis (Li et al., 2019b). SipB, a SPI-1 effector, is known to activate capase-1 within macrophages, leading to apoptosis, further pointing to the importance of SPI-1 downregulation (Hersh et al., 1999). If *S.* Typhimurium successfully survives the assault of macrophage defense and continues to replicate, it gains access to further systemic sites including the lymph nodes, spleen, and liver. Thus, survival within macrophages is a key element in *Salmonella* infection and disease progression

Role of macrophages in *Salmonella* infection

Macrophages are considered a first-line of defense against invasive pathogens and play an important role in immunity. Macrophages differentiate from circulating monocytes when exposed to macrophage colony-stimulating factor (M-CSF; Hamilton, 2008). While monocytes are rounded cells with a kidney-bean-shaped nucleus, macrophages can assume multiple cell shapes depending on their role and polarization state (McWhorter et al., 2013). Macrophages provide defense against pathogens, but also contribute to the clearance of dying cells, wound healing, and tissue repair. Infection, inflammation, or tissue damage trigger chemotaxis of macrophages to the site of damage, where they can phagocytose pathogens and cell debris. Further presentation of antigen to T lymphocytes will lead to an antigen-specific response. Through these effector functions,

macrophages can quickly and aggressively respond to infectious pathogens and present a serious challenge to intracellular bacteria such as *Salmonella*.

Macrophage phagocytosis relies on the recognition and binding of antibodies via Fc (fragment crystallizable) receptors on the cell surface (Mellmen et al., 1988). Through such antibody-dependent phagocytosis, the macrophage can internalize a pathogen or other particulate structure and proceed with ROS-mediated killing or enzymatic digestion. ROS production is an important function of macrophages and can be induced by complement receptors and TLRs (Kim et al., 2017; West et al., 2011; Samsted et al., 2014). The p22 and gp91 subunits of NADPH oxidase are located on the phagosome membrane and can assemble with cytosolic subunits to form active NADPH oxidase, leading to an oxidative burst (Anrather et al., 2006). The phagosome is also highly acidic and limits access to co-factors such as Mg^{2+}, contributing to bacterial killing (Russell et al., 2010; Cunrath and Bumann, 2019). Degraded microbial peptides are loaded onto major histocompatibility complex II (MHC-II) proteins and transported to the cell surface for presentation to T-cells (Neefjes et al., 2011). Recognition of PAMPs and TLR signaling will also trigger NF-κB signaling, which enhances expression of IL-8, TNFα, and IL-1β (Liu et al., 2017). IL-8 acts as a chemoattractant, triggering chemotaxis of neutrophils and other granulocytes to the site of damage, while IL-1b and TNFα promote an inflammatory program (Baggiolini and Clark-Lewis, 1992; Weber et al., 2010).

While macrophages are commonly associated with inducing inflammation, alternative activation by IL-4 and IL-13 can lead to an anti-inflammatory, pro-resolution phenotype, commonly known as M2 polarization (Gordon and Martinez, 2010). The canonical

polarization state, M1, is induced by inflammatory signals, including TNFα, interferon-γ, and LPS, and is characterized by the release of pro-inflammatory cytokines such as IL-1β and IL-6 as well as the enhanced production of MHC-II, ROS, and nitric oxide synthase. (Gordon and Martinez, 2010). In contrast, M2 macrophages promote tissue repair and inflammatory resolution through production of TGFβ, IL-10, and arginase (Orecchioni et al., 2019). Macrophage polarization is understood as a spectrum rather than an absolute binary state, but the phenotypic and functional alterations still provide useful insights into how macrophages can adapt to changing circumstances in the tissue. However, polarization can also provide an opportunity for pathogens to exploit macrophage dynamics for their own survival. *Salmonella* has evolved mechanisms to evade the bactericidal M1 macrophage while also promoting polarization to the more permissive M2 macrophages. *Salmonella* effector SteE enables the phosphorylation of signal transducer and activator of transcription 3 (STAT3), which promotes IL-4 dependent activation of M2-associated genes such as arginase-1 (Mosser and Edwards, 2008; Mauer et al., 2014; Gibbs et al., 2020; Panagi et al., 2020). Further, SteE neutralizes TNFα signaling in granuloma macrophages to promote M2 polarization, providing a permissive niche for bacterial persistence (Pham et al., 2020). In M1 macrophages, *Salmonella* is either efficiently killed and cleared from the cell, or lapses into a dormant state of non-growth, suggesting the bacteria could also operate in “stealth mode” to avoid recognition by intracellular immune receptors (Saliba et al., 2016; Lathrop et al., 2015). Thus, the ability of *Salmonella* to influence macrophage polarization is critical in the pursuit of survival, replication, and dissemination throughout the host.

During *Salmonella* infection, macrophage phagocytosis provides an outlet through which the bacteria can be contained and destroyed. However, *Salmonella* has evolved specific escape mechanisms to avoid macrophage killing. The SCV constitutes a haven for intracellular bacteria, protecting *Salmonella* from the deleterious macrophage effectors. The SCV rapidly acidifies during maturation, which induces expression of key bacterial effectors that will promote survival (Chakraborty et al., 2015). In the face of nutrient limitation, the low pH in the SCV induces the PhoP two-component system which transcriptionally activates the magnesium transporter MtgB (Yeom et al., 2020). By protecting magnesium homeostasis, MtgB also confers resistance to oxidative stress (Yeom et al., 2020; Bourret et al., 2017). Macrophage oxidative bursts and inflammation can also benefit the metabolism of *Salmonella*, providing a competitive advantage over the microbiota in the inflamed gut. Colonic bacteria produce large amounts of hydrogen sulfide, a toxic compound that is converted to thiosulfate (Winter et al., 2010). During intestinal inflammation, nitric oxide radicals and ROS can react with thiosulfate to produce tetrathionate and nitrate. Both nitrate and tetrathionate can act as terminal electron acceptors for *Salmonella* during anaerobic respiration, resulting enhanced metabolism and a competitive advantage over the gut microbiota (Winter et al., 2010; Lopez et al., 2012). These conditions result in *Salmonella* overgrowth in the inflamed gut. *Salmonella* can also disrupt NF-κB signaling through the bacterial effector AvrA, a deubiquitinase that targets the inhibitors of NF-κB. IκBα inhibits NF-κB through binding and masking its nuclear localization signal, but during NF-κB activation, the IκB kinase phosphorylates IκBα, leading to its ubiquitination and degradation (Bonizzi and Karin, 2004). AvrA deubiquitinates IκBα, resulting in inhibition of NF-κB nuclear translocation and activation (Ye al., 2007). Even in non-replicating conditions, *Salmonella* can persist in macrophages, opening the door for further dissemination. Upon phagocytosis, if *Salmonella* cannot successfully replicate and overcome nutrient limitation, the bacteria

induce expression of toxin-antitoxin genes that promote a non-replicating, viable persister state (Helaine et al., 2014). A proportion of these non-replicating persisters can resume growth and metabolic activity if engulfed by a naïve macrophage, contributing to a resurgence in infection (Helaine et al., 2014). Finally, *Salmonella* can manipulate the mobility of macrophages to promote dissemination to target organs. The SPI-2 effector SteC is the only known *Salmonella* kinase and phosphorylates host myosin light chain protein Myl12a, resulting in actin rearrangement and enhanced migration of the macrophage (Dai et al., 2024). While this activity does not affect intracellular replication in macrophages, it is essential for *Salmonella* dissemination past the gut-vascular barrier and into target organs (Dai et al., 2024). In all, *Salmonella* wields multiple tools to promote survival and replication within the macrophage, as well as future proliferation within the host.

S. Typhimurium evasion of autophagy

A key cellular defense mechanism is the process of macroautophagy, through which targeted proteins, organelles, or bacteria (xenophagy) are captured in autophagosomes and delivered to lysosomes for fusion and destruction. Autophagy is a stress response mechanism that can clear unwanted materials and provide recycled molecular building blocks during starvation. Autophagosome formation begins with phagophores, double-membraned structures that encircle targeted material. The phagophore assembly site (PAS) forms on the endoplasmic reticulum (ER) in areas of the membrane that are rich in PI3P (Hollenstein and Kraft, 2020). One of the first factors to target the PAS is the ULK1 (Unc-51-like autophagy activating kinase 1) complex, consisting of the ULK1 kinase, autophagy related protein 13 (ATG13) and focal adhesion kinase family interacting protein of 200 kD (FIP200) (Lin and Hurley, 2017). This complex is essential

to autophagosome formation, and controls much of the downstream autophagic processes through activation of Beclin-1 and the class III phosphoinositide 3-kinase VPS34 (vacuolar protein sorting 34) (Russell et al., 2013). Autophagy-related proteins (ATGs) cluster at the PAS, including ATG9 which works with ATG2 to deliver phospholipids from the ER (Yamamoto et al., 2012; Gomez-Sanchez et al., 2019). The growing membrane is further modified by the addition of microtubule-associated protein 1 light chain 3 beta (LC3B) which is conjugated with phosphatidylethanolamine (PE) (Kabeya et al., 2000). Finally, the nascent autophagosome edges form a pore that is closed through scission by the endosomal sorting complexes required for transport (ESCRT)-III complex (Zhou et al., 2019).

The regulation of autophagy is tightly linked to nutrient availability and starvation conditions in the cell. At the forefront of this regulation is mTORC1, a master regulator of growth and potent suppressor of autophagy. During starvation, mTORC1 is diffusely localized to the cytosol and inactive. When nutrients and amino acids are sufficient, mTORC1 is recruited to the surface of lysosomes by the Rag GTPases (Sancak et al., 2008). There, the Rag GTPases interact with the Ragulator complex which acts as an activation scaffold for mTORC1 (Sancak et al., 2010). Activation of mTORC1 is accomplished by the small GTPase Rheb and is mediated by v-ATPase (Long et al., 2005; Zoncu et al., 2011). Sensors for specific nutrients and amino acids control the activity of these complexes. In particular, arginine and cholesterol within lysosomes are sensed by the lysosomal solute carrier SLC38A9 to promote interaction with Ragulator and stimulate activation of mTORC1 (Castellano et al., 2017). Once active, mTORC1 controls a plethora of growth-related mechanisms including translation, ribosome biogenesis, and nucleotide synthesis. The most well studied substrates of mTORC1

kinase activity are the eukaryotic translation initiation factor 4E (eIF4E) which directs ribosomes to mRNA caps and the ribosomal S6 kinase (S6K) which phosphorylates the ribosomal protein subunit 6 to stimulate ribosome biogenesis (Ma and Blenis, 2009). Concurrently, mTORC1 suppresses autophagy through inhibitory phosphorylation of ULK1 (Kim et al., 2011).

During *S.* Typhimurium infection, SCVs are initially targeted by the autophagic machinery due to membrane damage caused by the SPI-1 T3SS. This damage affects both the host cell and the SCV. The T3SS is known to damage eukaryotic cell membranes, and the resulting damage allows the escape of amino acids, triggering a starvation response in the host cell (Tattoli et al., 2012b). This results in enhanced autophagy, which can attenuate *S.* Typhimurium infection. The SPI-1 T3SS creates similar damage in the SCV membrane, allowing cytosolic ubiquitin, cathepsins, and LC3B to bind the bacteria and target them for autophagic clearance (Birmingham et al., 2006). This initial response is combatted by the SPI-1 effector SopF, which ADP-ribosylates the vATPase and blocks its recruitment of the autophagic scaffold protein ATG16L1 (Xu et al., 2022). However, as SPI-1 expression is downregulated, the presence of SopF concurrently decreases as infection progresses (Xu et al., 2022). How *S*. Typhimurium continues to escape autophagy during the later stages of infection has remained unclear.

Another mechanism of *S.* Typhimurium autophagy evasion depends on the activation of host kinases Focal Adhesion Kinase (FAK) and protein kinase B (Akt). In this pathway, FAK and Akt are recruited to the SCV within 5 hours of infection (Owen et al., 2014).

FAK associates with focal adhesions and is autophosphorylated to mediate transmit adhesion-mediated signals to the cell interior (Parsons, 2003). Among its activities, FAK recruits and phosphorylates the PI3 kinase, which is responsible for the activation of Akt (Reiske et al., 1999; Alessi et al.,1997). Once activated, Akt phosphorylates the tuberous sclerosis complex (TSC), which is responsible for sequestering Rheb (Huang et al., 2009). Through this inhibitory phosphorylation, TSC releases Rheb so that it may activate mTORC1, thus Akt activity leads to the activation of mTORC1 and the suppression of autophagy. By recruiting FAK/Akt to the SCV during infection, *S.* Typhimurium controls activation of mTORC1 and can suppress autophagy for its own survival.

FAK/Akt activation and cholesterol accumulation during *S.* Typhimurium infection

The discovery of FAK/Akt activation during *S.* Typhimurium infection led to questions on how this activation was achieved. The activation is SPI-2-dependent, and was recently discovered to be dependent on a single SPI-2 effector, SseJ (Owen et al., 2014; Greene et al., 2021). SseJ is a RhoA-activated cholesterol acyltransferase that can generate cholesterol esters from free cholesterol and localizes to the cytoplasmic face of the SCV during infection (Freeman et al., 2003; Ohlson et al., 2005; Nawabi et al., 2008). Recent work from our lab demonstrated that that SseJ is important for the activation of FAK and Akt, leading to a signaling cascade that affects host cholesterol homeostasis (Greene et al., 2021). Active Akt phosphorylates the transcription factors TAL1 (T-cell acute lymphocytic leukemia protein 1) and FOXO3 (forkhead box O3) in an inhibitory manner, preventing their ability to control transcription (Frechin et al., 2015). Among the genes controlled by TAL1 and FOXO3 is ATP-binding cassette subfamily member 1 (*Abca1*), which encodes a major transporter of cholesterol (Frechin et al., 2015). ABCA1 functions

as a cholesterol efflux pump at the PM, and is the primary exporter of cholesterol in macrophages (Oram and Heinecke, 2005). By suppressing expression of *Abca1*, *S.* Typhimurium infected macrophages accumulate massive amounts of cholesterol (Greene et al., 2021). This cholesterol accumulation benefits *S.* Typhimurium through mechanisms that have remained unknown.

Cholesterol accumulation on the SCV and throughout the endolysosomal system is a phenomenon that has been observed in both epithelial and macrophage cell lines (Brumell et al., 2001; Catron et al., 2002). Cholesterol begins to accumulate by 8 hours post infection and reaches a maximum 18-20 hours post infection (Catron et al., 2002). Much of the accumulated cholesterol is centered in and around the SCV, as well as on SIFs (Catron et al., 2002). The majority of this cholesterol is likely derived from internalized low-density lipoprotein (LDL), as *Salmonella* cannot synthesize sterols and inhibition of host sterol synthesis does not impact bacterial survival or recruitment of cholesterol to the SCV (Catron et al., 2002). This accumulation is dependent on both the presence and activity of SseJ, as cells infected with *S.* Typhimurium that lacks SseJ or contains a catalytically inactive form of SseJ do not accumulate cholesterol (Greene et al., 2021). Restoration of cholesterol efflux through pharmacological upregulation of *Abca1* or deletion of *sseJ* attenuates intracellular survival, suggesting that high levels of intracellular cholesterol enhance survival (Greene et al., 2021). However, the mechanisms through which cholesterol accumulation promotes survival have remained poorly understood.

Cholesterol trafficking and homeostasis in the eukaryotic cell

The level of free cholesterol is tightly regulated in eukaryotic cells due to its importance in membranes and signaling. Cholesterol is a neutral lipid that regulates the fluidity, rigidity, and permeance of membranes. In the PM, cholesterol is often complexed with sphingomyelin and glycosylphosphatidylinositol-anchored proteins, forming microdomains that regulate trafficking and signal transduction (Simons and Ikonen, 1997). Excess cholesterol can induce cytotoxicity, while insufficient amounts can disrupt membranes and signaling pathways. Cholesterol homeostasis refers to the delicate balance between cholesterol uptake from extracellular sources, the *de novo* synthesis of cholesterol intracellularly, and the export of cholesterol out of the cells (Figure 1-4).

Extracellular cholesterol uptake occurs via the LDL receptor at the PM, which enables endocytosis of LDL (Brown and Goldstein, 1979). The LDL-LDLR complex is internalized in clathrin-coated pits, forming an endosome (Brown and Goldstein, 1979). The LDL is further delivered to lysosomes, where the cholesterol esters are hydrolyzed by a lysosomal lipase into free cholesterol (Goldstein et al., 1975). This cholesterol can then be exported from the lysosomal lumen to the limiting leaflet via Niemann Pick disease Type C 1/2 (NPC1/2) (Infante et al., 2008). NPC2 removes cholesterol from the luminal leaflet of the lysosome and transfers it to NPC1, a polytopic integral membrane protein that flips the cholesterol across the membrane to the cytosolic leaflet where it can be further trafficked (Subramanian and Balch, 2008). The exact fate of free cholesterol after this point is less well defined, although a major pathway appears to involve transfer to the PM enroute to the ER (Das et al., 2014). Transfer to the ER is known to involve specific cholesterol transport proteins, the GRAM domain family, which operate at PM-ER membrane contact sites (MCSs) (Naito et al., 2019). From the ER, cholesterol can

be redistributed to other organelles, including lysosomes, endosomes, and the TGN via MCSs mediated by oxysterol binding protein 1 (OSBP) and its less ubiquitous relative OSBP related protein 4 (ORP4) (Subra et al., 2023; Wang et al., 2002).

Balanced with LDL uptake, cholesterol biosynthesis is an alternative method of obtaining new cholesterol. Almost all cells can synthesize cholesterol, but it is an energetically expensive procedure and thus is tightly regulated. The majority of cellular cholesterol resides in the PM, while the ER, the site of *de novo* synthesis, contains less than 5 mol% (Lange, 1991). As a result, the ER is exquisitely sensitive to changes in cholesterol concentration. Cholesterol biosynthesis is predominately regulated by the sterol regulatory element-binding protein 2 (SREBP2), which in turn is retained in the ER by interactions with SREBP2 cleavage activating protein (SCAP) (Horton et al., 2002). When ER cholesterol levels are sufficient, cholesterol binds to SCAP, triggering its interaction with insulin-inducing gene 1 (Insig), an ER resident protein that provides further control over biosynthesis. Oxysterols can also bind Insig, enhancing retention of SCAP (Yabe et al., 2002). When the ER is depleted of cholesterol, the SCAP-SREBP2 complex binds to COPII and is released to translocate to the Golgi (Espenshade et al., 2002). Without SCAP binding, Insig is rapidly targeted for ubiquitylation and degradation (Gong et al., 2006). The Golgi is home to the site 1 and site 2 proteases (S1P and S2P) which cleave the N-terminal of SREBP2 into an active transcription factor (Horton et al., 2002). Translocation to the nucleus allows active SREBP2 to bind sterol regulatory elements (SREs) on target genes, namely the genes for 3-hydroxy-3-methyl-glutaryl-CoA-reductase (HMGCR) and squalene monooxygenase (Horton et al., 2002). HMGCR is the rate-limiting enzyme for *de novo* cholesterol synthesis, responsible for converting HMG-CoA to mevalonate, while squalene monooxygenase catalyzes the oxidation of

squalene to 2,3-oxidosqualene (Gill et al., 2011). In all, the ER is intricately sensitive to cholesterol levels and uses that sensitivity to control cholesterol biosynthesis.

While most cells can synthesize cholesterol, very few can catabolize it, thus excess cholesterol must be stored as esters within lipid droplets or exported from the cell. Within macrophages, the primary cholesterol export proteins are ABCA1 and ABC sub family G 1 (ABCG1). The primary acceptor for ABCA1 is Apolipoprotein A-I, whereas ABCG1 exports cholesterol to high-density lipoprotein (HDL) particles (Gelissen et al., 2005). Transcription of both exporters is upregulated by liver-X-receptors (LXRs) (Tontonoz and Mangelsdorf, 2003). Both ABCA1 and ABCG1 localize to the PM, but ABCG1 may also be found on recycling endosomes where it could redistribute sterols away from the ER (Tarling and Edwards, 2011). In addition to export, excess cholesterol can be stored as esters mediated by acyl coenzyme A:cholesterol acyltransferase (ACAT). ACAT is primarily an ER resident where it catalyzes the transfer of acyl chains to cholesterol from Acyl-CoA, generating cholesterol esters (Anderson et al., 1998). Esterified cholesterol is stored in lipid droplets in the cytosol, where they can be later accessed in the case of starvation. In this manner, the cell contains multiple systems of control through which cholesterol homeostasis can be maintained.

Connection between lysosomal cholesterol levels and suppression of autophagy

Intriguingly, endolysosomal cholesterol has been implicated in the activation of mTORC1. The recent discovery of SLC38A9, which binds cholesterol and arginine to directly stimulate mTORC1, demonstrates that cholesterol is also an essential mTORC1 activator (Castellano et al., 2017). Further research demonstrated that ER-lysosome

contacts mediated by Vesicle-associated membrane protein (VAMP) Associated Protein (VAP) and oxysterol binding protein 1 (OSBP) allow cholesterol transfer from the ER to the cytosolic face of the lysosome to directly activate mTORC1 and suppress autophagy (Lim et al., 2019). These developments have major implications for diseases driven by mTORC1 hyperactivation, however this connection has not yet been applied to the study of intracellular pathogens.

OSBP is the founding member of the OSBP-related protein (ORP) family of lipid transfer proteins which are responsible for delivering various species of lipids at unique MCSs (Subra et al., 2023). The majority of the ORP family features a pleckstrin-homology (PH) domain that binds to phosphatidylinositol lipids in a target membrane and a two phenylalanines in an acidic tract (FFAT) motif that binds to ER-resident VAP (Subra et al., 2023). Lipid transfer performed by a lipid transfer domain (ORD) extracts the specified lipid from the ER membrane and delivers it to the target membrane. OSBP was first described at the ER-Golgi interface, where it delivers cholesterol from the ER in exchange for PI(4)P from the Golgi (Balla et al., 2005). Subsequent research has uncovered that OSBP also plays a large role at ER-lysosome contact sites where it controls cholesterol levels in the lysosome (Lim et al., 2019). Importantly, OSBP has also been described in *S.* Typhimurium pathogenesis, where it interacts with SPI-2 effectors SseJ and SseL to promote vacuolar stability (Kolodziejek et al., 2019). However, the role of OSBP in modulating lipid levels during infection is unknown.

In this thesis, we demonstrate that *Salmonella*-induced cholesterol accumulation is important for the recruitment and activation of mTORC1 to SCVs during infection of macrophages. This mTORC1 activation suppresses autophagy induction and aids

bacterial survival. We further demonstrate that the lipid transfer activity of OSBP is necessary for mTORC1 activation and suppression of autophagy during infection. If OSBP activity is inhibited, bacterial survival worsens. These findings highlight a new mechanism through which *Salmonella* exploits host signaling pathways to benefit its own survival.

Summary and thesis rationale:

S. Typhimurium is a pervasive pathogen that can cause severe disease if left untreated. Key to its infection strategy is the ability to survive in hostile cell types such as macrophages. If the macrophage is breached and bacteria continue to replicate, dissemination to secondary sites of infection can lead to worsened outcomes. Thus, understanding the mechanisms that *S.* Typhimurium uses to survive in macrophages is of great importance. *S.* Typhimurium infection induces cholesterol accumulation which is protective to the bacteria through an unknown mechanism. This accumulation occurs through a signaling pathway driven by the SPI-2 effector SseJ, resulting in downregulation of the cholesterol exporter *Abca1* (Greene et al., 2021). Recent studies have revealed the important role of lysosomal cholesterol in the activation of mTORC1 and suppression of autophagy, which is mediated by lipid transport protein OSBP (Lim et al., 2019). In Chapter 2, we investigate the function of cholesterol accumulation in mTORC1 activation during *S.* Typhimurium infection, providing new insights into the mechanisms by which *S.* Typhimurium evades autophagy. We also assess the role of OSBP lipid transfer activity on mTORC1 activation and suppression of autophagy and we demonstrate new findings on how OSBP activity impacts bacterial survival. Finally, in Chapter 3, we report the first known lipidome of *S.* Typhimurium infected macrophages, detailing the vast changes in the lipid environment that occur during infection. In all,

these findings provide greater understanding to the complexity of *S.* Typhimurium evasion of autophagy, particularly in macrophages, and may allow for future research that will indirectly treat *Salmonella* infections through the modulation of lipid homeostasis.

Figure 1-1

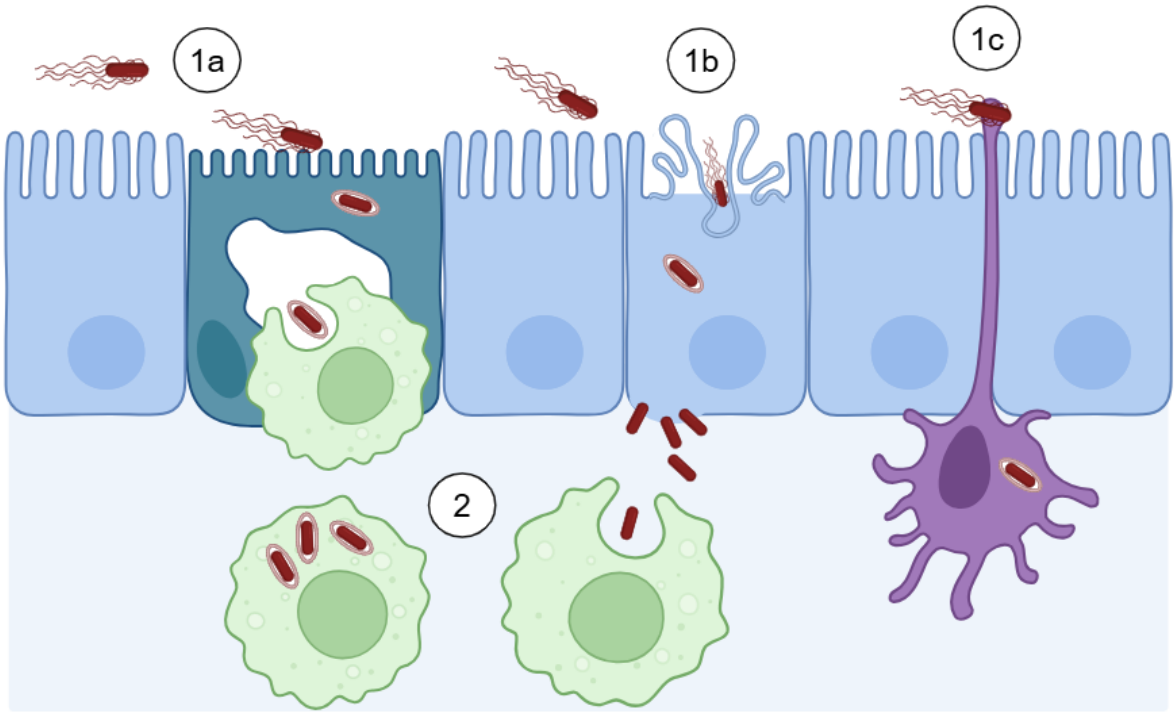

Figure 1-1. Invasion of host cells by *S.* Typhimurium.

Following ingestion of contaminated food or water, *S.* Typhimurium proceeds to the distal ileum of the small intestine where it invades the epithelial layer in a variety of ways. M cell sampling (1a) is thought to be a major route for internalization *in vivo*. M cells sample the contents of the gut lumen and deliver *S.* Typhimurium to the associated macrophage in the basolateral pocket. Direct invasion of epithelial cells (1b) occurs through a concerted effector of the SPI-1 T3SS which delivers effectors across the host cell membrane that will induce actin polymerization and membrane ruffling, triggering bacterial uptake. Once within the cell, *S.* Typhimurium resides in the specialized SCV compartment, and will proceed to the basolateral side of the cell where it is released by exocytosis. *S.* Typhimurium can also be captured directly by dendritic cells (1c). Once *S.* Typhimurium has breached the epithelial layer, it gains access to the lamina propria

which is rich in resident macrophages. The phagocytes will internalize *S.* Typhimurium (2) in an attempt to clear the infection. However, *S*. Typhimurium utilizes the SCV to withstand bactericidal attacks, replicating within the macrophage. This ability to survive and replicate in macrophages enables dissemination to secondary sites of infection such as the lymph nodes and liver.

Figure 1-2

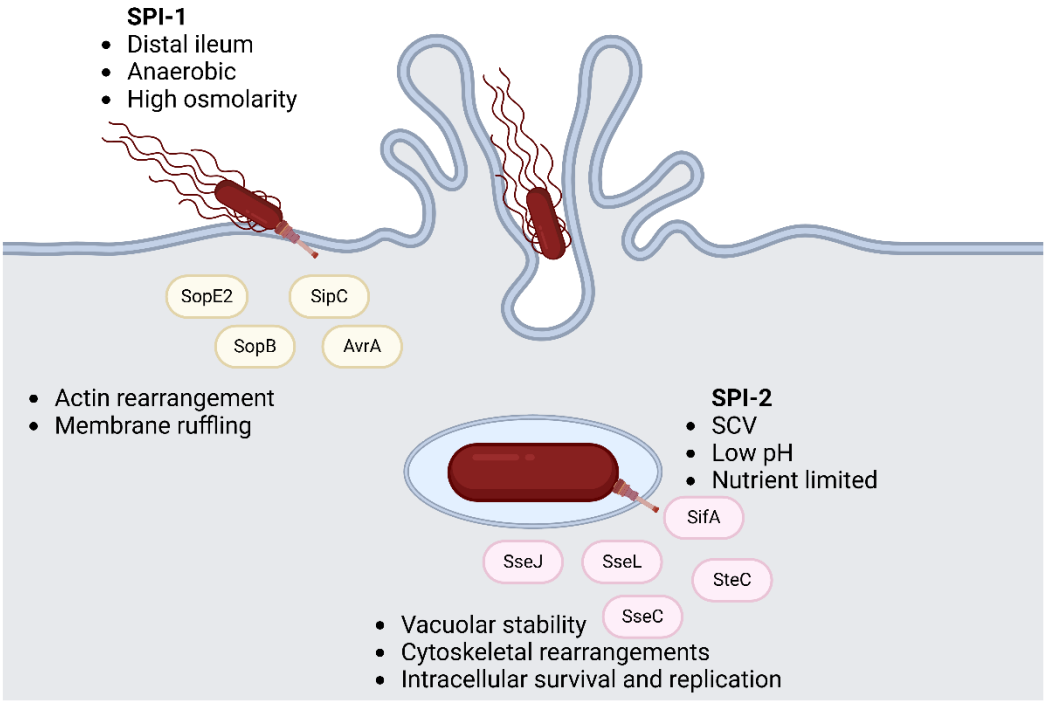

Figure 1-2. *Salmonella* Pathogenicity Islands and Type III Section Systems

S. Typhimurium utilizes two T3SSs, encoded by the SPIs, to enable invasion and infection of host cells. The SPI-1 T3SS is upregulated by the environment of the gut lumen, and secretes effector proteins that will induce actin rearrangements, membrane ruffling, and the initial evasion of autophagic clearance. The SPI-2 T3SS is induced by the low pH of the SCV and is upregulated during intermediate to late maturation of the SCV. SPI-2 effectors aid with vacuolar stability, bacterial replication, and cytoskeletal rearrangements.

Figure 1-3

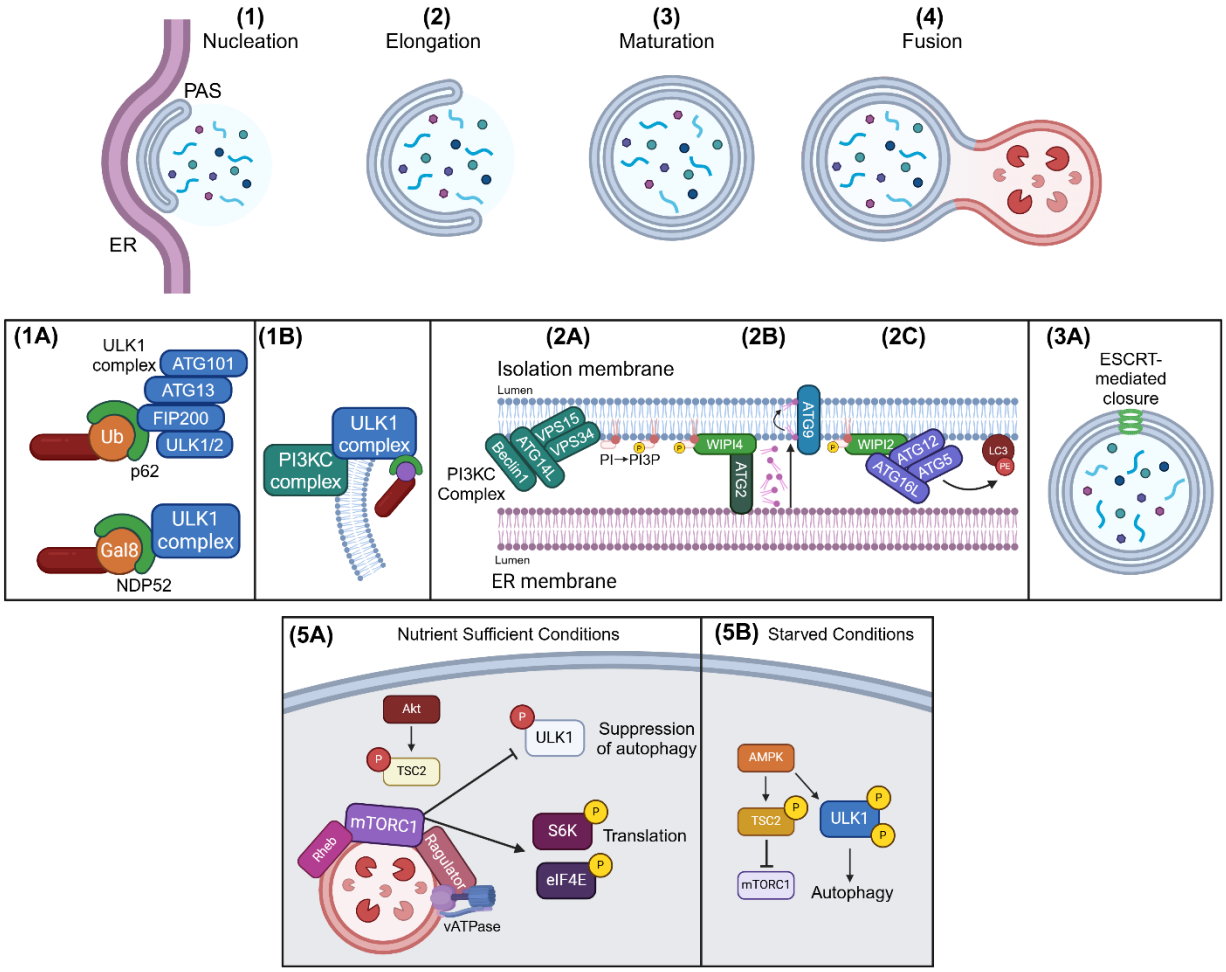

Figure 1-3. Autophagosome biogenesis and the regulation of autophagy. The process of autophagosome formation can be broadly summarized in four steps: nucleation (1), elongation (2), maturation (3), and fusion (4). Autophagosome biogenesis begins when the target cargo is recognized by ubiquitin, LC3, or galectins. These targeting molecules are recognized by selective autophagy receptors such as p62 and NDP52. FIP200, part of the ULK1 complex, contains an LC3 and p62 binding domain, and will bind the autophagy receptors and their cargo, triggering the nucleation of an

autophagosome at the ER (1A). ULK1 recruits and activates the PI3KC complex, containing Beclin1, ATG14L, VPS15, and VPS34, to the PAS (1B). The PI3KC complex generates PI3P from PI at the phagophore membrane, allowing the recruitment of WIPI proteins (2A). WIPI4 interacts with ATG2, which forms a channel from the ER to the isolation membrane, allowing the flow of phospholipids to the growing phagophore (2B). ATG9 flips these phospholipids from the cytosolic leaflet to the luminal, allowing for expansion of the membrane (2B). Concurrently, WIPI2 binds to PI3P to recruit ATG5, ATG12, and ATG16L which direct LC3 to the phagophore and conjugate it with PE (2C). As the autophagosome matures, it closes with the assistance of ESCRT-III (3A). The autophagosome will then fuse with a lysosome, degrading the cargo (4). In nutrient sufficient conditions, mTORC1 is directed to the lysosome by the Ragulator complex where it will bind vATPase and be activated by Rheb (5A). Regulation is provided by TSC2, which is phosphorylated and inhibited by Akt during fed conditions. Downstream mTORC1 effectors include S6K and eIF4E, which mediate protein translation and growth. mTORC1 also inhibits ULK1 through phosphorylation. During starvation, AMPK (AMP-activated protein kinase) phosphorylates and activates TSC2, allowing it to sequester Rheb and prevent mTORC1 activation. Concurrently, AMPK activates ULK1, initiating autophagy (5B).

Figure 1-4

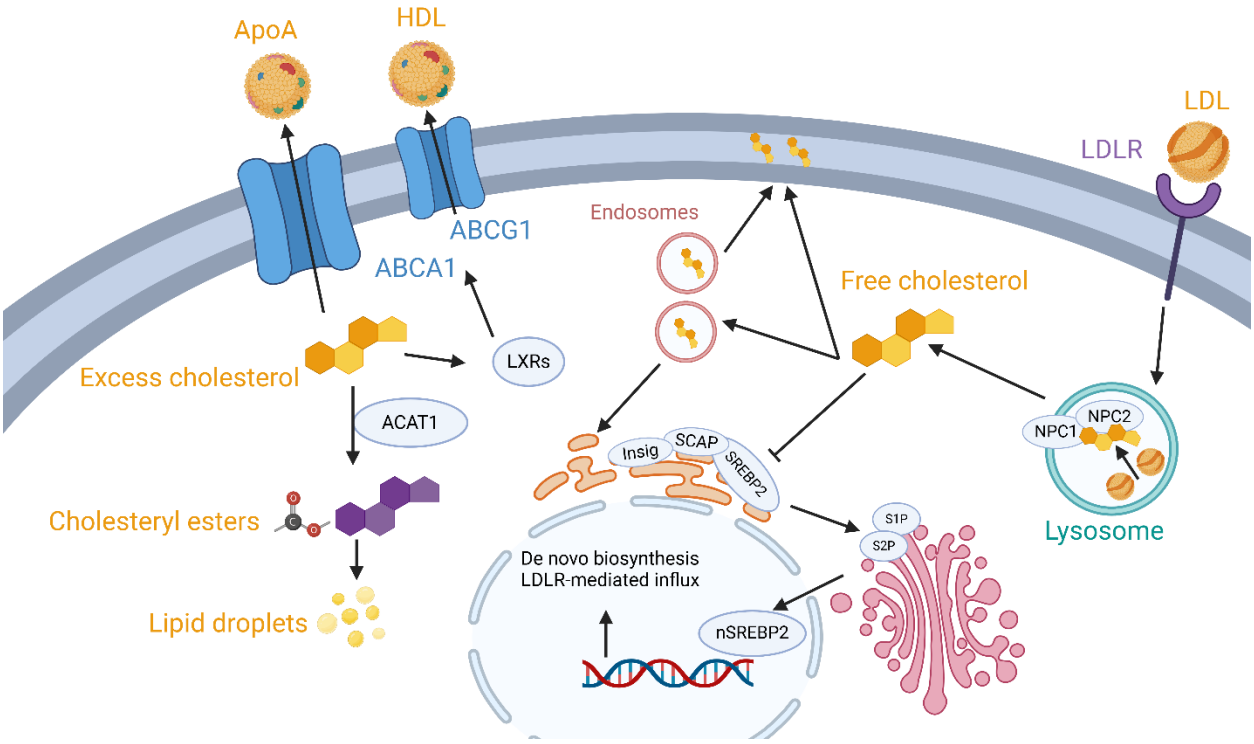

Figure 1-4. Summary of cholesterol homeostasis.

A brief summary of cholesterol uptake, intracellular trafficking, biosynthesis, storage, and efflux. LDL is internalized via the LDLR into lysosomes, where the LDL is hydrolyzed into free cholesterol. NPC1/2 shuttle free cholesterol from the lumen of the lysosome to the cytosolic leaflet, allowing its trafficking throughout the cell. A significant population of cholesterol is trafficked to the PM before reaching the ER. Lipid transfer proteins such as the ORP and GRAMD families facilitate cholesterol transfer between the various organelles. Sufficient levels of cholesterol in the ER signals Insig to retain SCAP and SREBP2 in the ER. If cholesterol is depleted from the ER, Insig releases SCAP, allowing translocation of SCAP and SREBP2 to the Golgi where SREBP2 is proteolytically cleaved into an active transcription factor. NSREBP2 will bind to SRE elements on target genes, upregulating *de novo* cholesterol biosynthesis. Excess cholesterol can be

esterified by ACAT into cholesterol esters and stored within lipid droplets or exported from the cell via ABCA1 or ABCG1. Excess cholesterol will also stimulate the Liver X Receptor (LXR) transcription factors which will upregulate expression of *Abca1* to encourage efflux.

Chapter 2:

Salmonella-induced cholesterol accumulation in infected macrophages suppresses autophagy via mTORC1 activation

The following work has been published:

Torsilieri, H.M., Upchurch, C.M., Leitinger, N., and Casanova, J.E. *Salmonella*-induced cholesterol accumulation in infected macrophages suppresses autophagy via mTORC1 activation. *Molecular Biology of the Cell*. 2024.

Torsilieri, H.M., performed all experiments and analysis shown in Chapter 2, and wrote the publication. Upchurch, C.M. performed the lipid mass spectrometry experiments (described in Chapter 3) and analyzed the preliminary data. Leitinger, N., provided experimental guidance and funding. Casanova, J.E. provided experimental guidance, funding, and review and revision of the manuscript

Abstract

Salmonella enterica serovar Typhimurium is a Gram-negative bacillus that infects the host intestinal epithelium and resident macrophages. Many intracellular pathogens induce an autophagic response in host cells but have evolved mechanisms to subvert that response. Autophagy is closely linked to cellular cholesterol levels; mTORC1 senses increased cholesterol in lysosomal membranes, leading to its hyperactivity and suppression of autophagy. Previous studies indicate that *Salmonella* infection induces dramatic accumulation of cholesterol in macrophages, a fraction of which localizes to *Salmonella* containing vacuoles (SCVs). We previously reported that the bacterial effector protein SseJ triggers cholesterol accumulation through a signaling cascade involving Focal Adhesion Kinase (FAK) and Akt. Here we show that mTORC1 is recruited to SCVs and is hyperactivated in a cholesterol-dependent manner. If cholesterol accumulation is prevented pharmacologically or through mutation of *sseJ*, autophagy is induced and bacterial survival is attenuated. Notably, the host lipid transfer protein OSBP is also recruited to SCVs and its activity is necessary for both cholesterol transfer to SCVs and mTORC1 activation during infection. We propose that *S.* Typhimurium induces cholesterol accumulation through SseJ to activate mTORC1, preventing autophagic clearance of bacteria.

Introduction

Salmonellae are Gram-negative, enteric bacilli that cause a range of human diseases from self-limiting gastroenteritis to severe typhoid fever. Key to systemic *Salmonella* infection is invasion of phagocytes within the Peyer's patches of the ileum (Darwin and Miller, 1999). *Salmonella* can survive and replicate within these phagocytes, leading to dissemination of the bacteria to the lymphatics, bloodstream, liver, and spleen (Richter-

Dahlfors et al., 1997). Colonization of these susceptible organs can lead to systemic disease and more severe outcomes. The ability to survive within a professional phagocyte like a macrophage is key to *Salmonella* pathogenesis, thus understanding how *Salmonella* accomplishes this warrants further understanding.

The *Salmonella* pathogenicity islands (SPI-1 and SPI-2) are essential for *Salmonella* infection, as each encodes a Type III Secretion System (T3SS) and most of the associated effector proteins that are secreted through them (Moest and Méresse, 2013). SPI-1 effectors primarily aid in the initial invasion of epithelial cells (Raffatellu et al., 2005). After internalization into a host cell, SPI-1 and its effectors are coordinately downregulated, while SPI-2 and its secreted effectors are induced by the phagosomal environment. The combined action of SPI-2 effectors drives remodeling of the phagosome into a specialized, non-degradative membrane-bound compartment, referred to as the *Salmonella*-containing vacuole (SCV) (Knuff-Janzen et al., 2020). Maturation of the SCV resembles endosome maturation, initially acquiring early endosomal markers EEA1 (early endosome antigen 1) and Rab5, and later recruiting Rab7 and lysosomal-associated membrane proteins (LAMP1 and LAMP2) (Steele-Mortimer, 2008; Rathman et al., 1997). However, the SCV avoids fusion with host lysosomes and actively excludes mannose-6-phosphate receptors and their cargo lysosomal hydrolases (Garcia-del Portillo and Finlay, 1995; Rathman et al., 1997; McGourty et al., 2012).

The ability of *Salmonella* to survive within host cells is due, in part, to avoidance of the host's autophagic response (Casanova, 2017). Autophagy is a cellular stress process that acts to capture bits of cytosol, damaged organelles, misfolded proteins, or intracellular pathogens (referred to as xenophagy). The core mechanism of

macroautophagy involves the sequestering of target proteins or organelles into double-membraned autophagosomes, which are ultimately delivered to lysosomes for degradation (Kirkegaard et al. 2004). During *Salmonella* infection, SCVs are initially targeted by the autophagic machinery due to membrane damage caused by the SPI-1 T3SS (Birmingham et al., 2006; Tattoli et al., 2012b). This initial response is attenuated by the SPI-1 effector SopF, which ADP-ribosylates the vacuolar H^+-ATPase, blocking its recruitment of the autophagic scaffold protein ATG16L1 (Xu et al., 2019). However, SopF expression peaks at one hour post-infection in macrophages and is barely detectable at 4 hours post-infection (Lau et al., 2019). This timing coincides with the induction of the SPI-2 T3SS and its effectors. We recently reported that *S.* Typhimurium actively suppresses autophagy in macrophages in a SPI-2-dependent manner, through recruitment of the host kinases Focal Adhesion Kinase (FAK) and protein kinase B (Akt) to the cytosolic face of the SCV, leading to activation of the master metabolic regulator, mechanistic target of rapamycin (mTOR) (Owen et al., 2014). We subsequently discovered that FAK/AKT recruitment is dependent on a single SPI-2 effector, SseJ (Greene et al., 2021).

SseJ is a RhoA-activated cholesterol acyltransferase that can generate cholesterol esters from free cholesterol and localizes to the cytoplasmic face of the SCV during infection (Nawabi et al., 2008; Ohlson et al., 2005; LaRock et al., 2012). Our recent work demonstrated that SseJ is important for the activation of FAK and Akt (Greene et al. 2021). The signaling cascade downstream of FAK/Akt activation leads to transcriptional downregulation of a key cholesterol exporter, ATP-binding cassette subfamily member 1 (ABCA1) (Frechin et al. 2015). Reduced sterol efflux results in massive cholesterol accumulation within cells, benefiting *S.* Typhimurium survival through mechanisms that have remained unknown (Greene et al. 2021). Cholesterol accumulation on the SCV and

throughout the endolysosomal system is a phenomenon that has been observed in both epithelial and macrophage cell lines (Brumell et al., 2001; Catron et al., 2002). Much of the accumulated cholesterol is centered in and around the SCV, as well as on the *Salmonella*-induced filaments (SIFs) that protrude from the SCV at late stages of infection (Brumell et al., 2001; Catron et al., 2002). The majority of this cholesterol is likely derived from internalized LDL, as *Salmonella* cannot synthesize sterols and inhibition of host sterol synthesis does not impact bacterial survival or recruitment of cholesterol to the SCV (Catron et al., 2002; Catron et al., 2004; Gilk et al., 2013). We also found that restoration of cholesterol efflux through pharmacological upregulation of *Abca1* or deletion of *sseJ* attenuated intracellular survival, suggesting that high levels of intracellular cholesterol enhance survival (Greene et al., 2021). However, the mechanisms through which cholesterol accumulation promotes survival remain poorly understood.

Intriguingly, endolysosomal cholesterol has been implicated in the activation of the master metabolic regulator, mTORC1. Canonical mTORC1 signaling relies on amino acid and nutrient signals to trigger the recruitment of mTORC1 to the surface of the lysosome by the Rag GTPase complexes (Sancak et al., 2010). At the lysosome, the small GTPase Rheb activates mTORC1, stimulating its downstream activities promoting protein synthesis through phosphorylation of p70 S6 kinase (p70 S6K), and inhibiting autophagy by phosphorylation of ULK1 (Long et al., 2005; Hay and Sonenberg, 2004; Kim et al., 2011). However, the recent discovery of a lysosomal amino acid transporter, SLC38A9, that can bind cholesterol and directly stimulate mTORC1 demonstrates that cholesterol is also an essential mTORC1 activator (Castellano et al. 2017). Lim et al (2019) further demonstrated that ER-lysosome contacts mediated by Vesicle-associated membrane protein (VAMP) Associated Protein (VAP) and oxysterol binding protein 1

(OSBP) allow cholesterol transfer from the ER to the cytosolic face of the lysosome to directly activate mTORC1 and suppress autophagy. These developments have major implications for diseases driven by mTORC1 hyperactivation, however this connection has not yet been applied to the study of intracellular pathogens.

Here, we show that *S.* Typhimurium-induced cholesterol accumulation suppresses autophagy through the recruitment and activation of mTORC1. We demonstrate that mTOR is robustly recruited to the surface of SCVs in infected murine macrophages, and that this recruitment is dependent on *S.* Typhimurium-induced cholesterol accumulation. We subsequently show that mTORC1 activation, which is elevated during *S.* Typhimurium infection, returns to uninfected levels when cholesterol accumulation is prevented. Concurrently, the formation of autophagosomes is increased when cholesterol accumulation is blocked. Finally, we find that the cholesterol transporter OSBP, previously reported to interact with SseJ (Kolodziejek et al., 2019), is important for both activation of mTORC1 and *S.* Typhimurium survival. We show that inhibition of OSBP lipid transfer activity, even in the presence of SseJ, reduces mTORC1 activation, leading to increased autophagosome formation and decreased bacterial survival. These findings demonstrate the ability of intracellular pathogens like *Salmonella* to subvert cellular lipid trafficking and signaling to survive and propagate disease.

Results:

Salmonella Typhimurium induces cholesterol accumulation in infected macrophages.

Previous work has demonstrated that *S.* Typhimurium (*St*) induces cholesterol accumulation in both cultured macrophages (Catron et al., 2002) and primary bone marrow-derived macrophages (BMDMs) (Greene et al., 2021). Early experiments were

performed using the fluorescent cholesterol-binding dye filipin, while our recent work used a fluorescent cholesterol analog, BODIPY-cholesterol (TopFluor) (Greene et al., 2021). Here, we demonstrate that cholesterol accumulation in immortalized BMDMs can be monitored by staining of endogenous cholesterol with the purified Domain 4 (D4H*) of the Perfringolysin O toxin. When expressed in cells, this probe binds selectively to free cholesterol in the cytoplasmic leaflets of the plasma membrane and organelle membranes where cholesterol is greater than 10 mole percent (Maekawa et al., 2017; Lim et al., 2019).

During *St* infection, the SPI-1 T3SS becomes highly cytotoxic to macrophages, and its expression is downregulated during passage through the intestinal epithelium (Hersh et al. 1999). Since the SPI-1 T3SS is not required for macrophage infection, we utilized a strain of *St* (Δ*invG*) that lacks InvG, the ring protein of the SPI-1 T3SS (Sanowar et al. 2010). This model allowed us to directly infect macrophages without the associated toxicity of the SPI-1 T3SS. Previous studies have shown that immortalized murine bone marrow-derived (iBMDMs) behave similarly to primary BMDMs during *St* infection (Greene et al., 2021). The iBMDMs were derived from C57/BL6 mice, which are widely used to model systemic *S.* Typhimurium infection in mice due to their deficiency in the Nramp iron/manganese transporter (Collins, 1972; Vidal et al., 1995). To demonstrate cholesterol accumulation using the D4H* probe, iBMDMs were infected with Δ*invG St* for 18 hours prior to fixation and permeabilization with a liquid nitrogen pulse (Lim et al. 2019). Endogenous cholesterol was then detected with the purified recombinant biosensor D4H*-mCherry (Figure 2-8A). As previously described in non-phagocytic cells (Lim et al., 2019), D4H*-mCherry weakly labeled the cytoplasmic leaflet of lysosomes and endosomes in uninfected iBMDMs (Figure 2-1A, Figure 2-9A), indicating that these membranes contain less than 10% cholesterol. *St* infection significantly elevated D4H*-

mCherry levels, with high levels of enrichment at the SCV (as defined by co-staining with *St* and LAMP1 antibodies), as well as throughout the lysosomal system (Figure 2-1A, Figure 2-9A). *St* infected iBMDMs exhibited over 80% more D4H*-mCherry staining than uninfected iBMDMs imaged from the same culture (Figure 2-1A-B, Figure 2-9A), confirming previous findings that *St* induces massive cholesterol accumulation within infected macrophages (Catron et al., 2002; Greene et al., 2021). In agreement with previous research (Greene et al., 2021), we found that the loss of *sseJ* significantly reduced D4H*-mCherry labeling in infected macrophages, indicating reduced cholesterol accumulation (Figure 21A-B, Figure 2-9A). Finally, our previous work demonstrated that SseJ-induced cholesterol accumulation can be prevented by treatment with T0901317, an LXR agonist that upregulates *Abca1*, nullifying the actions of SseJ (Repa et al., 2000; Greene et al., 2021). To demonstrate this, we treated iBMDMs with 10 μM T0901317 24 hours prior to infection and maintained treatment throughout infection. T0901317 pre-treatment completely blocked *St*-induced cholesterol accumulation as D4H*-mCherry labeling within pre-treated, infected iBMDMs was not significantly changed from that of uninfected cells (Figure 2-1A-B, Figure 2-9B), indicating that downregulation of *Abca1* is necessary for cholesterol accumulation during *St* infection.

Excess sterols signal the downregulation of *hmgcr*, the rate-limiting enzyme for sterol biosynthesis (Siperstein and Guest, 1960), through the activity of sterol regulatory element binding protein 2 (SREBP2; Hua et al., 1993). Thus, we measured *hmgcr* transcript levels as a readout of sterol synthesis during *St* infection. Notably, *de novo* cholesterol biosynthesis is seemingly unaffected by the massive cholesterol increase in *St* infected cells, as expression of *hmgcr* is slightly elevated, albeit not significantly, during *St* infection (Figure 2-9C). Overall, our findings using the purified D4H*-mCherry

probe agreed with previous research and highlighted a new method for studying cholesterol accumulation in *St*-infected macrophages.

By 5 hours post-infection, expression of SPI-2 T3SS effectors, including *sseJ*, is highly induced (Cirillo et al., 1998). Due to this early expression pattern of *sseJ*, we sought to understand the kinetics of cholesterol accumulation in iBMDMs. We infected iBMDMs with GFP-expressing bacteria for 5, 8, 12 and 18 hours, then stained with purified D4H*-mCherry to label endogenous cholesterol. Our results demonstrate that although expression of the SPI-2 T3SS is highly induced at 5 hours post-infection, cholesterol does not begin to significantly accumulate until at least 8 hours post-infection, with maximum levels of accumulation occurring at 18 hours post-infection, as previously reported (Figure 2-1C; Catron et al., 2002). To determine if cholesterol accumulation is cell-autonomous, we compared D4H*-labeling in uninfected cells from uninfected cultures to that in uninfected cells from *St*-infected cultures (“bystander” cells) at various time points post-infection. We found that “bystander” uninfected cells did not have significantly altered levels of endogenous cholesterol compared to uninfected cells at any time point (Figure 2-1C). Consequently, at 18 hours post-infection *St*-infected cells had three-fold higher levels of cholesterol than “bystander” cells (Figure 2-1C), indicating that cholesterol accumulation is restricted to the infected cells in a given culture. Due to this observation, all subsequent experiments used uninfected cells from the same culture as negative controls.

Salmonella-induced cholesterol accumulation is important for mTOR localization to the SCV

Previous studies have demonstrated that mTOR re-localizes to SCVs early in epithelial cell infection, however the presence of mTOR on SCVs during macrophage infection has not been verified (Tattoli et al., 2012a; Owen et al., 2014). Given the importance of mTOR localization to its activation, we sought to assess the localization of mTOR during *St* infection of iBMDMs. Confocal microscopy of infected iBMDMs revealed that mTOR is readily found on the surface of LAMP1^{+}, *St*$^{+}$ SCVs (Figure 2-2A, Figure 2-9A). Given the recent discovery of cholesterol-mediated activation of mTORC1, we asked if cholesterol accumulation was important for mTOR localization to the surface of the SCV. When iBMDMs were pre-treated with T0901317 prior to infection, mTOR intensity at the SCV decreased nearly 2-fold (Figure 2-2A-B, 2-S2A) compared to untreated, infected macrophages. Similarly, iBMDMs infected with Δ*sseJ::pACYC184* had significantly lower mTOR recruitment to the SCV than macrophages infected with the wildtype Δ*invG* strain (Figure 2-2A-B, Figure 2-9A). The catalytic activity of SseJ was also important for mTOR localization to the SCV, as macrophages infected with Δ*sseJ::H384N*, a mutant that lacks the acyltransferase activity of SseJ, had similarly reduced levels of mTOR localization to the SCV. We also assessed the activation of mTORC1, using phosphorylation of p70 S6 kinase as a readout. After 18 hours of infection, *St*-infected macrophages exhibited over 4-fold increase in mTORC1 activation compared to uninfected macrophages (Figure 2-2C-D). This activation of mTORC1 in response to infection was dependent on cholesterol accumulation and the activity of SseJ, as macrophages treated with T0901317 or infected with an SseJ-deficient strain were unable to activate mTORC1 above uninfected levels (Figure 2-2C-D). Notably, both mTOR localization to the SCV and mTORC1 activation were rescued by infection with

the complemented strain Δ*sseJ::sseJ*, indicating that the cholesterol accumulation induced by SseJ is necessary to recruit and activate mTOR at the SCV.

Salmonella suppresses autophagosome formation via cholesterol accumulation

Activated mTORC1 phosphorylates ULK1, inhibiting the initiation of autophagy (Hosokawa et al., 2009; Kim et al., 2011). We therefore next investigated how autophagosome formation is affected during *St* infection. For this purpose, we infected iBMDMs with fluorescent *St*, then stained for LC3, a canonical marker of autophagosome biogenesis. We found that iBMDMs infected with WT Δ*invG* exhibited no significant increase in LC3 intensity compared to uninfected cells (Figure 2-3A-B, Figure 2-9B). Notably, Δ*sseJ::pACYC184* infection induced a three-fold increase in LC3 intensity, compared to uninfected cells (Figure 2-3A-B, Figure 2-9B). Neither Δ*invG* nor Δ*sseJ::pACYC184* infection resulted in any change in LAMP1 levels, suggesting that the overall number of lysosomes is not altered in response to infection (Figure 2-8D). The elevated LC3 intensity phenotype was reduced by infection with Δ*sseJ::sseJ* but not by infection with Δ*sseJ::H384N*, suggesting that the activity of SseJ is necessary for suppression of autophagy. T0901317 treatment amplified LC3 intensity in all infection conditions, which suggests that the cholesterol accumulation induced by SseJ is necessary for suppressing autophagy during *St* infection (Figure 2-3A-B).

During the formation of phagophores and autophagosomes, LC3B-I becomes conjugated with phosphatidylethanolamine (PE) (Ichimura et al., 2000). This lipidated form (LC3B-II) is essential for phagophore expansion (Xie et al., 2008). Immunoblotting of LC3B-I and LC3B-II revealed that iBMDMs infected with Δ*invG St* had no significant change in the ratio of LC3B-II:LC3B-I compared to uninfected cells (Figure 2-3C-D). However, infection with Δ*sseJ::pACYC184* or Δ*sseJ::H384N St* increased the LC3B-

II:LC3B-I ratio by 1.5-fold. This increase in lipidated LC3 was rescued by infection with Δ*sseJ::sseJ* (Figure 2-3C-D). In agreement with our immunofluorescence experiments, T0901317 treatment significantly increased the ratio of LC3B-II:LC3B-I for all samples, regardless of the presence or absence of functional SseJ (Figure 2-3C-D). These results confirm that cholesterol accumulation during *St* infection impairs autophagosome formation. In our previous study, we demonstrated that SseJ-induced cholesterol accumulation is essential for *St* survival during macrophage infection, although it was unclear how cholesterol was affecting bacterial survival (Greene et al., 2021). Together these results suggest that cholesterol accumulation leads to the suppression of autophagy, which benefits bacterial survival within the macrophage.

Cholesterol transfer activity by OSBP is important for mTOR activation and autophagy suppression during *Salmonella* infection

The SCV is a major site of cholesterol accumulation during infection, however how cholesterol is trafficked to this compartment remains unclear. Recently, the cholesterol transporter OSBP, which delivers cholesterol from the ER to the Golgi and endolysosomal membranes, was implicated as an essential contributor to mTORC1 activation by cholesterol (Lim et al., 2019). Intriguingly, OSBP has been identified at the SCV during *St* infection, where it interacts with effectors SseJ and SseL to promote vacuolar stability (Kolodziejek et al., 2019). However, the role of OSBP in cholesterol transport at the SCV is unknown. Since OSBP has been implicated as a key mediator of mTOR recruitment and activation at the lysosome, (Lim et al., 2019), we inquired if OSBP activity was important for the localization of mTOR to the SCV. We pretreated macrophages with the OSBP inhibitor OSW1 (10 nM) prior to infection with fluorescent *St*. OSW1 is a potent OSBP and ORP4 inhibitor that competitively binds to the lipid

binding domain, leading to a significant decrease in OSBP cholesterol transfer activity (Burgett et al., 2011; Mesmin et al., 2017). ORP4 shares close homology with OSBP, however in contrast to the ubiquitous expression of OSBP, ORP4 is almost exclusively expressed in brain, heart, and testis tissue (Wang et al., 2002). As shown above, *St* infection stimulated mTOR localization to the SCV in an SseJ-dependent manner in infected cells (Figure 2-4A-B, Figure 2-10A). OSW1 treatment completely reversed mTOR localization to the SCV in all strains, indicating that the ability of OSBP to deliver cholesterol to the SCV is necessary for mTOR recruitment during *Salmonella* infection (Figure 2-4A-B, Figure 2-10A). We also assessed mTORC1 activation by measuring p70 S6K phosphorylation and found that OSW1 treatment reduced mTORC1 activation to uninfected, untreated levels (Figure 2-4C-D). Together, these findings suggest that OSBP activity is important for both mTOR localization and activation during *Salmonella* infection.

We evaluated autophagy during OSW1 treatment and found that OSW1 dramatically increases LC3 intensity in both uninfected and *St* infected cells (Figure 2-5A-B, Figure 2-10B). Notably, this increase in autophagosome formation is not rescued by infection with WT Δ*invG* bacteria, or with the Δ*sseJ::sseJ* rescue strain that retains SseJ functionality (Figure 2-5A-B, Figure 2-10B). Furthermore, OSW1 treatment dramatically elevated the ratio of LC3B-II:LC3B-I detected in *St* infected iBMDMs, with over 5-fold increase compared to uninfected, control cells (Figure 2-5C-D). This agrees with previous findings where OSW1 induced autophagic flux (Lim et al., 2019), and provides further evidence that inhibition of OSBP during *Salmonella* infection can induce autophagy. While SseJ induces cholesterol accumulation, OSBP must then deliver excess cholesterol to the cytoplasmic face of the SCV to activate mTORC1 and suppress autophagy.

In support of this hypothesis, we found that OSW1 treatment significantly decreases bacterial survival, as measured by a standard gentamicin protection assay. In untreated cells, Δ*sseJ::pACYC184* or Δ*sseJ::H384N* have a significant survival defect, which is rescued in macrophages infected with the Δ*sseJ::sseJ* strain (Figure 2-6A, C). However, OSW1 treatment significantly reduced bacterial survival of all strains by over 70% compared to untreated macrophages (Figure 2-6A). OSW1 did not affect the internalization rate of *St*, suggesting that this survival defect is due to the inhibition of OSBP activity, and not to off-target toxicity (Figure 2-6B). To further validate these findings, we tested the effects of 25-hydroxycholesterol (25-HC) on bacterial survival. 25-HC is a well-known OSBP inhibitor that functions similarly to OSW1 in competitively binding the lipid binding domain of OSBP (Ridgway et al., 1992). As shown in Figure 2-6C-D, 25-HC treatment reduced bacterial survival by approximately 50% in all strains, which concurs with previous findings that OSW1 is nearly 1000 times more potent than 25-HC (Mesmin et al., 2017). In summary, these results demonstrate that the ability of OSBP to bind and deliver cholesterol is essential to *St* survival during macrophage infection.

While OSBP recruitment to the SCV has been established (Kolodziejek et al., 2019), we sought to confirm the presence of cholesterol along with OSBP at the SCV surface. We transiently expressed EGFP-OSBP and mCherry-D4H plasmids in iBMDMs, then infected with *St* for 18 hours. We found that EGFP-OSBP and mCherry-D4H-labeled cholesterol are closely associated at the SCV membrane, which is denoted by *St* and LAMP1 antibody staining (Figure 2-7E, Movie 1). OSBP and cholesterol decorated the SCV in a patch-like pattern, which supports our hypothesis that OSBP is delivering cholesterol to the SCV. Because it has been reported that SseJ and SseL redundantly recruit OSBP to the SCV, we infected cells with WT Δ*invG*, Δ*sseJ*, or Δ*sseL* strains of *St* and assayed whole cell

cholesterol accumulation, along with mCherry-D4H and OSBP localization to the SCV. In iBMDMs infected with Δ*sseL*, total cellular cholesterol levels were increased by two-fold compared to uninfected cells, with no significant difference from iBMDMs infected with Δ*invG* (Figure 2-7A-B). In contrast, iBMDMs infected with the Δ*sseJ* strain showed no significant change in cholesterol levels compared to uninfected cells, underscoring that SseJ, but not SseL, is responsible for cholesterol accumulation during *St* infection (Figure 2-7B). Furthermore, cholesterol levels at the SCV were decreased in iBMDMs infected with Δ*sseJ*, supporting our previous findings that SseJ is necessary for cholesterol accumulation (Figure 2-7C). These results also agree with our previous findings that BMDMs infected with a Δ*sseL* strain of *St* retained elevated FAK and Akt activation (Greene et al., 2021). OSBP localization to the SCV was not perturbed by the single deletions of *sseJ* or *sseL*, reiterating the redundancy of these effectors (Figure 2-7D).

Taken together, our results suggest a model in which *St* induces cholesterol accumulation through the activity of SseJ, which is responsible for *Abca1* downregulation (Figure 2-7E). As cholesterol levels increase throughout the cell, it is delivered to the cytoplasmic face of the SCV by OSBP. Cholesterol on the SCV surface then recruits and activates mTORC1, leading to suppression of the autophagic response and consequently increased bacterial survival. If this manipulation of host signaling is inhibited at any point – through mutation or loss of *sseJ*, pharmacological upregulation of *Abca1*, or inhibition of OSBP activity – autophagy is triggered and bacterial survival is attenuated.

Discussion:

The ability of *Salmonella* to escape autophagy and survive in restrictive cell types such as macrophages plays a major role in systemic infection and negative clinical outcomes. Recent work has demonstrated that *Salmonella* can effectively suppress autophagy within the first 4-5 hours post infection in both epithelial and macrophage cells (Owen et al., 2014; Tattoli et al., 2012a; Xu et al., 2022). However, as bacterial replication progresses later in infection, it is unclear how *Salmonella* continues to avoid the autophagic response. Here, we provide evidence that *Salmonella* leverages cholesterol accumulation within the macrophage to activate mTORC1 and suppress autophagy. Our results demonstrate that *Salmonella* utilizes the SPI-2 effector SseJ to induce cellular cholesterol accumulation, which is necessary for both mTOR recruitment to the SCV and mTORC1 activation. This pathway relies on the lipid transfer activity of the host cholesterol transporter OSBP, which is recruited to the SCV, and is essential for activation of mTORC1 and the suppression of autophagy. These results highlight a novel method through which intracellular pathogens can manipulate the host response.

Role of mTORC1 during infection

Early studies have demonstrated mTOR recruitment to the SCV within several hours post infection in epithelial cells (Tattoli et al., 2012a). However, this same phenomenon has not been demonstrated in macrophages or at time points past the onset of bacterial replication. Here, we demonstrate that mTOR robustly localizes to the SCV 18 hours post infection of macrophages. Notably, this localization is dependent on both the presence and catalytic activity of the SPI-2 effector SseJ, which was recently implicated in *Salmonella*-induced cholesterol accumulation (Greene et al., 2021). SseJ is critical for the recruitment and activation of host kinases FAK and Akt, which both localize to the

SCV during infection (Owen et al., 2014; Greene et al., 2021). Akt mediates the inhibitory phosphorylation of transcription factors FOXO3 and TAL1, which drive the expression of the major cholesterol export protein ABCA1 (Frechin et al., 2015). In this manner, SseJ activity suppresses the expression of *Abca1*, resulting in massive cholesterol accumulation that benefits bacterial survival through a previously unknown mechanism. We now demonstrate that SseJ-induced cholesterol accumulation is necessary for the localization of mTOR to the SCV and activation of mTORC1. These results parallel a similar process in uninfected cells, where high levels of cholesterol in the cytosolic leaflet of lysosome membranes (such as occurs in Niemann-Pick type C disease) can recruit and activate mTORC1 (Lim et al., 2019). What remains unknown is how this localization to SCVs impacts lysosomal recruitment of mTOR. Future studies will be required to determine if there is preferential recruitment of mTOR to SCVs compared to lysosomes, or if lysosome-localized mTOR contributes to the massive induction of mTORC1 activity observed in *Salmonella*-infected macrophages.

OSBP cholesterol transfer activity

The observation that mTOR localizes to the SCV in a cholesterol-dependent manner raises further questions about how cholesterol is delivered to the SCV. Cholesterol trafficking is highly regulated in eukaryotic cells, and is primarily handled by lipid transfer proteins that operate through membrane contact sites (MCSs). Endocytosed LDL is trafficked to lysosomes, where liberated cholesterol is de-esterified and then shuttled across the lysosomal membrane via NPC1/2 and other parallel export mechanisms (Infante et al., 2008). From there, the fate of free cholesterol is less well defined, although a major pathway appears to involve transfer to the plasma membrane enroute to the ER (Das et al., 2014). Transfer to the ER is known to involve specific GRAMD1

transporters operating at plasma membrane-ER MCSs (Naito et al., 2019). From the ER, cholesterol can be redistributed to other organelles, including lysosomes, endosomes, and the TGN via OSBP and its less ubiquitous relative ORP4 by the coupled counter-transport of phosphatidylinositol-4-phosphate (PI4P) (Ridgway et al., 1992; Dong et al., 2016; Mesmin et al., 2013). Recently, OSBP has also been linked to cholesterol-mediated mTORC1 activation at the lysosome (Lim et al., 2019). Our work has now clarified that OSBP is necessary for both mTOR localization to the SCV and mTORC1 activation during *Salmonella* infection. These findings are supported by previous research that identified OSBP at the SCV where it interacts with SPI-2 effectors SseJ and SseL (Kolodziejek et al., 2019). OSBP is redundantly recruited to the SCV by these effectors and can be recruited even in the presence of 25-hydroxycholesterol, suggesting that this recruitment via SPI-2 effectors is robust. Our findings have clarified that OSBP-mediated cholesterol transfer is necessary to suppress autophagy during infection, as infected cells treated with the OSBP inhibitor OSW1 showed a robust increase in LC3 puncta and LC3-II:LC3-I ratio. These results suggest that OSBP is directed to the SCV via SseJ/SseL to deliver cholesterol, which then acts to recruit and activate mTORC1. Notably, while SseJ and SseL may act redundantly to recruit OSBP to the SCV, our findings demonstrated that SseL is not necessary for the cholesterol accumulation that occurs during *St* infection. OSBP is a major consumer of PI4P at its target membranes, consuming most of the PI4P present in the TGN (Mesmin et al., 2017). Additionally, the affinity of OSBP for a membrane depends on local PI4P concentration due to the binding requirement of its PH domain for PI4P (Mesmin et al., 2013). Thus, the question arises regarding how the SCV sustains continued OSBP binding, and if PI4P is continually supplied or generated at the SCV surface. An interactome of *Salmonella* effector protein-protein interactions revealed that SseL interacts with the PI-4 kinase PI4KIIα in RAW264.7 macrophages (Walch et al., 2021),

which may explain how the SCV is supplied with PI4P to sustain OSBP activity. Further research will be needed to determine how the dynamics of OSBP recruitment and activity are affected by the lipid composition of the SCV membrane.

Notably, despite the nearly 4-fold increase in endogenous cholesterol in *St* infected macrophages, expression of *hmgcr*, the rate-limiting enzyme in cholesterol biosynthesis, was not suppressed, suggesting that biosynthetic cholesterol is produced at a rate similar to that of uninfected cells. This result implies that either the regulatory machinery that senses ER cholesterols levels (e.g. SREBP2) is impaired during *Salmonella* infection or that cholesterol is transferred away from the ER (via OSBP and/or other transporters) as it enters, preventing its accumulation in the ER.

SseJ and FAK/Akt activation

SseJ plays an essential role in *Salmonella* infection. Localized to the surface of the SCV, SseJ is important for both activation of FAK/Akt and interaction with OSBP, in parallel with SseL (Greene et al., 2021; Kolodziejek et al., 2019). We now report that the catalytic activity of SseJ is necessary for the induction of cholesterol accumulation and subsequent mTORC1 activation, leading to suppression of autophagy. How SseJ activates FAK/Akt remains an open question. One possibility is through direct interaction between SseJ and FAK, however a recent study of *Salmonella* effector interactions did not detect any interactions between SseJ and FAK or Akt in RAW264.7 cells (Walch et al., 2021). Another option is through modification of the lipid composition of the SCV. FAK activation depends on the conformation of its N-terminal FERM domain, which mediates autoinhibition by occluding the kinase domain (Lietha et al., 2007). Binding of the FERM domain to integrins relieves autoinhibition, allowing the kinase domain to

autophosphorylate residue Tyr 397, leading to activation (Schaller et al., 1994). In addition to integrin and growth factor binding, FAK activation can also be triggered by phospholipid binding. Direct binding of $PI(4,5)P_2$ to the FERM domain triggers clustering of FAK on lipid membranes, leading to conformational changes that release autoinhibition and allow for activation (Goñi et al., 2014). Given the role of SseJ in modifying the lipid environment of the SCV, the recruitment and activation of FAK to the SCV may involve intricate changes in the lipid profile of the membrane rather than direct interaction with SseJ.

Salmonella suppression of autophagy

Salmonella infection involves a complex relationship with autophagy. Early in infection (1-4 hours), the SPI-1 T3SS forms pores in the plasma membrane, causing transient amino acid starvation (Tattoli et al., 2012a). The SPI-1 T3SS also damages the early SCV membrane, resulting in recognition of the damaged vacuoles by cytosolic galectins (Kreibich et al., 2015). Both events trigger an early autophagic response, which *Salmonella* contains through the SPI-1 effector SopF (Xu et al., 2022). SopF ADP-ribosylates the ATP6V0C subunit of V-ATPase, preventing recruitment of the core autophagy component ATG16L and subsequent xenophagy initiation (Xu et al., 2019).

Further autophagic control is provided by the SPI-2 effector SopB, which modulates PI3P levels on the SCV to prevent fusion with autophagosomes (Chatterjee et al., 2023). Clearly *Salmonella* has evolved multiple pathways to evade the host autophagic response. While earlier work has focused on time points from 1 to 8 hours post infection, our studies have addressed later points, when bacteria have replicated. At this stage, macrophages laden with replicating bacteria can pose a serious threat as they begin to

circulate, spreading the infection through the body. Cholesterol accumulation also peaks at 18 hours post infection and is beneficial to bacterial survival (Greene et al., 2021). Cholesterol levels and autophagy have been closely linked in recent studies of uninfected cells, but our data define a novel pathway through which an intracellular pathogen manipulates host cholesterol trafficking to suppress autophagy. This pattern of cholesterol accumulation during infection is not unique to *Salmonella*, but rather shared by several other intracellular pathogens that infect macrophages. Notably, the *Legionella pneumoniae* vacuole is also known to accumulate cholesterol, and the bacteria modulate mTORC1 activity to promote lipogenesis and vacuolar stability (Abshire et al., 2016; Ondari et al., 2023). Similarly, *Mycobacterium tuberculosis* induces both LDL uptake and cholesterol biosynthesis during infection, leading to increased cellular cholesterol levels that promote persistence and are used as a carbon source by the bacteria (Chen et al., 2024; Pandey et al., 2008). Whether cholesterol accumulation also suppresses autophagy in these contexts remains unknown.

In summary, our work details an intricate process through which *Salmonella* utilizes the SPI-2 effector SseJ to induce cholesterol accumulation and suppress autophagy through mTORC1 activation. Key to this process is the cholesterol transporter OSBP, which delivers cholesterol from the ER to the lysosome, and in the context of *Salmonella* infection, to the SCV. If OSBP cholesterol transfer activity is perturbed, mTORC1 activation is reduced to below uninfected levels and the cells exhibit increased autophagosome formation, along with decreased bacterial survival. In this manner, *Salmonella* evades the autophagic response at late time points in macrophage infection to promote survival.

Materials and Methods

Cell culture

The iBMDMs were a kind gift from Dr. Johnathan Kagan (Children's Hospital, Boston). iBMDMs were grown on tissue-culture-treated petri dishes (Fisher) in Dulbecco's Modified Eagle Medium (DMEM; Genessee Scientific) supplemented with 10% fetal bovine serum (FBS) and 1% penicillin/streptomycin/amphotericin B (PSF). Primary BMDMs were isolated from the hind leg bones of mice, plated onto untreated petri dishes (Fisher), and cultured in RPMI (Genesee Scientific) supplemented with 10% heat-inactivated FBS, 10% L929-conditioned media, and 1% PSF.

Bacterial strains and culture

Bacterial strains used in this study are described in Table 2-1. The SPI-1-deficient Δ*invG* mutant strain of *Salmonella* Typhimurium SL1344 was a kind gift from Beth McCormick (University of Massachusetts). The mutant Δ*sseJ::pACYC184,* Δ*sseJ:: sseJ*, and Δ*sseJ::H384N* strains were previously described (Greene et al. 2021) and are on a Δ*orgA* background. The Δ*sseJ* and Δ*sseL* strains were a kind gift from Denise Monack (Stanford University), and are on a Δ*orgA* background. For infection of iBMDMs, bacteria were grown under non-invasion-inducing conditions. Briefly, each strain was grown statically overnight in LB broth containing the appropriate antibiotics. Bacteria were harvested the following morning at OD_{600} 0.6-0.8.

Bacterial Infection

One hour prior to infection, cells were washed three times with 1X PBS, then incubated in fresh DMEM containing 10% heat-inactivated FBS and no antibiotics (infection media). Bacteria were collected, spun down, and resuspended in infection media. Cells

were infected with the indicated strain and multiplicity of infection (MOI) for 30 minutes. After 30 minutes, cells were washed three times in 1X PBS, then incubated in fresh infection media containing gentamicin (100 ug/mL, Fisher) for 60 minutes to kill extracellular bacteria. After 90 minutes total infection, the media was replaced with fresh infection media containing 10 ug/mL gentamicin for the remainder of the assay.

Immunofluorescence Microscopy

The day before infection, iBMDMs were plated on fibronectin-coated glass coverslips (Electron Microscopy Services) in a 24-well dish (Corning). Cells were infected with the indicated bacterial strain at an MOI of 75 for 18 hours. The coverslips were washed once with 1X PBS prior to fixation with 4% paraformaldehyde (PFA), then blocked with 3% bovine serum albumin (BSA) in 0.1% Triton-X-100 in PBS for 1 hour. Cells were additionally blocked in Mouse-On-Mouse Blocking Reagent (Vector) to prevent Fc receptor non-specific binding. The coverslips were incubated with primary antibodies for 1 hour at room temperature. Cells were then washed three times with 0.1% Triton-X-100 in PBS and incubated with Alexa Fluor conjugated secondary antibodies for 1 hour at room temperature. After staining, cells were washed 3 times with 1X PBS, then mounted on glass slides using Prolong Gold mounting media. Coverslips were cured overnight prior to imaging. The following antibodies were used in this study for immunofluorescence: rat anti-LAMP1 (DSHB); rabbit anti-mTOR (Cell Signaling Technologies); mouse anti-LC3 (MBL International); rabbit anti-*Salmonella* antigen (ThermoFisher); donkey anti-rabbit 488; donkey anti-mouse 488; goat anti-rat 647; and donkey anti-rabbit 405 (all Alexa Fluor antibodies from ThermoFisher). Coverslips were imaged using a Nikon AX-R resonant scanning confocal microscope fitted with an Apo TIRF 100x Oil DIC N2 objective. Z-stacks of the entire cell were taken with 0.25-0.5 µm slices, and a maximum Z projection was generated using FIJI software. Images were

analyzed using the Nikon Elements software. Laser power and gain settings were identical between all conditions. D4H*-mCherry intensity was measured by the whole-cell Corrected Total Cellular Fluorescence (CTCF, see formula below) of the D4H*-mCherry signal. Quantification of mTOR is described below. LC3 intensity was measured by the whole-cell ratio of LC3 CTCF to LAMP1 CTCF.

CTCF = Integrated Density – (Average background x ROI Area)

Quantification of mTOR on SCVs

To quantify the CTCF of mTOR on SCVs, ROIs were created by first thresholding on the LAMP1 signal and creating a binary mask that represented all lysosomal and SCV structures. A second binary mask was generated by thresholding on the *Salmonella* structures. By adding the interaction of the two masks using Nikon Elements Software, we generated ROIs that were positive for both LAMP1 and *Salmonella*, indicating an SCV. The mean intensity of mTOR and the area of these ROIs were recorded, enabling CTCF calculation.

Purification of GST-D4H*-mCherry

The pGEX-KG-D4H*-mCherry plasmid was a gift from Roberto Zoncu (Addgene plasmid #13604). BL21 *Escherichia coli* expressing pGEX-KG-D4H*-mCherry were grown overnight, then expanded and induced for plasmid expression using 0.4 mM ITPG for 16 hours at 20 degrees C. Bacteria were pelleted and resuspended in Buffer A (20 mM Tris-Cl pH 8.0, 0.1 M NaCl, 1 mM DTT, and 1:1000 dilution of HALT Protease Cocktail Inhibitor (Thermofisher), followed by incubation with 0.35 mg/mL lysozyme for 30 minutes on ice. The lysate was then sonicated on ice for 12 cycles of 10s followed by a 10s pause. Next, 0.5% Triton X-100 was added to the lysate, which was shaken at 4 deg

C for 15 minutes. The lysate was then spun at 17,000 x g for 30 min at 4 deg C. The resulting supernatant was added to equilibrated Glutathione Sepharose 4B Beads (GE Healthcare) and shaken at 4 deg C overnight. The GST-D4H*-mCherry protein was eluted with 10 mM reduced glutathione in 50 mM Tris, 150 mM NaCl, pH 8.0. The GST tag was cleaved with thrombin (Biovision) and the eluted protein was filtered using 30 kDa centrifugal filter units (Millipore). The size and quality of the purified protein was validated with Gel Code Blue staining and immunoblotting.

D4H*-mCherry staining

For intracellular staining of endogenous cholesterol, cells were plated and infected as described above. After 18 hours of infection, the coverslips were fixed with 4% PFA then flash-permeabilized in liquid nitrogen for 30s. The cells were blocked in 3% BSA in PBS for 1 hour, then blocked in Mouse-on-Mouse Blocking Reagent (Vector) for 2 hours at room-temperature. Cells were then stained with 40 µg/mL of purified D4H*-mCherry diluted in 3% BSA in PBS for 2 hours at room-temperature. After D4H* staining, cells were washed three times with 1X PBS, refixed with 4% PFA, and stained with LAMP1 and *Salmonella*-antigen antibodies for 1 hour at room-temperature. After primary antibody incubation, cells were washed three times with 1X PBS then incubated with Alexa-Fluor conjugated secondary antibodies for 1 hour at room temperature. Cells were then washed three times with 1X PBS and mounted using Prolong Gold.

Drug Treatments

Prior to infection, cells were pre-treated either: overnight with 10 uM T0901317 (Tocris); for 1 hour with 10 nM OSW1 (Cayman Chemical Company); or for 1 hour with 5 uM 25-HC (Avanti Polar Lipids). All drug treatments were maintained throughout the course of

the infection. For untreated, control cells (- Tx) cells were treated with the drug vehicle (DMSO).

Western Blotting

Cells were seeded at 5 x 10^5 cells/well on 6-well tissue-culture-treated dishes (Corning) prior to infection at an MOI of 150. After 18 hours of infection, cells were rinsed three times with cold 1X PBS, then lysed in Triton X-100 lysis Buffer (50 mM Tris pH 7.4, 1% Triton X-100, 150 mM NaCl, and 2 mM EDTA), supplemented with 1 mM sodium vanadate, 50 mM sodium fluoride, 1:1000 dilution of HALT protease cocktail inhibitor (ThermoFisher), and 0.1 mM PMSF. Samples were loaded onto 4-20% SDS-polyacrylamide gels (BioRad), transferred onto PVDF membranes using the Transblot Turbo Transfer system (BioRad), and probed using the following antibodies: rabbit anti-p-p70 S6K (CST); rabbit anti-p70 S6K (CST); rat anti-LAMP1 (DSHB); rabbit anti-LC3B (Cell Signaling); goat anti-β-actin (Santa Cruz); anti-rabbit HRP (Amersham); IRDye 680RD anti-rat IgG; and IRDye 800 CW anti-goat IgG. For HRP-linked antibodies, membranes were developed with SuperSignal Pico PLUS Chemiluminescent Substrate (Thermo), and imaged on a ChemiDoc (Biorad). For IRDye-linked antibodies, membranes were imaged using a Li-Cor Odyssey. Densitometry was performed using ImageLab software (BioRad).

RNA extraction and qPCR

Cells were seeded at 1 x 10^6 cells/well in 6-well tissue-culture-treated plates prior to infection at an MOI of 150. After 18 hours of infection, RNA was extracted using the RNeasy PLUS Mini kit (Qiagen). cDNA was prepared using the ProtoScript II Reverse Transcriptase kit with Oligo dT primers. Real-time PCR analysis was performed using the Applied BioSystems 7500 Real Time PCR machine, Taqman 2X Master Mixer

(Applied Biosystems) and the following Taqman primer-probe sets: Mm01282499_m1 Hmgcr FAM-MBG; 18s rRNA VIC-TAMRA. The ddCT method was used to quantify all relative mRNA levels, using 18s rRNA as the reference.

Gentamicin Protection Assay:

Cells were seeded at 5 x 10^4 in 24-well dishes 18 hours prior to infection at an MOI of 75. Cells were lysed in 0.2% Triton-X-100 PBS at 30 minutes, 1 hour, or 18 hours post-infection. Lysates were diluted and plated onto LB agar to enumerate CFUs. Internalization rate = CFU at 1 hour/CFU at 0.5 hour. Survival rate = CFU at 18 hours/CFU at 1 hour.

Transfection and plasmids

The pEGFP-OSBP plasmid was subcloned from pmCherry-OSBP (a kind gift from Bruno Antonny, Institut Curie) using the BamHI site. The pmCherry-D4H plasmid was a kind gift from Gregory Fairn (Dalhousie University). For transfection, iBMDMs were seeded at 5 x 10^4 on fibronectin-coated coverslips 24 hours prior to transfection with the BAPtofect-25 (Phoreus Biotech) transfection reagent. Cells were used 24 hours after transfection. The transfected iBMDMs were infected with Δ*invG* as described above for 18 hours at MOI 75. The coverslips were fixed and stained with LAMP1 and *Salmonella*-antigen antibodies prior to imaging.

Statistics

For the comparison of two independent groups, a Student's t-test was used. For the comparison of more than two independent groups, two-way ANOVA with Dunnett's or Tukey's multiple comparison was used. The exact test used in each figure may be found

in the corresponding legend. All tests were performed with GraphPad Prism10, and p-values of 0.05 or less were considered statistically significant.

Acknowledgements

Figures were made using BioRender and Inkscape. We thank Johnathan Kagan (Children's Hospital, Boston) for the iBMDMs; Beth McCormick (University of Massachusetts) for the Δ*invG* strain; Denise Monack (Stanford University) for the Δ*sseJ* and Δ*sseL* strains; and Gregory Fairn (Dalhousie University) for the mCherry-D4H plasmid. This work was funded by NIH grants to J.E. Casanova (R01DK58536 and R01AI136073), N. Leitinger (R01AI168194), and the Global Biothreats Training Grant (T32AI055432).

Figure 2-1

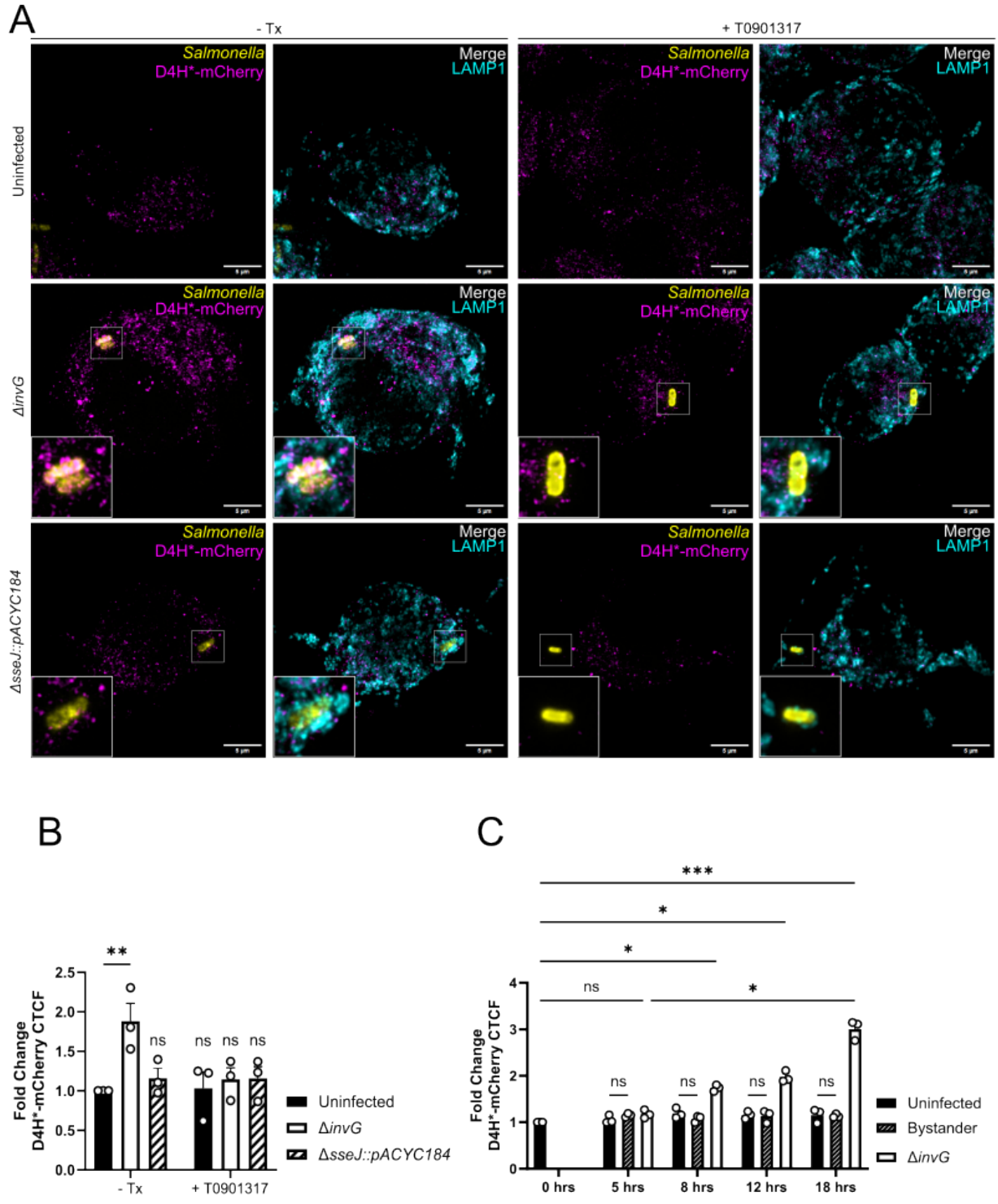
A
- Tx
+ T0901317
Uninfected
ΔinvG
ΔsseJ::pACYC184
Salmonella
D4H*-mCherry
Merge
LAMP1
B
Fold Change
D4H*-mCherry CTCF
**
ns
- Tx
+ T0901317
Uninfected
ΔinvG
ΔsseJ::pACYC184
C
***
*
ns
0 hrs
5 hrs
8 hrs
12 hrs
18 hrs
Bystander

Figure 2-1: *Salmonella* Typhimurium infection induces cholesterol accumulation in immortalized bone marrow-derived macrophages. (A) Vehicle (-Tx) or T0901317-treated (10 μM) bone marrow-derived macrophages (iBMDMs) were either uninfected or infected with the indicated *Salmonella* strain for 18 hours. Cells were fixed, permeabilized in liquid nitrogen, and stained with recombinant purified D4H*-mCherry (magenta) to label endogenous cholesterol. Cells were then stained for *Salmonella* (yellow) and LAMP1 (cyan) and imaged by confocal microscopy. Uninfected cells were imaged from the same coverslips as infected cells. The inset panel represents 2.5X zoom. Scale bar indicates 5 μm. The individual channel images can be found in Figure 2-8A-B. All images are maximum intensity projections of Z-stacks with 0.25 μm steps. (B) The corrected total cellular fluorescence (CTCF) of whole cell D4H*-mCherry signal was quantified. Bars indicate mean + standard error of the mean (SEM) of 3 experimental replicates with 10-20 cells measured per experimental replicate. ** $p < 0.01$; ns, not significant. Statistics represent the indicated groups compared to uninfected, untreated iBMDMs, two-way ANOVA with Dunnett's multiple comparison. (C) iBMDMs were left uninfected or infected with GFP-expressing Δ*invG* (yellow) bacteria for 5, 8, 12, or 18 hours. At the endpoint, cells were fixed, permeabilized in liquid nitrogen, and stained with recombinant purified D4H*-mCherry (magenta) and anti-LAMP1 (cyan). The CTCF of whole cell D4H*-mCherry signal was quantified. Uninfected cells are those imaged from uninfected coverslips. Bystander cells are uninfected cells imaged from Δ*invG*-infected coverslips. Bars indicate mean + SEM of 3 experimental replicates with 10-20 cells measured per experimental replicate. * $p < 0.05$; *** $p < 0.001$; ns, not significant. Two-way ANOVA with Tukey's multiple comparison.

Figure 2-2

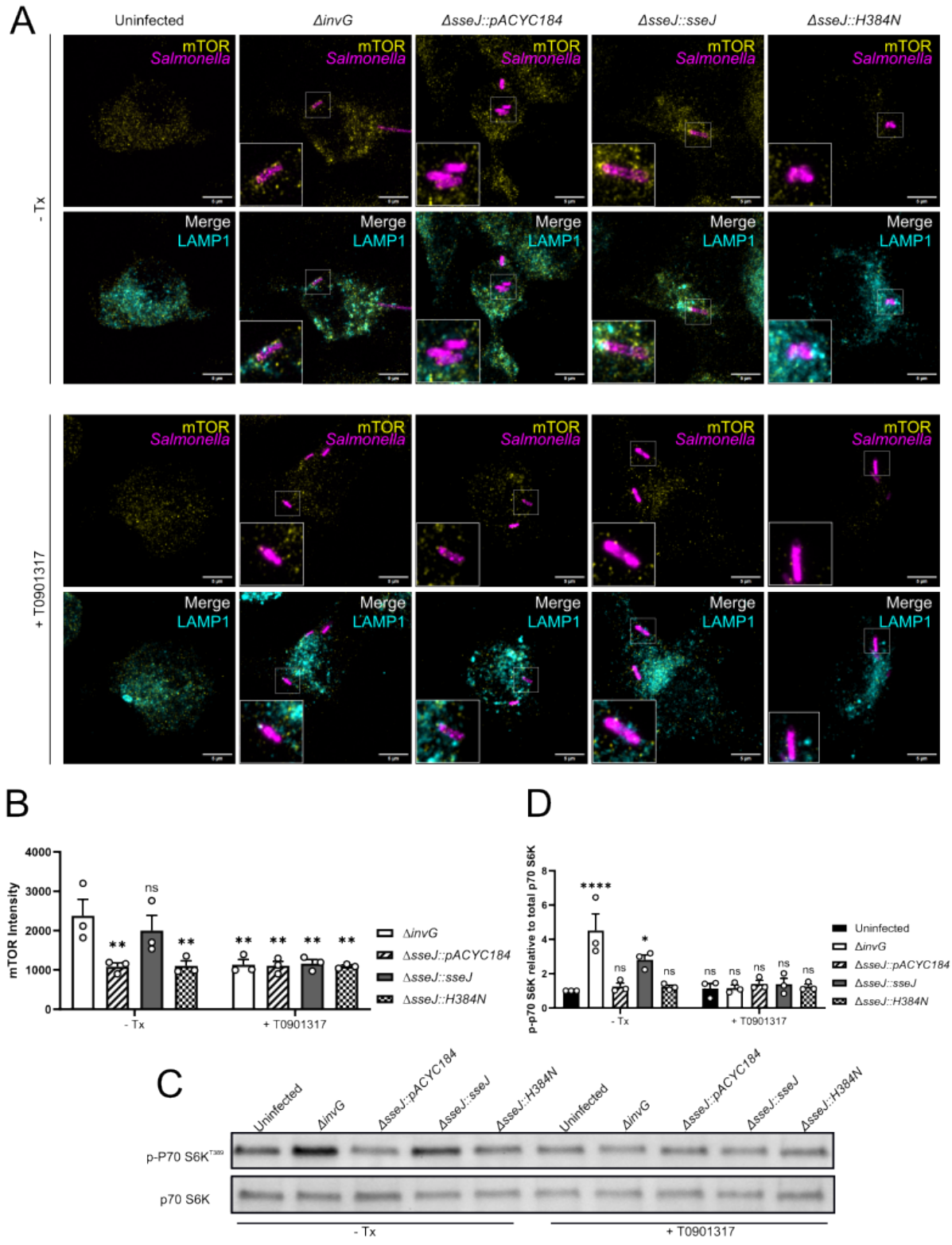
A
Uninfected
ΔinvG
ΔsseJ::pACYC184
ΔsseJ::sseJ
ΔsseJ::H384N
- Tx
+ T0901317
mTOR
Salmonella
Merge
LAMP1
B
mTOR Intensity
4000
3000
2000
1000
0
ns
**
- Tx
+ T0901317
ΔinvG
ΔsseJ::pACYC184
ΔsseJ::sseJ
ΔsseJ::H384N
D
p-p70 S6K relative to total p70 S6K
8
6
4
2
0
****
*
ns
Uninfected
C
p-P70 S6K
p70 S6K

Figure 2-2. *Salmonella* infection triggers mTOR localization to the SCV in a cholesterol-dependent manner. (A) iBMDMs were treated with the vehicle (-Tx) or 10 μM T0901317 prior to infection with RFP-expressing *Salmonella* (magenta) for 18 hours at MOI 75. Cells were fixed and stained for mTOR (yellow) and LAMP1 (cyan), then imaged with confocal microscopy. Uninfected cells were imaged from the same coverslips as infected cells. The inset panel represents 2.5X zoom. Scale bar indicates 5 μm. The individual channel images can be found in Figure 2-9A. All images are maximum intensity projections of Z-stacks with 0.25 μm steps. (B) The intensity of mTOR was measured by the CTCF on SCVs (*Salmonella*$^+$, LAMP1$^+$ structures. Bars indicate mean + SEM of 3 experimental replicates, with 15 cells measured per replicate. ** $p < 0.01$; ns, not significant. Statistics represent the indicated groups compared to uninfected, untreated iBMDMs. Two-way ANOVA with Dunnett's multiple comparison. (C) Vehicle (-Tx) or T0901317 (10 μM) treated iBMDMs were infected with *Salmonella* for 18 hours at MOI 150, then lysates were collected and immunoblotted for total and phosphor-p70 S6K. (D) Blots were quantified by measuring the densitometry of the total and phosphor-p70 S6K bands, and expressed as the ratio of phospho:total signal. Bars indicate mean + SEM of 3 experimental replicates. * $p < 0.05$; ** $p < 0.01$; **** $p < 0.0001$; ns, not significant. Statistics represent the indicated groups compared to uninfected, untreated iBMDMs. Two-way ANOVA with Dunnett's multiple comparison.

Figure 2-3

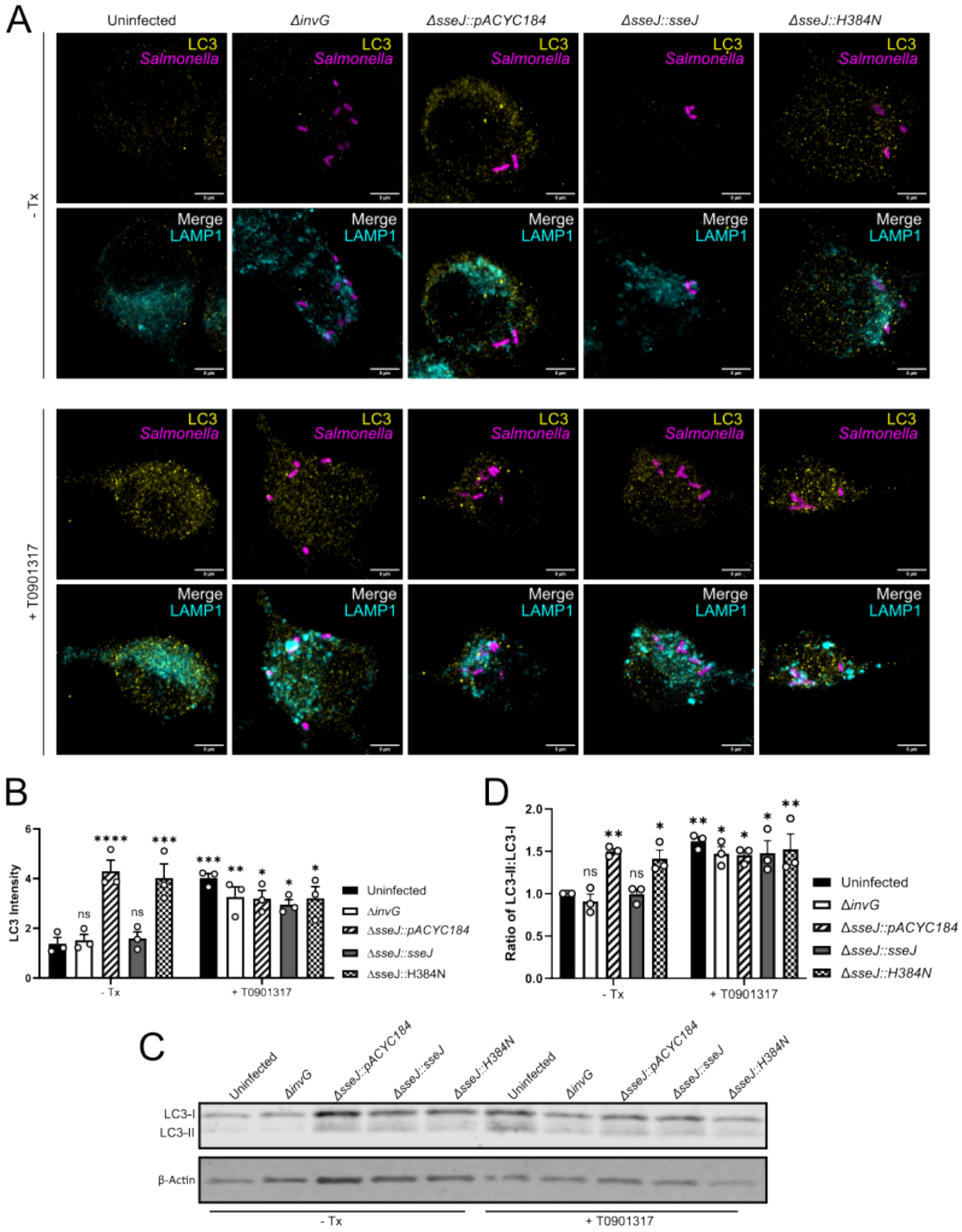
A
Uninfected
ΔinvG
ΔsseJ::pACYC184
ΔsseJ::sseJ
ΔsseJ::H384N
- Tx
+ T0901317
LC3
Salmonella
Merge
LAMP1
B
LC3 Intensity
ns
****
***
**
*
- Tx
+ T0901317
Uninfected
ΔinvG
ΔsseJ::pACYC184
ΔsseJ::sseJ
ΔsseJ::H384N
D
Ratio of LC3-II:LC3-I
C
LC3-I
LC3-II
β-Actin

Figure 2-3. Cholesterol accumulation suppresses autophagosome formation during *Salmonella* infection. (A) Vehicle (-Tx) or T0901317 (10 μM) treated iBMDMs were infected with RFP *Salmonella* (magenta) for 18 hours at MOI 75, then fixed and stained for LC3 (yellow) and LAMP1 (cyan). Uninfected cells were imaged from the same coverslips as infected cells. Scale bar indicates 5 μm. The individual channel images can be found in Figure 2-9B. All images are maximum intensity projections of Z-stacks with 0.25 μm steps. (B) LC3 intensity was measured by the whole-cell ratio LC3 CTCF:LAMP1 CTCF. Bars indicate mean + SEM of 3 experimental replicates, with 20 cells measured per replicate. Statistics represent the indicated bars compared to uninfected, untreated iBMDMs. * $p < 0.05$; ** $p < 0.01$; *** $p < 0.001$; **** $p < 0.0001$; ns, not significant. Two-way ANOVA with Dunnett's multiple comparison. (C) Vehicle (-Tx) or T0901317 (10 μM) treated iBMDMs were infected with *Salmonella* for 18 hours at MOI 150, then lysates were collected and immunoblotted for LC3B and β-actin. (D) Blots were quantified by measuring the densitometry of the LC3B-II and LC3B-I bands, and expressed as the ratio of LC3-II:LC3-I signal. Bars indicate mean + SEM of 3 experimental replicates. * $p < 0.05$; ** $p < 0.01$; ns, not significant. Statistics represent the indicated groups compared to uninfected, untreated iBMDMs. Two-way ANOVA with Dunnett's multiple comparison.

Figure 2-4

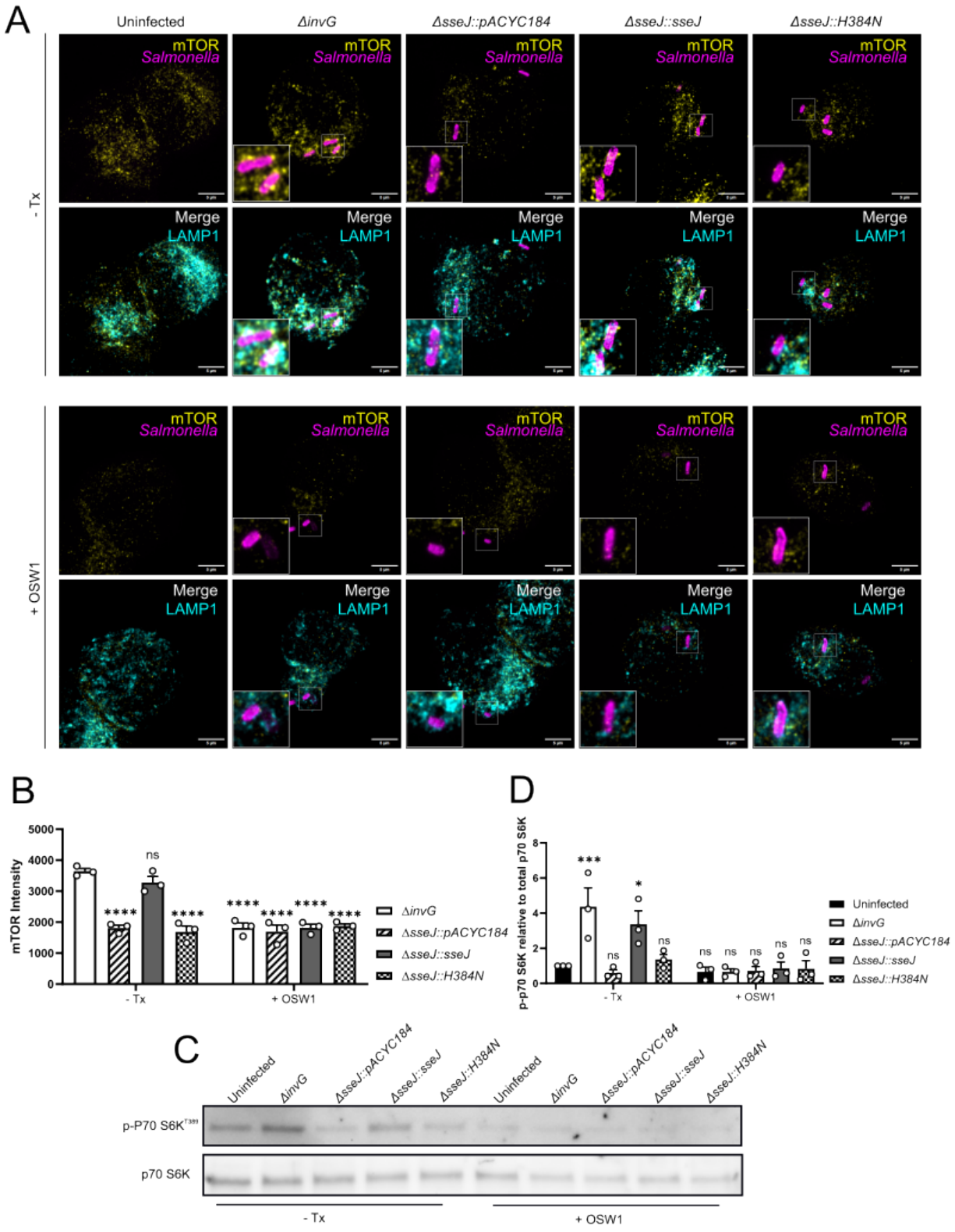
A
Uninfected
ΔinvG
ΔsseJ::pACYC184
ΔsseJ::sseJ
ΔsseJ::H384N
mTOR
Salmonella
Merge
LAMP1
- Tx
+ OSW1
B
mTOR Intensity
5000
4000
3000
2000
1000
0
ns
****
- Tx
+ OSW1
ΔinvG
ΔsseJ::pACYC184
ΔsseJ::sseJ
ΔsseJ::H384N
D
p-p70 S6K relative to total p70 S6K
8
6
4
2
0
***
*
ns
Uninfected
C
p-P70 S6K
p70 S6K

Figure 2-4. OSBP activity is important for mTOR localization to the SCV during *Salmonella* infection. (A) iBMDMs were treated with the drug vehicle (-Tx) or 10 nM OSW1 prior to infection with RFP-expressing *Salmonella* (magenta) for 18 hours at MOI 75. Cells were fixed and stained for mTOR (yellow) and LAMP1 (cyan), then imaged with confocal microscopy. Uninfected cells were imaged from the same coverslips as infected cells. The inset panel represents 2.5X zoom. Scale bar indicates 5 μm. The individual channel images can be found in Figure 2-10A. All images are maximum intensity projections of Z-stacks with 0.25 μm steps. (B) The intensity of mTOR was measured by the CTCF on SCVs (*Salmonella*$^+$, LAMP1$^+$ structures. Bars indicate mean + SEM of 3 experimental replicates, with 15 cells measured per replicate. **** $p < 0.0001$; ns, not significant. Statistics represent the indicated bars compared to uninfected, untreated iBMDMs. Two-way ANOVA with Dunnett's multiple comparison. (C) Vehicle (-Tx) or OSW1 (10 nM) treated iBMDMs were infected with *Salmonella* for 18 hours at MOI 150, then lysates were collected and immunoblotted for total and phosphor-p70 S6K. (D) Blots were quantified by measuring the densitometry of the total and phosphor-p70 S6K bands, and expressed as the ratio of phospho:total signal. Bars indicate mean + SEM of 3 experimental replicates. * $p < 0.05$; *** $p < 0.001$; ns, not significant. Statistics represent the indicated bars compared to uninfected, untreated iBMDMs. Two-way ANOVA with Dunnett's multiple comparison.

Figure 2-5

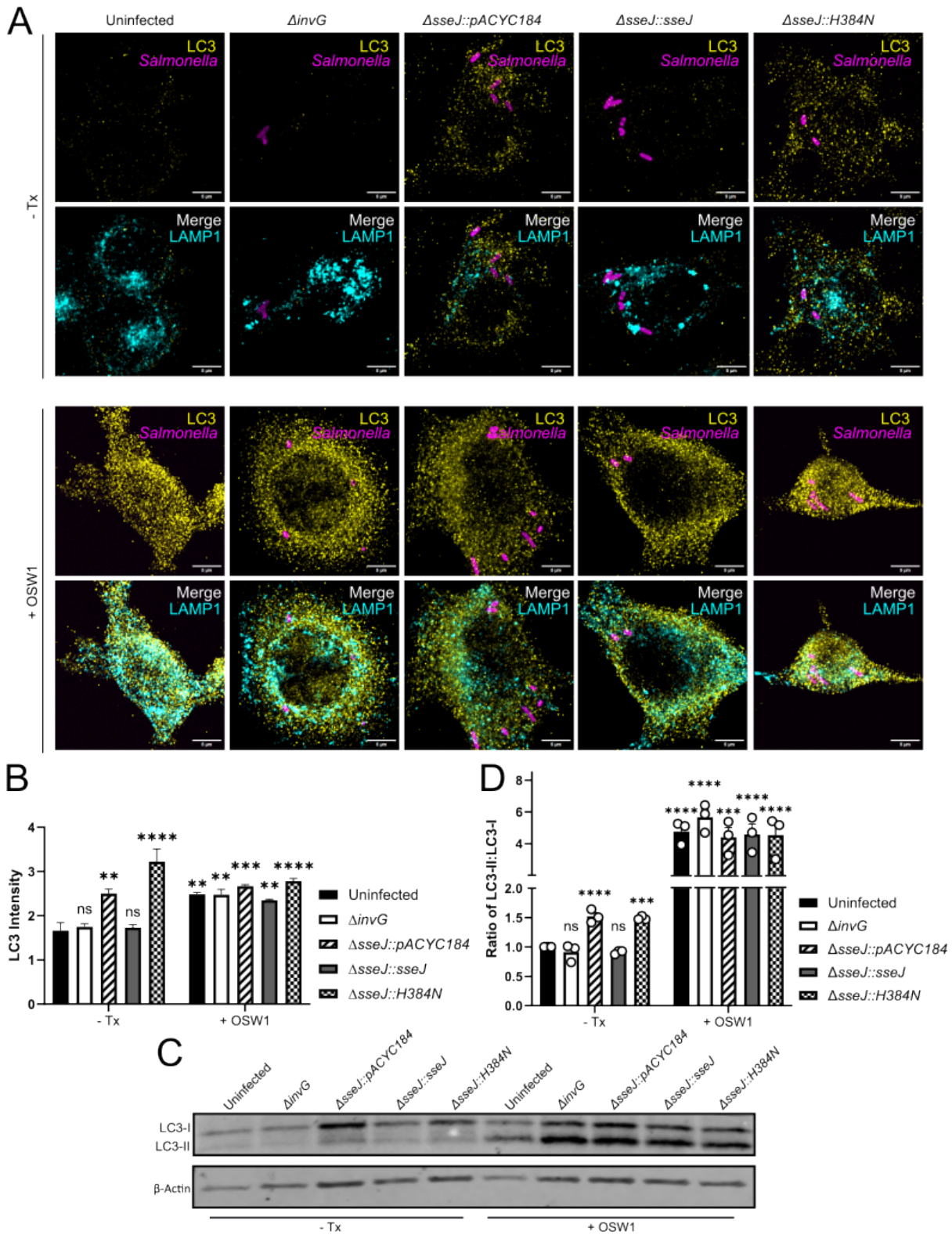
A
Uninfected
ΔinvG
ΔsseJ::pACYC184
ΔsseJ::sseJ
ΔsseJ::H384N
LC3
Salmonella
Merge
LAMP1
- Tx
+ OSW1
B
LC3 Intensity
ns
**
****
***
- Tx
+ OSW1
Uninfected
ΔinvG
ΔsseJ::pACYC184
ΔsseJ::sseJ
ΔsseJ::H384N
D
Ratio of LC3-II:LC3-I
C
LC3-I
LC3-II
β-Actin

Figure 2-5. OSBP activity suppresses autophagosome formation during *Salmonella* infection of macrophages. (A) Vehicle (-Tx) or OSW1 (10 nM) treated iBMDMs were infected with RFP *Salmonella* (magenta) for 18 hours at MOI 75, then fixed and stained for LC3 (yellow) and LAMP1 (cyan). Uninfected cells were imaged from the same coverslips as infected cells. Scale bar indicates 5 μm. The individual channel images can be found in Figure 2-10B. All images are maximum intensity projections of Z-stacks with 0.25 μm steps. (B) LC3 intensity was measured by the whole-cell ratio LC3 CTCF:LAMP1 CTCF. Bars indicate mean + SEM of 3 experimental replicates, with 20 cells measured per replicate. ** $p < 0.01$; *** $p < 0.001$; **** $p < 0.0001$; ns, not significant. Statistics represent the indicated bars compared to the uninfected, untreated iBMDM group. Two-way ANOVA with Dunnett's multiple comparison. (C) Vehicle (-Tx) or OSW1 (10 nM) treated iBMDMs were infected with *Salmonella* for 18 hours at MOI 150, then lysates were collected and immunoblotted for LC3B and β-actin. (D) Blots were quantified by measuring the densitometry of the LC3B-II and LC3B-I bands and expressed as the ratio of LC3-II:LC3-I signal. Bars indicate mean + SEM of 3 experimental replicates. *** $p < 0.001$; **** $p < 0.0001$; ns, not significant. -Tx: one way-ANOVA with Dunnett's multiple comparison. +OSW1: two-way ANOVA with Dunnett's multiple comparison. Statistics represent the indicated groups compared to uninfected, untreated iBMDMs.

Figure 2-6

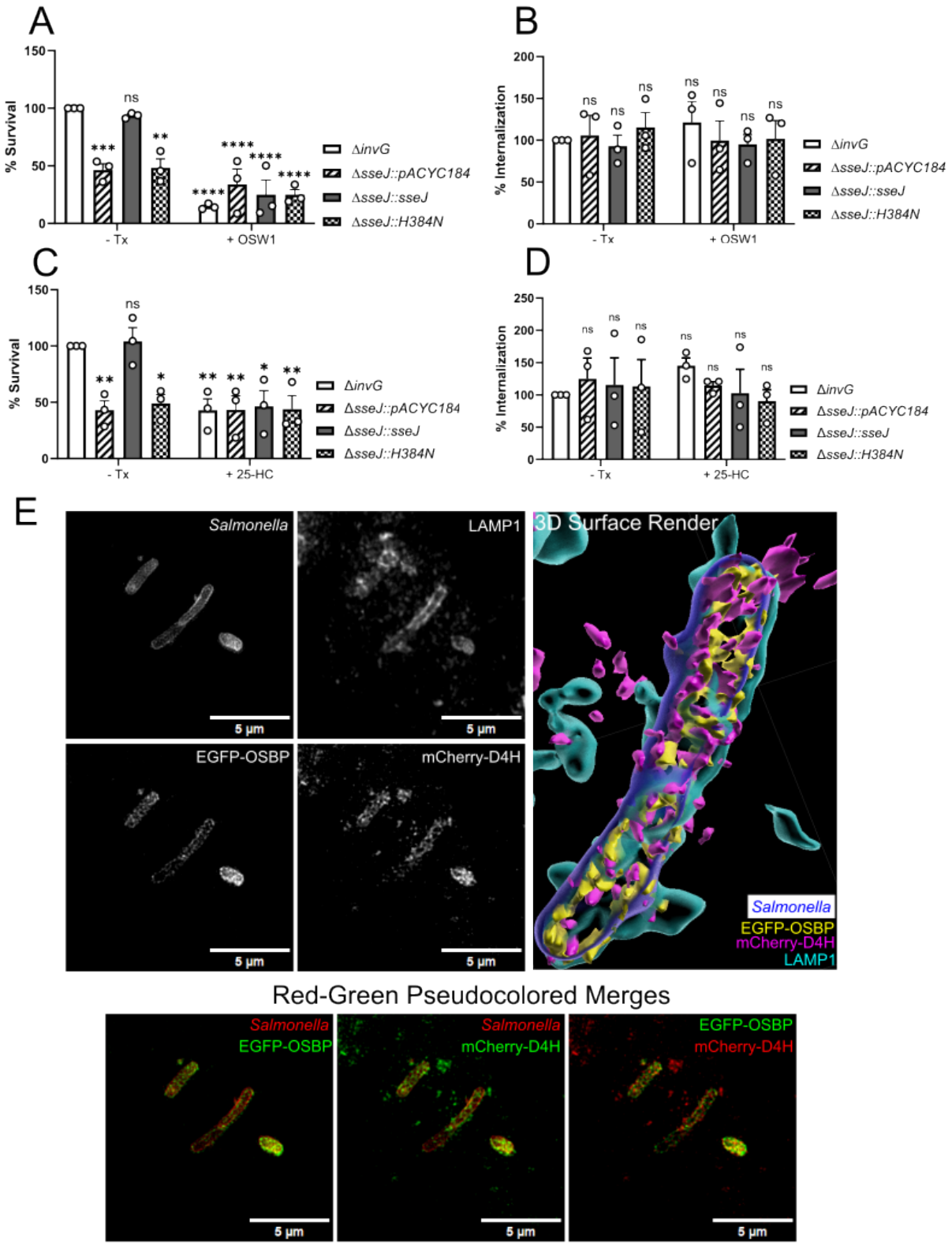
A
% Survival
150
100
50
0
ns
***
**
****
****
****
****
- Tx
+ OSW1
ΔinvG
ΔsseJ::pACYC184
ΔsseJ::sseJ
ΔsseJ::H384N
B
% Internalization
200
150
100
50
0
ns
- Tx
+ OSW1
ΔinvG
ΔsseJ::pACYC184
ΔsseJ::sseJ
ΔsseJ::H384N
C
% Survival
150
100
50
0
ns
**
*
**
**
*
**
- Tx
+ 25-HC
ΔinvG
ΔsseJ::pACYC184
ΔsseJ::sseJ
ΔsseJ::H384N
D
% Internalization
250
200
150
100
50
0
ns
- Tx
+ 25-HC
ΔinvG
ΔsseJ::pACYC184
ΔsseJ::sseJ
ΔsseJ::H384N
E
Salmonella
LAMP1
EGFP-OSBP
mCherry-D4H
5 μm
3D Surface Render
Salmonella
EGFP-OSBP
mCherry-D4H
LAMP1
Red-Green Pseudocolored Merges
Salmonella
EGFP-OSBP
Salmonella
mCherry-D4H
EGFP-OSBP
mCherry-D4H

Figure 2-6. Inhibition of OSBP cholesterol transfer activity attenuates *Salmonella* survival. iBMDMs were treated with the drug vehicle (-Tx), 10 nM OSW1 (A-B), or 5 μM 25-hydroxycholesterol (25-HC; C-D) prior to and throughout infection with the indicated strain at MOI 150 for 18 hours. Cells were lysed at 30 minutes, 1 hour, and 18 hours post infection, and the contents were plated on LB agar containing appropriate antibiotics for overnight growth. Colony forming units (CFUs) at each time were enumerated and used to calculate survival (CFUs at 18 hours/CFUs at 1 hour) and internalization (CFUs at 1 hour/CFUs at 30 minutes) rates. Bars indicate mean + SEM of 3 experimental replicates, with each experimental replicate being the mean of 3 technical replicates. * $p < 0.05$; ** $p < 0.01$; *** $p < 0.001$; **** $p < 0.0001$; ns, not significant. Statistics represent the indicated bars compared to untreated iBMDMs infected with Δ*invG*. Two-way ANOVA with Dunnett's multiple comparison. (E) iBMDMs were transiently transfected with EGFP-OSBP and mCherry-D4H prior to infection with *ΔinvG* at MOI 75 for 18 hours. Cells were then fixed and stained for *Salmonella* and LAMP1. All images are maximum intensity projections of Z-stacks with 0.50 μm steps. Pseudocolored red-green merges are shown for contrast. Scale bar represents 5 μm. The 3D surface render was generated using Imaris software.

Figure 2-7

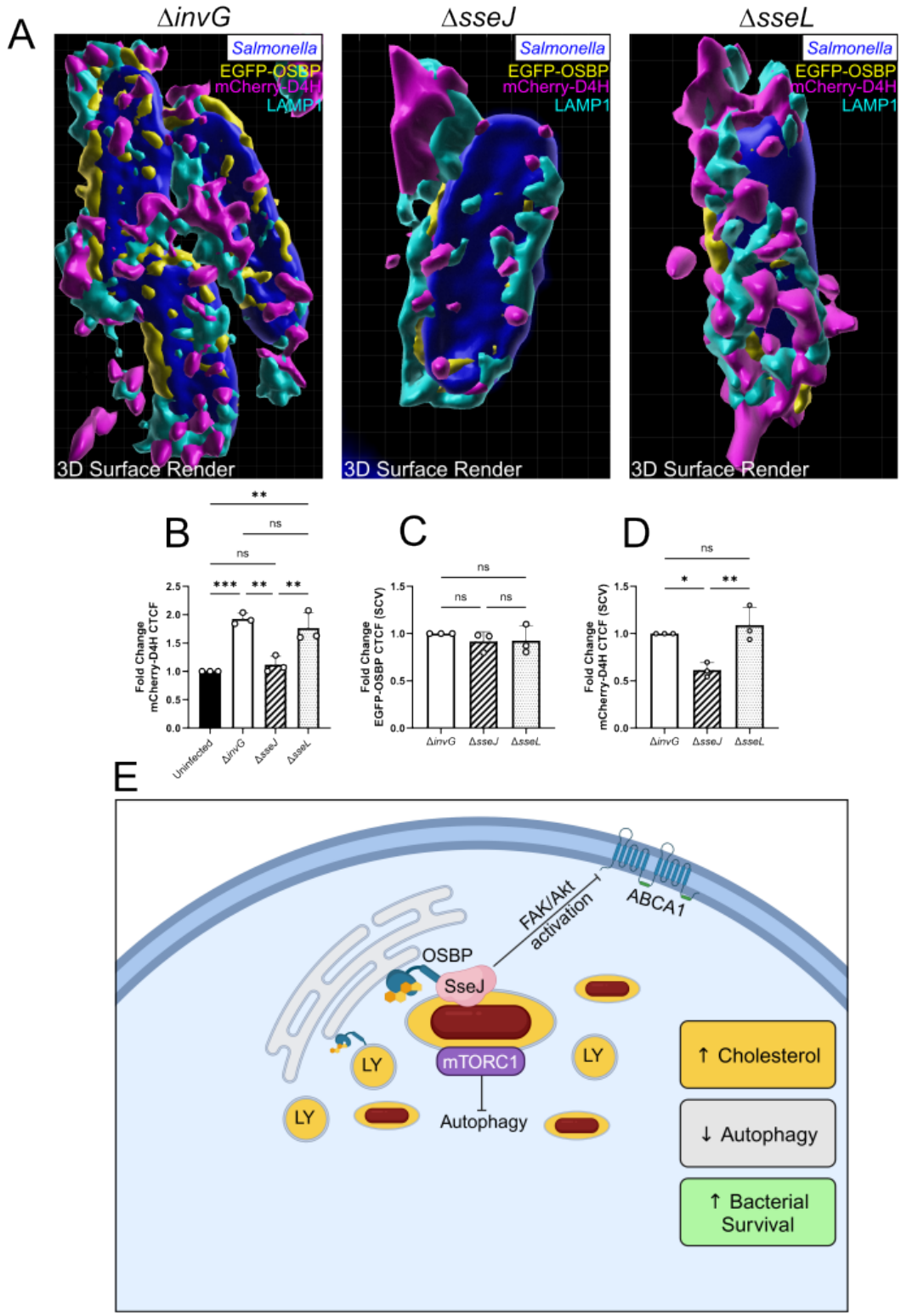
A
ΔinvG
ΔsseJ
ΔsseL
Salmonella
EGFP-OSBP
mCherry-D4H
LAMP1
3D Surface Render
B
C
D
Fold Change mCherry-D4H CTCF
Fold Change EGFP-OSBP CTCF (SCV)
Fold Change mCherry-D4H CTCF (SCV)
Uninfected
ΔinvG
ΔsseJ
ΔsseL
ns
E
FAK/Akt activation
ABCA1
OSBP
SseJ
mTORC1
LY
Autophagy
↑ Cholesterol
↓ Autophagy
↑ Bacterial Survival

Figure 2-7. SseJ, but not SseL, is required for cholesterol accumulation during *Salmonella* infection, leading to mTORC1 activation and suppression of autophagy**.** (A) iBMDMs were transiently transfected with EGFP-OSBP and mCherry-D4H prior to infection with the indicated strain at MOI 75 for 18 hours. Cells were then fixed and stained for *Salmonella* and LAMP1. 3D surface renders were generated using Imaris software. (B) The CTCF of whole cell mCherry-D4H signal was quantified. Bars indicate mean + SEM of 3 experimental replicates, with 10-20 cells measured per experimental replicate. ** $p < 0.01$; *** $p < 0.001$; ns, not significant. One-way ANOVA with Tukey's multiple comparison. (C-D) The CTCF of mCherry D4H (C) or EGFP-OSBP (D) signal on SCVs (*Salmonella*$^+$, LAMP1$^+$ structures) was quantified. Bars indicate mean + SEM of 3 experimental replicates with 10-20 cells measured per experimental replicate. * $p < 0.05$; ** $p < 0.01$; ns, not significant. One-way ANOVA with Tukey's multiple comparison. (E) During *Salmonella* infection, the SPI-2 effector SseJ triggers FAK and Akt activation, which lead to the downregulation of *Abca1*. With reduced export, cholesterol builds up throughout the endolysosomal system. Excess cholesterol is delivered to the cytoplasmic face of both lysosomes and SCVs through OSBP, which is recruited to the SCV and interacts with SseJ. OSBP cholesterol transfer activity is essential for the subsequent recruitment of mTOR by elevated cholesterol levels on the SCV. mTORC1 activation suppresses autophagy, leading to bacterial survival. Created with BioRender.

Figure 2-8

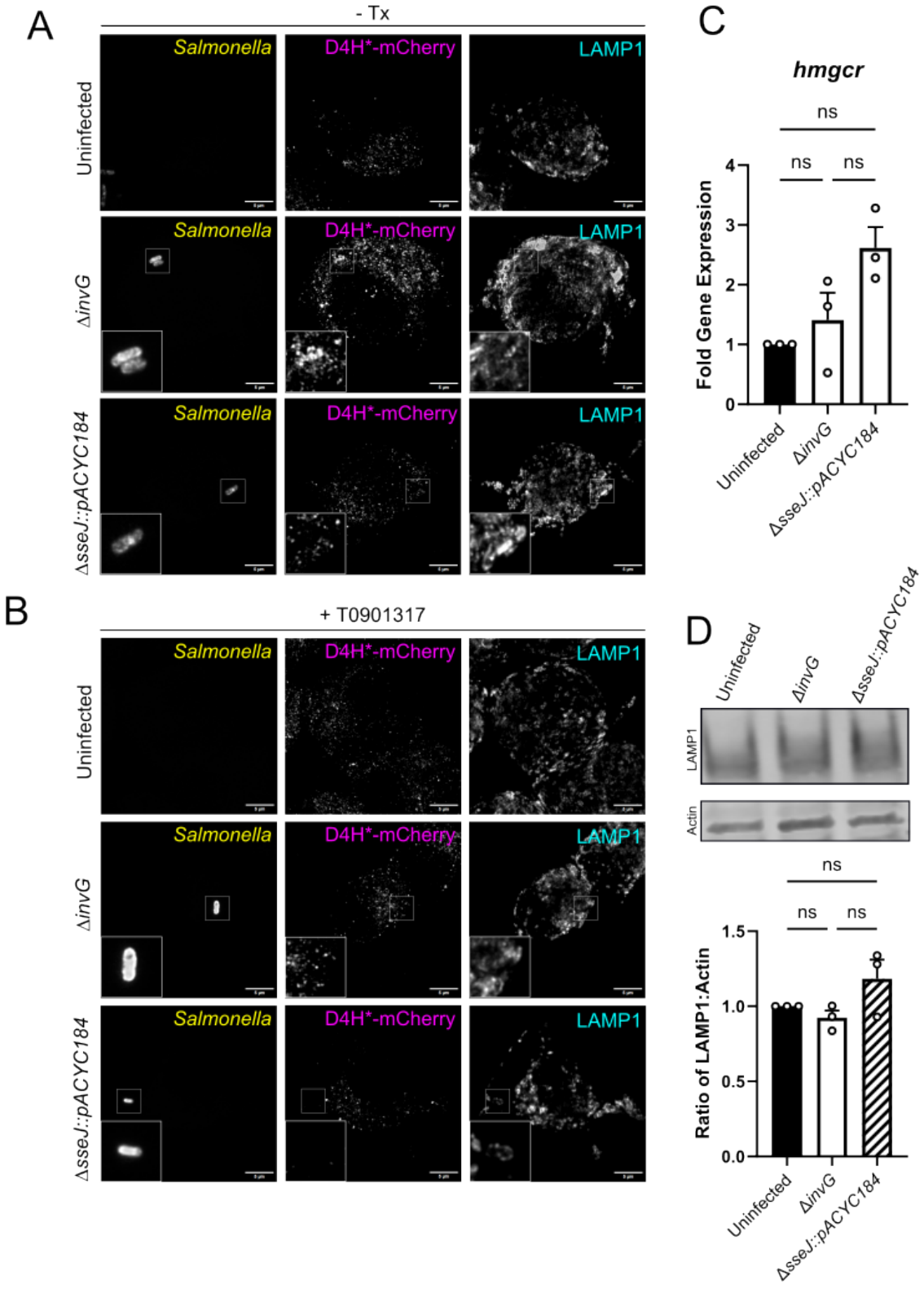
A
- Tx
Salmonella
D4H*-mCherry
LAMP1
Uninfected
ΔinvG
ΔsseJ::pACYC184
B
+ T0901317
C
hmgcr
ns
Fold Gene Expression
Uninfected
ΔinvG
ΔsseJ::pACYC184
D
LAMP1
Actin
Ratio of LAMP1:Actin

Figure 2-8. (A-B) Single channel images from Figure 2-1. Control or T0901317-treated (10 μM) bone marrow-derived macrophages (iBMDMs) were uninfected or infected with the indicated *Salmonella* strain for 18 hours. Cells were fixed, permeabilized in liquid nitrogen, and stained with recombinant D4H*-mCherry (magenta) to label endogenous cholesterol. Cells were then stained for *Salmonella* (yellow) and LAMP1 (cyan) and imaged with confocal microscopy. Uninfected cells were imaged from the same coverslips as infected cells. The inset panel represents 2.5X zoom. Scale bar indicates 5 μm. All images are maximum intensity projections of Z-stacks with 0.25 μm steps. (C) iBMDMs were infected with *Salmonella* at MOI 150 for 18 hours. The expression of *hmgcr* was measured using qPCR and ΔΔCT quantification. Bars indicate the mean of 3 experimental replicates, with each experimental replicate having 3 technical replicates, + SEM of the fold change normalized to uninfected levels. One-way ANOVA with Tukey's multiple comparison. (D) iBMDMs were infected with the indicated *Salmonella* strain for 18 hours at MOI 150, then lysed and immunoblotted for LAMP1 and actin. Blots were quantified through densitometry of the bands, and expressed as the ratio of LAMP1:actin. Bars indicate mean + SEM of 3 experimental replicates. Statistics represent the indicated bars compared to the uninfected iBMDM group. One-way ANOVA with Tukey's multiple comparison.

Figure 2-9

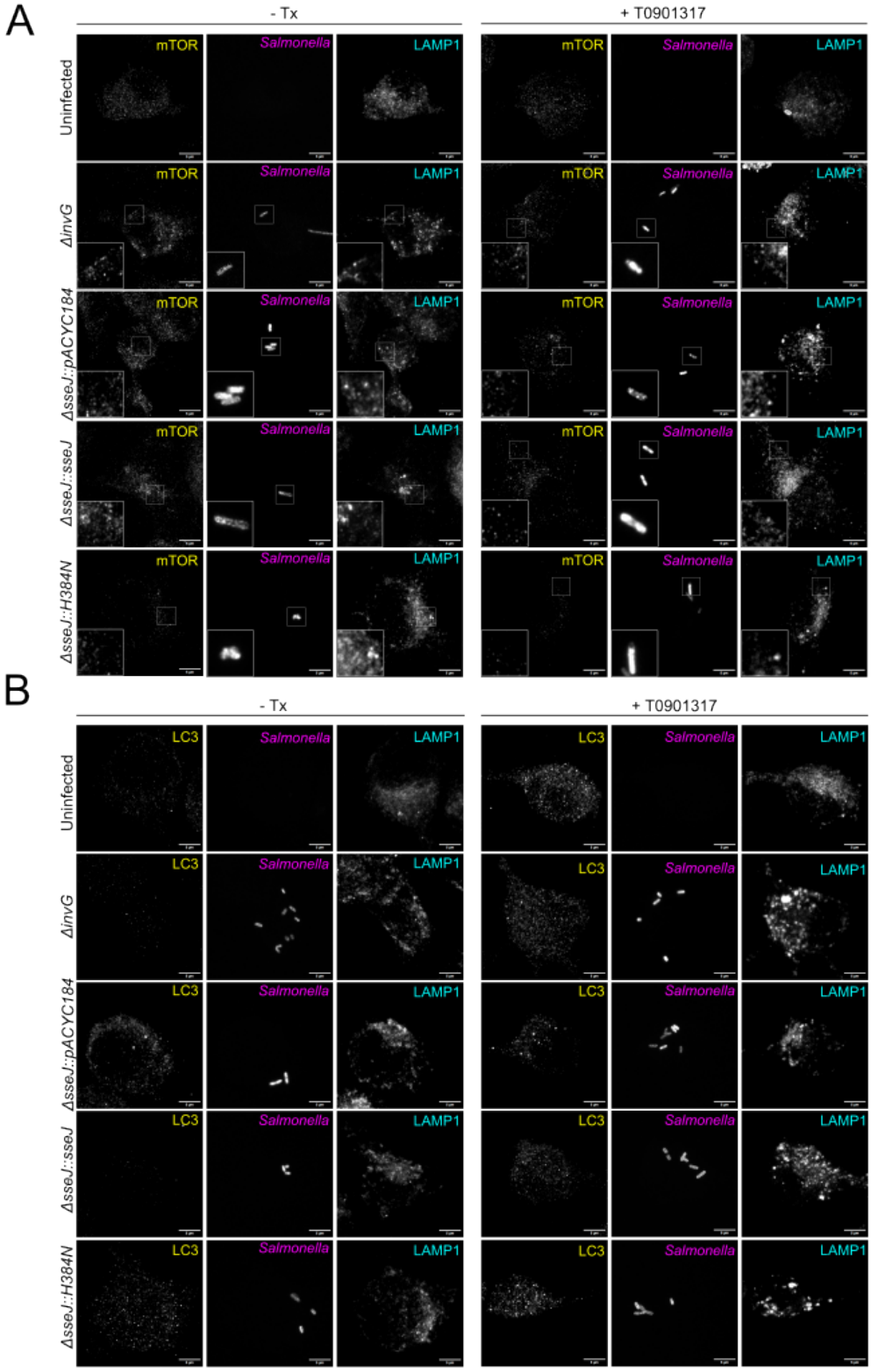
A
- Tx
+ T0901317
Uninfected
ΔinvG
ΔsseJ::pACYC184
ΔsseJ::sseJ
ΔsseJ::H384N
mTOR
Salmonella
LAMP1
B
- Tx
+ T0901317
LC3
Salmonella
LAMP1

Figure 2-9. Single channel images from Figures 2-3-4. (A) Untreated or T0901317 treated (10 μM) iBMDMs were infected with RFP-expressing *Salmonella* for 18 hours at MOI 75. Cells were fixed and stained for mTOR (yellow) and LAMP1 (cyan). (B) Control or T0901317 treated (10 μM) iBMDMs were infected with RFP-expressing *Salmonella* for 18 hours at MOI 75. Cells were fixed and stained for LC3 (yellow) and LAMP1 (cyan). Inset indicates 2.5X zoom. Scale bar represents 5 μm. All images are maximum intensity projections of Z-stacks with 0.25 μm steps.

Figure 2-10

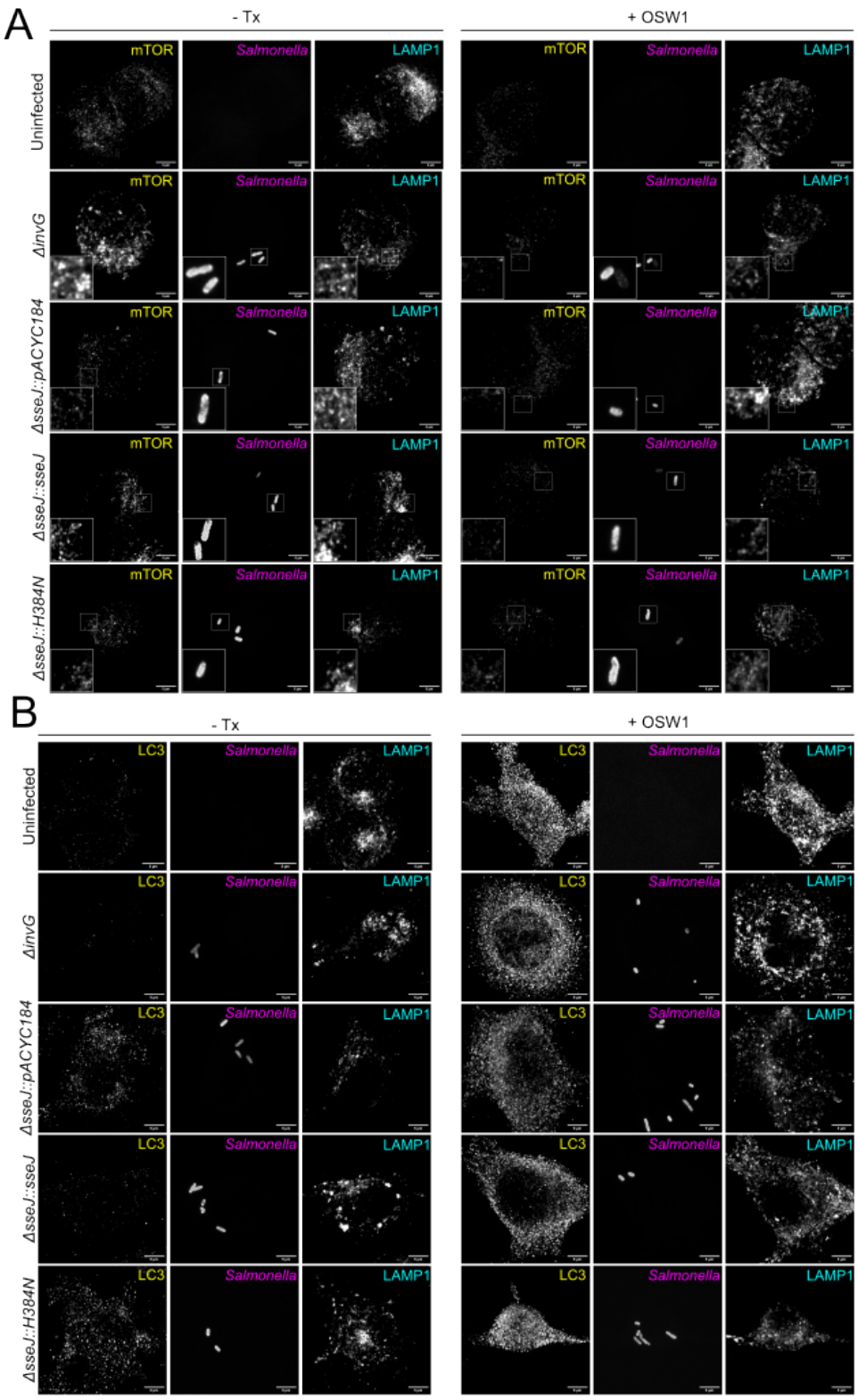
A
- Tx
+ OSW1
Uninfected
ΔinvG
ΔsseJ::pACYC184
ΔsseJ::sseJ
ΔsseJ::H384N
mTOR
Salmonella
LAMP1
B
- Tx
+ OSW1
Uninfected
ΔinvG
ΔsseJ::pACYC184
ΔsseJ::sseJ
ΔsseJ::H384N
LC3
Salmonella
LAMP1

Figure 2-10. Single channel images from Figures 5-6. (A) Untreated or OSW1 treated (10 nM) iBMDMs were infected with RFP-expressing *Salmonella* for 18 hours at MOI 75. Cells were fixed and stained for mTOR (yellow) and LAMP1 (cyan). (B) Control or OSW1-treated (10 nM) iBMDMs were infected with RFP-expressing *Salmonella* for 18 hours at MOI 75. Cells were fixed and stained for LC3 (yellow) and LAMP1 (cyan). Inset indicates 2.5X zoom. Scale bar represents 5 μm. All images are maximum intensity projections of Z-stacks with 0.25 μm steps.

Table 2-1

Name	Species	Strain	Background	Mutation	Description	Source
Δ*invG*	*S. enterica* serovar Typhimurium	SL1344	WT	Deletion of *invG*, ring protein for SPI-1 T3SS	SPI-1 deficient, SPI-2 competent	Beth McCormick
Δ*sseJ::pACYC184*	*S. enterica* serovar Typhimurium	SL1344	Δ*orgA*	Deletion of *sseJ*, complemented with an empty vector	SseJ deletion strain; SPI-1 deficient, SPI-2 competent	Greene et al., 2021
Δ*sseJ::sseJ*	*S. enterica* serovar Typhimurium	SL1344	Δ*orgA*	Deletion of *sseJ*, complemented with a functional copy of *sseJ*	SseJ rescue strain; SPI-1 deficient, SPI-2 competent	Greene et al., 2021
Δ*sseJ::H384N*	*S. enterica* serovar Typhimurium	SL1344	Δ*orgA*	Deletion of *sseJ*, complemented with a catalytically inactive copy of *sseJ*	Catalytically inactive SseJ strain; SPI-1 deficient, SPI-2 competent	Greene et al., 2021
Δ*sseJ*	*S. enterica* serovar Typhimurium	SL1344	Δ*orgA*	Deletion of *sseJ*	SseJ deletion strain; SPI-1 deficient, SPI-2 competent	Denise Monack
Δ*sseL*	*S. enterica* serovar Typhimurium	SL1344	Δ*orgA*	Deletion of *sseL*	SseL deletion strain; SPI-1 deficient, SPI-2 competent	Denise Monack

Table 2-1. List of *Salmonella* strains used throughout this research.

Chapter 3:

Salmonella Typhimurium manipulates the macrophage lipidome to promote a shift in lysophospholipids and cholesterol esters

The following work has been published:

Torsilieri, H.M., Upchurch, C.M., Leitinger, N., and Casanova, J.E. *Salmonella*-induced cholesterol accumulation in infected macrophages suppresses autophagy via mTORC1 activation. *Molecular Biology of the Cell*. 2024.

Torsilieri, H.M., performed all experiments and analysis shown in Chapter 2, the BMDM infections and lipid extractions in Chapter 3, and wrote the publication. Upchurch, C.M. performed the lipid mass spectrometry experiments and analyzed the preliminary data. Leitinger, N., provided experimental guidance and funding. Casanova, J.E. provided experimental guidance, funding, and review and revision of the manuscript

Wording and content have been modified from the published article.

Abstract

Macrophages reprogram their metabolism to respond to microbial infection and regulate inflammation. Pro-inflammatory M1 macrophages are known to restrict *Salmonella* infection, while pro-resolution M2 macrophages provide a replicative niche. Lipid metabolism is critical to macrophage polarization, with distinct lipid profiles supporting specialized functions. In this study we conduct the first known lipid mass spectrometry analysis of *Salmonella enterica* serovar Typhimurium infected macrophages. We found that *S.* Typhimurium manipulates macrophage lipid homeostasis via the SPI-2 effector SseJ. In particular, SseJ is necessary for the increase in lysophosphatidylcholine and cholesterol ester species found in infected macrophages. This lipid remodeling likely facilitates bacterial persistence by promoting an anti-inflammatory M2 polarization state, which is advantageous for long-term *Salmonella* survival. Our findings provide novel insights into the interplay between *S.* Typhimurium and macrophage lipid homeostasis, highlighting lipidomic reprogramming as a mechanism for bacterial survival and immune modulation.

Introduction

Macrophages are highly responsive immune cells that are known to reprogram their metabolic pathways to facilitate pathogen recognition, inflammation, and the resolution of these responses (O'Neill and Pearce, 2016). This reprogramming can target glycolysis, oxidative phosphorylation, and lipid biosynthesis, leading to unique cellular contents depending on the macrophage response. During atherosclerosis, for instance, foam cell macrophages increase their lipid metabolism and fatty acid oxidation (Moore et al., 2013). In contrast, tumor-associated macrophages shift metabolism to glycolysis and fatty acid synthesis, much like the Warburg effect in proliferating cancer cells (Reinfeld et

al., 2021). The consequences of this reprogrammed metabolism can lead to enhanced pathogen control; however, some microbes have evolved mechanisms to escape killing and manipulate the host macrophage metabolism to benefit intracellular survival.

The rapidly developing field of macrophage polarization now views polarization as a spectrum rather than binary states. However, the basic descriptions of M1 and M2 macrophages are still useful to understanding how they contribute to host defense. In this model, base state macrophages (M0) can be influenced into M1 or M2 activation depending on their exposure to certain cytokines. M1 and M2 polarization states bear unique metabolic and functional characteristics that enable macrophages to act in pro-inflammatory, antimicrobial defense (M1) or anti-inflammatory, tissue resolution (M2). The M1 state is induced by tumor necrosis factor (TNF) or interferon-γ (IFNγ) and is characterized by enhanced glycolysis and decreased oxidative phosphorylation. The citric acid cycle in M1 macrophages is interrupted, leading to the accumulation of itaconate, citrate, and succinate (Jha et al., 2015; Michelucci et al., 2013). Excess citrate supports the synthesis of fatty acids and pro-inflammatory lipids, while itaconate is an antimicrobial metabolite that restricts *S.* Typhimurium survival in infected macrophages (Michelucchi et al., 2013; Schuster et al., 2022). Succinate stabilizes the transcription factor HIF1α (hypoxia-inducible factor 1α), which upregulates pro-inflammatory cytokine interleukin 1β (IL-1β) (Tannahill et al., 2013). M1 macrophages also increase production of reactive oxygen species (ROS) through the pentose phosphate pathway which generates NADPH (Nagy and Haschemi, 2015). As a result of this metabolic reprogramming, M1 macrophages are highly pro-inflammatory and contain an arsenal of ROS, inducible nitric oxide synthase, and antimicrobial peptides. In contrast to the pro-inflammatory M1 macrophage, M2 macrophages commonly function to resolve

inflammation and repair tissue. M2 macrophages respond to IL-4 and IL-13 stimulation and are characterized by an intact citric acid cycle and enhanced oxidative phosphorylation that is fueled by both fatty acid oxidation and glucose (Tan et al., 2015; Huang et al., 2014). Among the M2 effectors are transforming growth factor β (TGFβ), IL-10, and arginase 1, which promote tissue healing and the resolution of inflammation (Orecchioni et al., 2019; Chen et al., 2023).

In addition to energetic pathways, macrophage lipid homeostasis is reprogrammed in response to activation. M1 macrophages are known to accumulate fatty acids within triglycerides and cholesterol esters, while M2 macrophages are enriched in glycerophospholipids, ether lipids, and sphingolipids (Morgan et al., 2021). These unique lipidomes enhance the specialized functions of polarized macrophages. In M1 macrophages, IFN signaling downregulates cholesterol biosynthesis, increases cholesterol esterification for fatty acid storage, and generates cholesterol derivatives such as 25-HC (Zhou et al., 2020; Blanc et al., 2011; Blanc et al., 2013). Meanwhile, fatty acid synthesis is necessary for membrane remodeling to mediate inflammatory signaling as well as induction of the NLR family pyrin containing 3 (NLRP3) inflammasome and release of pro-inflammatory cytokines IL-1β and IL-18 (Wei et al., 2016; Moon et al., 2015). In M2 macrophages, IL-4 modulates both fatty acid uptake via the receptor CD36 and lipolysis of triglycerides into fatty acids, thus providing the fuel necessary for FAO and oxidative phosphorylation (Huang et al., 2014).

Macrophage polarization can benefit or inhibit intracellular pathogens depending on the ability of the pathogen to evade or manipulate macrophage metabolism. *M. tuberculosis*

expresses a heat shock protein that stimulates expression of host IL-10, promoting M2 polarization (Parveen et al., 2013), while *Orienta tsutsugamushi* (the causative agent of scrub typhus) can survive and replicate in the presence of nitric oxide and thus promotes M1 polarization during infection (Ogawa et al., 2017; Tantibhedhyangkul et al., 2013). *S.* Typhimurium engages with macrophage polarization in a way that benefits long-term bacterial survival. Recent studies have demonstrated that *S.* Typhimurium persists in tissue by residing in granuloma macrophages (Goldberg et al., 2018). Furthermore, *S.* Typhimurium actively influences macrophage polarization through the secretion of SPI-2 effector SteE. The activity of SteE opposes TNF signaling which would normally polarize macrophages to the antimicrobial M1 state (Pham et al., 2020). SteE coordinates the phosphorylation of signal transducer and activator of transcription 3 (STAT3), which increases M2 polarization, thus enabling *S.* Typhimurium to overcome host restriction (Pham et al., 2020).

Given the connections between macrophage polarization and lipid homeostasis, we sought to understand how *S*. Typhimurium influences the macrophage lipidome during infection. We have generated the first known lipidome of *Salmonella* infected macrophages and found that *S*. Typhimurium induces broad changes in lipid homeostasis. In particular, *Salmonella* infection favors the formation of LPC, ChE, and plasmalogen species while decreasing production of triglycerides, which may provide new insights into how *Salmonella* influences macrophage polarization to benefit its own survival.

Results

Salmonella induces extensive changes in the lipid profile of infected macrophages

While the ability of *S.* Typhimurium (*St*) to manipulate cellular cholesterol levels is well-described, little is known about the fate of other lipid species within *St*-infected macrophages. To investigate this further, we performed lipid mass spectrometry on primary BMDMs that were uninfected or infected with Δ*invG*, the non-complemented SseJ-deficient strain Δ*sseJ::pACYC184,* or Δ*sseJ::sseJ* (a strain of Δ*sseJ St* that is complemented with a functional copy of *sseJ*; Figure 3-1A). Before performing lipid mass spectrometry, we analyzed the endogenous levels of free cholesterol in the samples and confirmed that BMDMs infected with Δ*invG* or Δ*sseJ::sseJ* had over threefold higher levels of endogenous cholesterol compared to uninfected BMDMs or those infected with the non-complemented strain Δ*sseJ::pACYC184* (Figure 3-1B, Figure 3-4).

Mass spectrometry revealed broad changes in the lipidomic profile of infected macrophages, including the previously reported increase in cholesterol esters (ChE; Figure 3-1C-F, Figure 3-4, Table 3-1) (Nawabi et al., 2008). SseJ is known to create cholesterol esters by cleaving the sn-1 acyl chain from glycerophospholipids and transferring it to the cholesterol backbone, but the phospholipid acyl donors have remained unidentified (Christen et al., 2009). We observed a marked SseJ-dependent increase in lysophosphatidylcholine (LPC), suggesting that phosphatidylcholine (PC) is the primary target of SseJ activity (Figure 3-1G, Figure 3-4). Intriguingly, several species of PC were increased in BMDMs infected with Δ*invG* or Δ*sseJ::sseJ*, but not in BMDMs infected with Δ*sseJ::pACYC184*, indicating that these specific species may be targeted by SseJ acyltransferase activity (Figure 3-1A, Figure 3-4).

We also observed significant SseJ-dependent increases in ceramide (Cer) and sphingomyelin (SM) species (Figure 3-2B, Figure 3-4). Free cholesterol preferentially binds SM in membranes, and this sequestration forms liquid ordered domains (Ridgway, 2000). Elevated Cer (a precursor for SM synthesis) and SM in infected macrophages may therefore suggest a cellular response to manage cholesterol accumulation through SM-mediated sequestering. *St*-infected BMDMs also displayed a significant, SseJ-independent reduction in levels of triglycerides (TG), with a greater than 50% decrease in all infected macrophages (Figure 3-2C, Figure 3-4). This shift in lipid composition is reminiscent of a previously described variance between M1 and M2 macrophages (Morgan et al., 2021). This observation also aligns with previous research suggesting that *St* infection triggers the polarization of macrophages to the M2 phenotype, which is more favorable for long-term replication and persistence (Pham et al., 2020; Panagi et al., 2020). Together, these findings suggest that *St* has major effects on the lipid profile of infected cells and may use those changes to create an advantageous niche with the macrophage.

To further dissect changes in PC and LPC during *St* infection, particularly in iBMDMs, we validated these findings using targeted mass spectrometry (Figure 3-3A-J, Figure 3-4, Table 3-2). Compared to primary BMDMs, the changes in immortalized macrophages were less dramatic, but still suggested a SseJ-dependent change in LPC species, specifically in LPC 18:1 and LPC 20:4 (Figure 3-3C and 3E, Figure 3-4). PC 36:4 and PC 32:0 were elevated in all *St* infected conditions, which may imply a general response to *St* infection (Figure 3-3F-H, Figure 3-4). Overall, this targeted approach with iBMDMs validated our initial findings in primary macrophages and confirmed that SseJ can use its acyltransferase activity to generate LPC species from PC.

Discussion

The accumulation of cholesterol in *Salmonella*-infected macrophages has been a subject of interest for many years, however the status of other lipids during infection has not been established. Here, we demonstrate that *Salmonella* infection leads to a significant shift in the lipidomic profile of both primary and immortalized BMDMs. We noted a nearly 4-fold increase in short-chain cholesterol esters (ChE 2:0), as well as an SseJ-dependent increase in lysophosphatidylcholine (LPC). These results, along with SseJ-dependent increases in certain PC species, suggest that SseJ acyl-transferase activity acts primarily on PC species. Notably, the increased ChE species contained extremely short acyl chains, while the identified LPC species were of longer chain length. These results suggest that further processing may occur to ChE species after receiving acyl chains from SseJ. Whether this modification occurs through unknown properties of SseJ or by unidentified enzymes is unclear. Beyond the activity of SseJ, the importance of increased LPC levels during infection remains unknown. Lysophospholipids are widely thought to render membranes more fluid, and it is plausible that increased LPC in the membranes of SCVs facilitates the formation or organization of SIFs (Ailte et al., 2016). However, whether there is a physiological role or signaling pathway that is fulfilled by LPC during infection will require further study.

Interestingly, we found that LPC plasmalogen species were also elevated, suggesting that SseJ does not have specificity for the backbone of its target, but rather the headgroup. Plasmalogens are ether-linked glycerolipids that are abundant throughout the body and contribute about 20% of total phospholipid mass in cell membranes (Braverman and Moser, 2012). Ether lipids also serve as ligands for peroxisome proliferator-activated receptors (PPARs), which promote the M2 polarization state

(Davies et al., 2001; Bouhlel et al., 2007). Further, PPARγ is upregulated in *Salmonella*-infected macrophages and enhances bacterial replication, suggesting that ether lipids may play a role in promoting M2 polarization and the establishment of a replicative niche (Eisele et al., 2014). As plasmalogen synthesis begins in peroxisomes, further research will investigate whether peroxisomes play a role in *Salmonella* pathogenesis (Nagan et al., 1997).

In addition to these findings, there was a significant downward trend in triglyceride levels in *Salmonella* infected macrophages. These results are intriguing when paired with recent findings that M1 macrophages have higher levels of triglycerides than M2 macrophages (Morgan et al., 2021). Elevated TG levels are also implicated in enhanced macrophage inflammatory response, further cementing that TG can play a role in controlling pathogens (Castoldi et al., 2020). Intriguingly, OSBP ligands such as OSW1 and 25-HC increase TG levels in macrophages, leading to sustained secretion of pro-inflammatory signals such as IL-6 (Diercks et al., 2024). Thus *S.* Typhimurium may also use its control of OSBP lipid trafficking activity to further dampen the inflammatory response. Our results present additional evidence that *Salmonella* can manipulate the metabolic and lipidomic environment of macrophages to promote survival.

Materials and Methods

Mice

All experiments were performed in strict accordance with the recommendations in the Guide for the Care and Use of Laboratory Animals of the National Institutes of Health. Protocols were approved by the Institutional Animal Care and Use Committee at the University of Virginia (Protocol number 3488). All efforts were made to minimize animal

suffering during this study. Mice were kept in pathogen-free conditions and given free access to food and water.

Cell culture

The iBMDMs were a kind gift from Dr. Johnathan Kagan (Children's Hospital, Boston). iBMDMs were grown on tissue-culture-treated petri dishes (Fisher) in Dulbecco's Modified Eagle Medium (DMEM; Genessee Scientific) supplemented with 10% fetal bovine serum (FBS) and 1% penicillin/streptomycin/amphotericin B (PSF). Primary BMDMs were isolated from the hind leg bones of mice, plated onto untreated petri dishes (Fisher), and cultured in RPMI (Genesee Scientific) supplemented with 10% heat-inactivated FBS, 10% L929-conditioned media, and 1% PSF.

Bacterial strains and culture

Bacterial strains used in this study are described in Table 2-1. The SPI-1-deficient Δ*invG* mutant strain of *Salmonella* Typhimurium SL1344 was a kind gift from Beth McCormick (University of Massachusetts). The mutant Δ*sseJ::pACYC184,* and Δ*sseJ:: sseJ*, strains were previously described (Greene et al. 2021) and are on a Δ*orgA* background. For infection of iBMDMs, bacteria were grown under non-invasion-inducing conditions. Briefly, each strain was grown statically overnight in LB broth containing the appropriate antibiotics. Bacteria were harvested the following morning at OD_{600} 0.6-0.8.

Bacterial Infection

One hour prior to infection, cells were washed three times with 1X PBS, then incubated in fresh DMEM containing 10% heat-inactivated FBS and no antibiotics (infection media). Bacteria were collected, spun down, and resuspended in infection media. Cells were infected with the indicated strain and multiplicity of infection (MOI) for 30 minutes.

After 30 minutes, cells were washed three times in 1X PBS, then incubated in fresh infection media containing gentamicin (100 ug/mL, Fisher) for 60 minutes to kill extracellular bacteria. After 90 minutes total infection, the media was replaced with fresh infection media containing 10 ug/mL gentamicin for the remainder of the assay.

Lipid Extraction and Endogenous Cholesterol Assay

Primary BMDMs were infected with the indicated strains for 18 hours, then lipids were extracted using a modified Bligh and Dyer method (Bligh and Dyer, 1959). Cell pellets were resuspended in HPLC grade H2O in glass test tubes, and each sample was split in half – half was used for an internal control Amplex Red assay, while the other half was used for lipid MS/MS. For the MS samples, 1:100 dilution of Splash Lipidomix Mass Spec Standard (Avanti) in 1 mL of methanol was added, while 1 mL of methanol was added to each Amplex Red sample. For the targeted MS, 500 ng of 18:1 LPC-d7 was added to each MS sample as a standard. After this initial step, all samples were treated equally. Lipids were extracted from cell pellets using 1:1:1 HPLC-grade water: methanol: chloroform. Samples were extracted three times, and the resulting organic fraction was dried under nitrogen. Dried samples were resuspended in HPLC methanol (MS samples) or 9:1 isopropanol: NP:40 (Amplex red samples). Samples intended for the Amplex Red endogenous cholesterol assay were assayed immediately following a protocol from Robinet et al. (2010). Lipid samples were aliquoted into a 96-well plate (Costar) and treated with bovine catalase (Sigma), before addition of cholesterol oxidase (Sigma), HRP (Sigma), and ADHP (Invitrogen). Fluorescence was measured using a Cytation 1 plate reader (Biotek).

Lipid Mass Spectrometry and Analysis

We analyzed the cellular lipidome using a Thermo Q Exactive coupled with a Vanquish UHPLC and identified lipid species using LipidSearch (version 4.1.1.16). Samples were separated using a Thermo Scientific Acclaim 120 (C18 5 µm 120 Å 4.6 x 100 mm) column (operated at 35 °C) using reverse phase conditions with 50% acetonitrile, 50% water, and 0.1% formic acid with 10 mM ammonium formate (mobile phase A) and 88% isopropanol, 10% acetonitrile, 2% water, and 0.02% formic acid with 2 mM ammonium formate (mobile phase B) at a flow rate of 400 µL/min. The following gradient was used for coverage of the lipidome: 0 to 6 min, 0% B; 6 to 8 min, 0 to 30% B; 8 to 12 min, 30% to 60% B; 12 to 18 min, 60 to 80% B; 18 to 23 min, 80 to 90% B; 23 to 32 min, 90 to 100% B; 32 to 52 min, 100% B; 52 to 55 min, 100 to 0% B; 55 to 60 min, 0% B. Mass spectra were collected in positive mode using Full MS/dd-MS^2 Top5 using the following settings: Full MS -- Resolution – 35,000; AGC Target – 1e5; Maximum IT – 128 ms; Scan Range – 200 to 1500 m/z; dd-MS^2 -- Resolution – 17,500; AGC Target – 2e5; Maximum IT – 64 ms; Loop count – 5; TopN – 5; Scan Range – 200 to 2000 m/z; Normalized Collison Energy – 40; Minimum AGC Target – 8e3; Dynamic Exclusion – 3.0s (6.0 ppm). Lipids were identified using LipidSearch with the follow settings: Search – Q Exactive Database; precursor tolerance – 5.0 ppm; product tolerance – 8.0 ppm; Alignment – alignment method – mean; retention time tolerance – 0.25 min. Internal standards were analyzed using parallel reaction monitoring with the following settings: Resolution – 17,500; AGC Target - 5e4; Maximum IT – 64 ms; Normalized Collision Energy – 35. Lipid abundances for each sample were normalized to cell number and adjusted based on the average extraction efficiency of the following internal standards: 18:1-d7 LysoPC, 18:1-d7 LysoPE, 15:0-18:1-d7 PC, 15:0-18:1-d7-15:0 TAG.

Targeted Mass Spectrometry:

We developed a targeted mass spectrometry method to assess the relative concentrations of the following 10 phospholipids: 16:0 LysoPC (1-palmitoyl-2-hydroxy-sn-glycero-3-phosphocholine), 18:0 LysoPC (1-stearoyl-2-hydroxy-sn-glycero-3-phosphocholine), 18:1 LysoPC (1-oleoyl-2-hydroxy-sn-glycero-3-phosphocholine), 18:2 LysoPC (1-linoleoyl-2-hydroxy-sn-glycero-3-phosphocholine), 20:4 LysoPC (1-Arachidonoyl-glycero-3-phosphocholine), 32:0 PC (1,2-dipalmitoyl-sn-glycero-3-phosphocholine), 36:1 PC (1-stearoyl-2-oleoyl-sn-glycero-3-phosphocholine), 36:2 PC (1-stearoyl-2-linoleoyl-sn-glycero-3-phosphocholine), 34:2 PC (1-palmitoyl-2-linoleoyl-sn-glycero-3-phosphocholine), and 36:4 PC (1-palmitoyl-2-arachidonoyl-sn-glycero-3-phosphocholine). In brief, lipids were extracted from cell pellets as previously described. The resulting extracts were separated chromatographically using a Phenomenex Kinetex 1.7 µm EVO C18 100 Å (50 x 1.0 mm) column under reverse phase conditions with 75% water and 25% methanol with 10 mM ammonium acetate (mobile phase A) and 50% methanol and 50% isopropanol with 10 mM ammonium acetate (mobile phase B) at a flow rate of 200 µL/min and a column temperature of 35°C. The following gradient was used: 0% B, 0 to 0.99 min; 0 - 45% B, 0.99 to 1 min; 45% B, 1 to 2.99 min; 45 – 75% B, 2.99 to 3.00 min; 75% B, 3 – 9.7 min; 75 – 0% B, 9.7 – 10 min; 0% B, 10 – 12 min. Retention times for each standard were determined. Mass spectra were collected in positive mode using parallel reaction monitoring with the following settings: Full MS settings – Scan Range – 400 – 1000 m/z; Resolution – 17,500; Microscans – 3; AGC target – 2e5; Sheath Gas Flow Rate – 25; Aux Gas Flow Rate – 5; Sweep Gas Flow Rate – 1; Spray Voltage – 3 kV; Capillary Temperature – 275°C; Aux Gas Heater Temperature – 35°C; MS^2 settings – Microscans – 1; Resolution – 17,500; AGC target – 2e4; Max IT – 64 ms; NCE – 35. Retention times were assigned based on commercially available standards or predicted retention time based on chemical structure. Thermo Scientific Xcalibur 4.1.31.9 was used to quantify the targeted lipid species using parent

mass with an accuracy tolerance of 5 ppm in conjunction with a product mass of 184.073 m/z and expected retention time. Resulting peak areas were normalized to extraction efficiency using the internal standard 18:1-d7 LysoPC (1-oleoyl(d7)-2-hydroxy-sn-glycero-3-phosphocholine) and cell number.

Acknowledgements

Figures were made using BioRender and Inkscape. We thank Johnathan Kagan (Children's Hospital, Boston) for the iBMDMs; Beth McCormick (University of Massachusetts) for the Δ*invG* strain; and Denise Monack (Stanford University) for the Δ*sseJ* strain. This work was funded by NIH grants to J.E. Casanova (R01DK58536 and R01AI136073), N. Leitinger (R01AI168194), and the Global Biothreats Training Grant (T32AI055432).

Figure 3-1

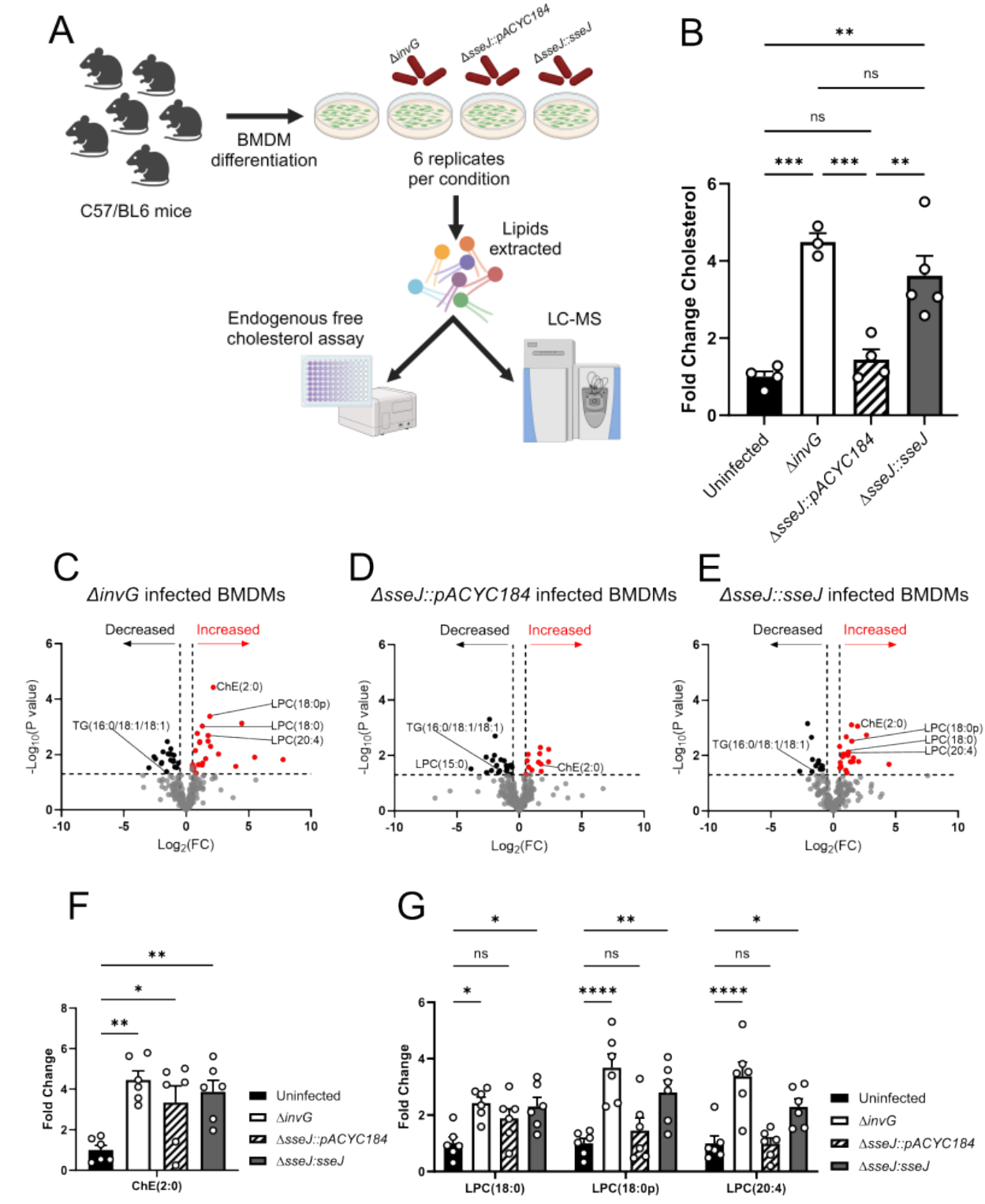
A
C57/BL6 mice
BMDM differentiation
ΔinvG
ΔsseJ::pACYC184
ΔsseJ::sseJ
6 replicates per condition
Lipids extracted
Endogenous free cholesterol assay
LC-MS
B
Fold Change Cholesterol
Uninfected
ΔinvG
ΔsseJ::pACYC184
ΔsseJ::sseJ
C
ΔinvG infected BMDMs
D
ΔsseJ::pACYC184 infected BMDMs
E
ΔsseJ::sseJ infected BMDMs
Decreased
Increased
-Log10(P value)
Log2(FC)
ChE(2:0)
LPC(18:0p)
LPC(18:0)
LPC(20:4)
TG(16:0/18:1/18:1)
LPC(15:0)
F
Fold Change
ChE(2:0)
G
LPC(18:0)
LPC(18:0p)
LPC(20:4)

Figure 3-1. *Salmonella* infection induces broad changes in the macrophage lipidomic profile. (A) Schematic of the lipidomics workflow. Briefly, BMDMs were isolated from C57BL/6 mice, then uninfected or infected with the indicated strain for 18 hours. The cells were collected and the pellets from each sample split in half for use in the endogenous cholesterol assay or lipid mass spectrometry. Image made with BioRender (B) Lipids were extracted from the cells and quantified using an Amplex Red assay for endogenous cholesterol. Values are normalized to uninfected cells. Bars indicate the mean of 3-6 experimental replicates + SEM. ** $p < 0.01$; *** $p < 0.001$; ns, not significant. Two-way ANOVA with Tukey's multiple comparison. (C-E) Levels of lipid species in Δ*invG* (C), Δ*sseJ::pACYC184* (D), or Δ*sseJ::sseJ* (E) infected macrophages, relative to uninfected macrophages. Dots depict increased species (red, FC > 0.5) and decreased species (black, FC < -0.5). Cholesterol ester (ChE); triglyceride (TG); lysophosphatidylcholine (LPC). (F-G) Relative quantities of ChE (F) or LPC (G) species in infected BMDMs. Values are normalized to uninfected cells. Bars indicate the mean of 6 experimental replicates + SEM. Statistics represent the indicated groups compared to uninfected iBMDMs. * $p < 0.05$; ** $p < 0.01$; **** $p < 0.0001$; ns, not significant. Two-way ANOVA with Tukey's multiple comparisons.

Figure 3-2

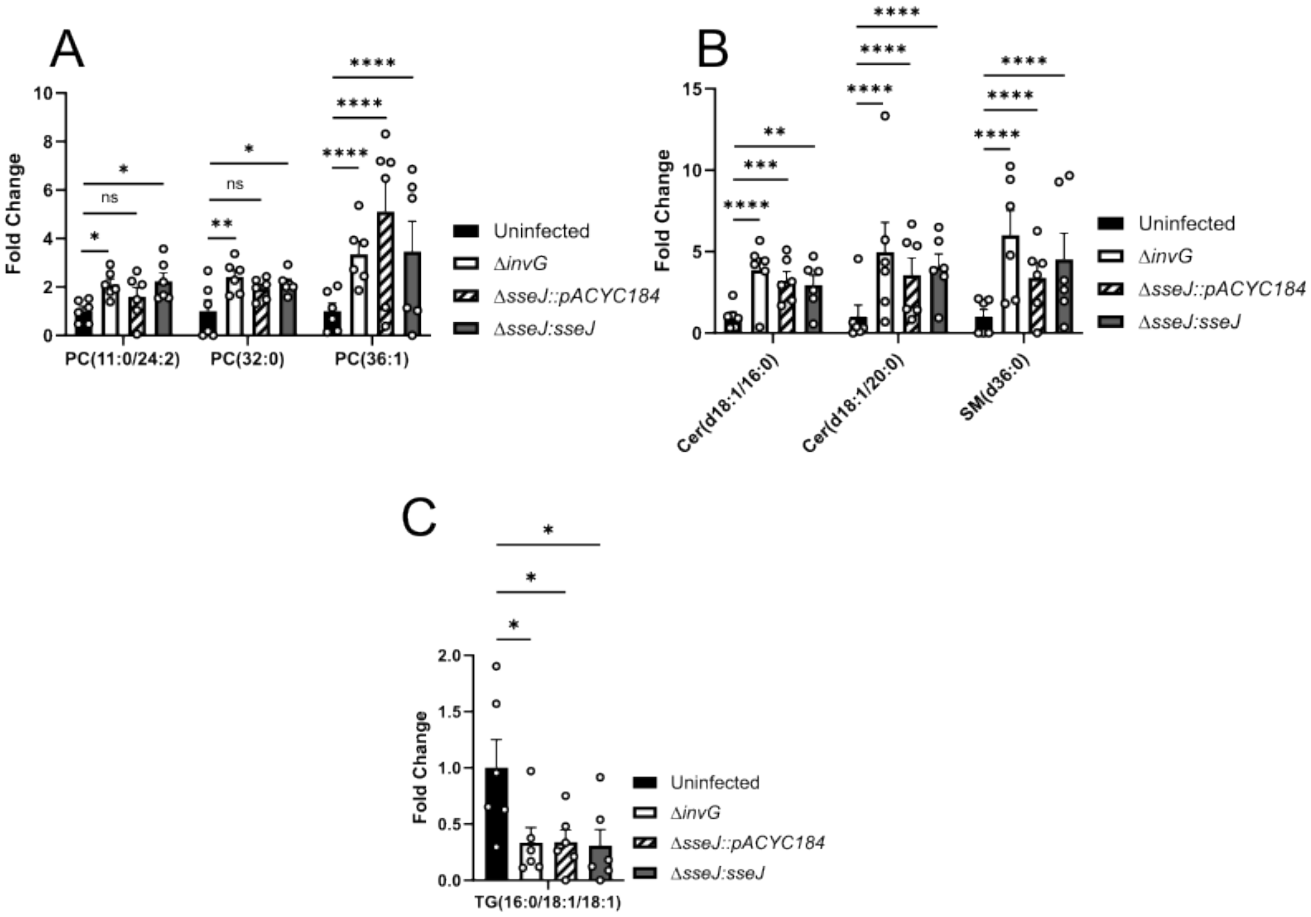

Figure 3-2. Relative quantities of phosphatidylcholine (PC, A), ceramide (Cer) and sphingomyelin (SM, B), and triglyceride (TG, C) species in infected BMDMs compared to uninfected BMDMs. Bars indicate the mean of 6 experimental replicates + SEM. * $p < 0.05$; ** $p < 0.01$; *** $p < 0.001$; **** $p < 0.0001$. Two-way ANOVA with Dunnett's multiple comparison.

Figure 3-3

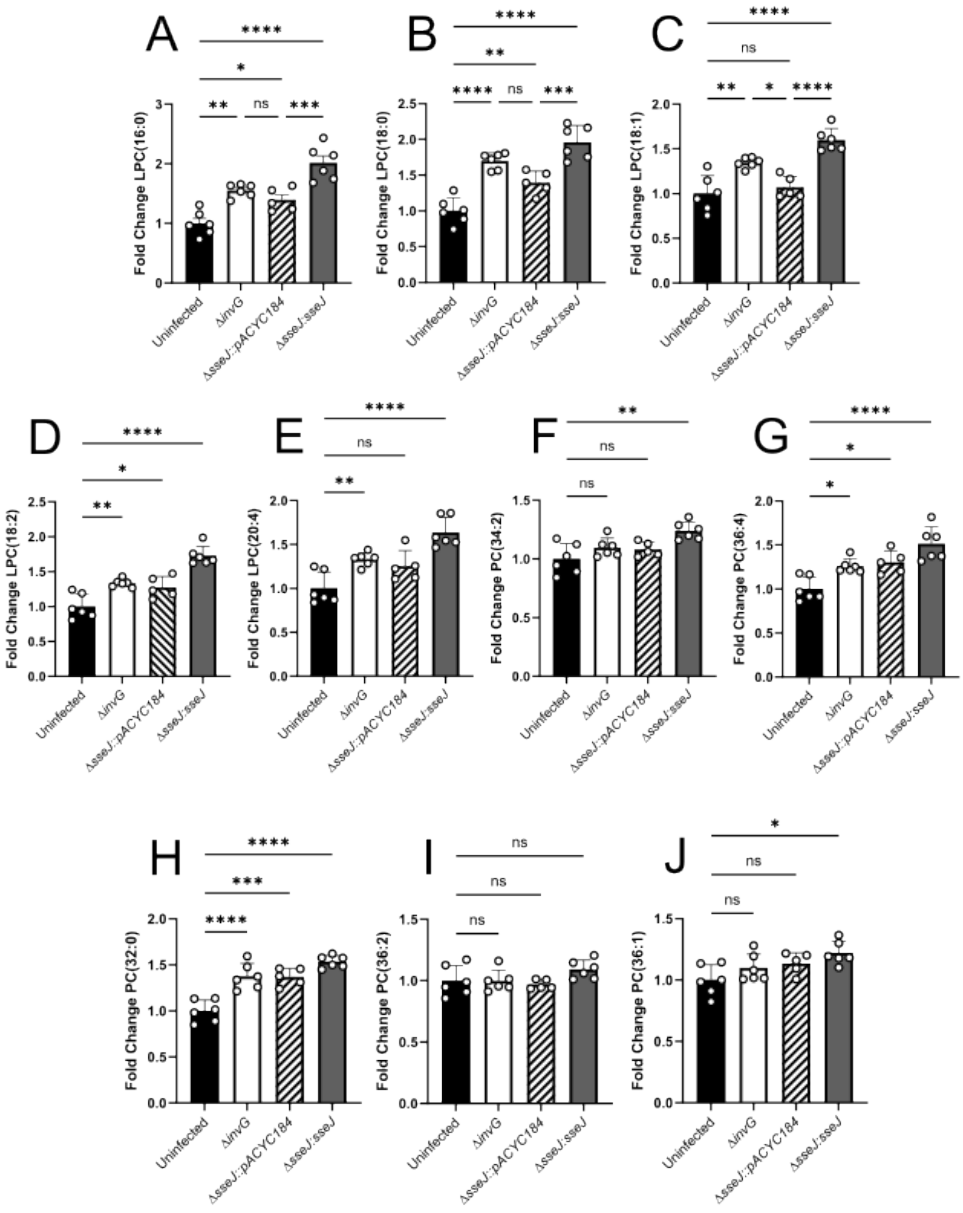

Figure 3-3. (A-J) Relative quantities of select LPC and PC species from targeted mass spectrometry of iBMDMs, compared to uninfected iBMDMs. Bars indicate the mean of 6 experimental replicates + SEM. * $p < 0.05$; ** $p < 0.01$; *** $p < 0.001$; **** $p < 0.0001$; ns, not significant. Two-way ANOVA with Tukey's multiple comparison.

Figure 3-4

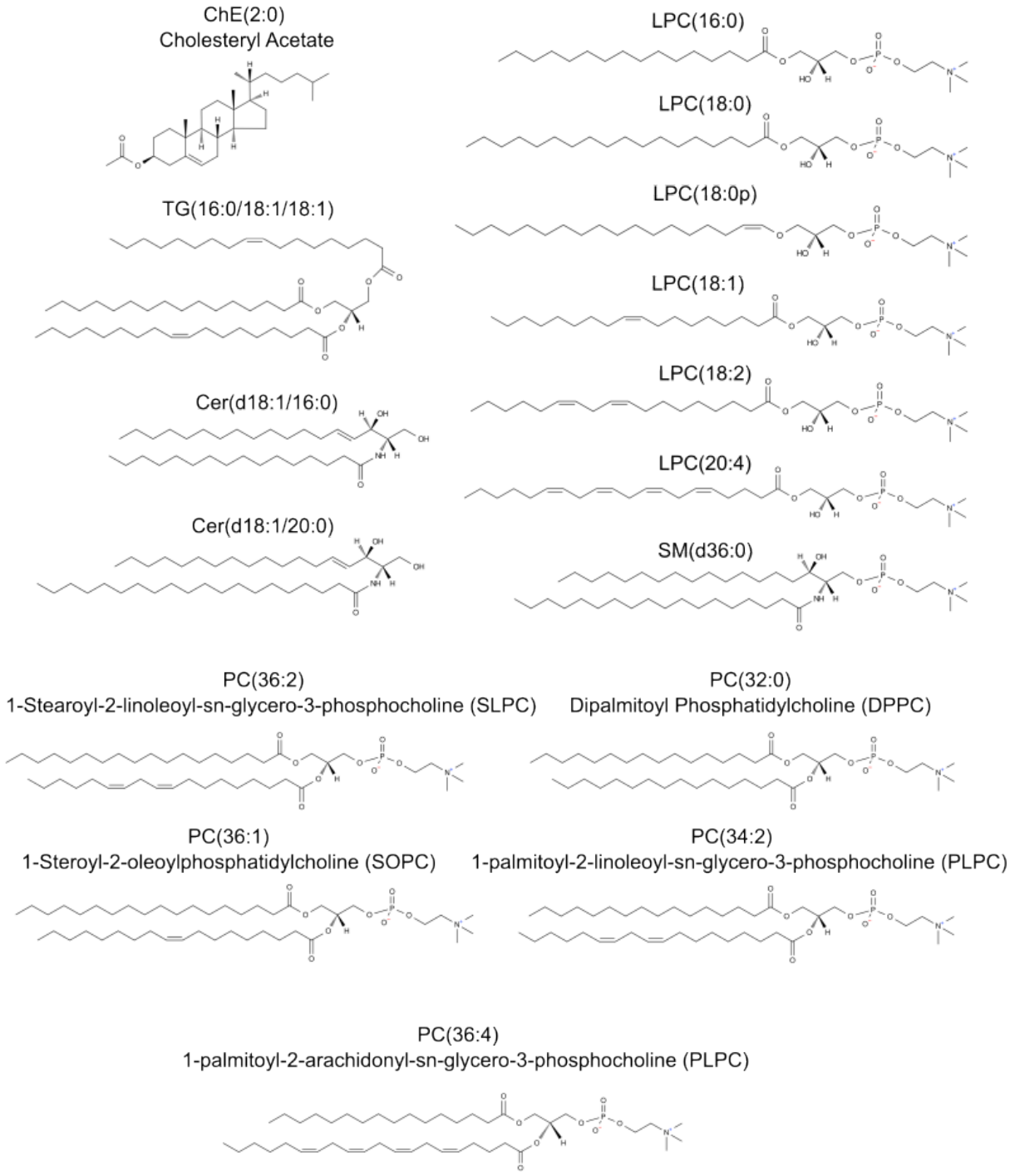

Figure 3-4. Structures of lipids shown in graphs from Figures 3-1-3. Structures accessed from LIPIDMAPS database. The abbreviated headgroup and side chains are shown above each structure, with alternative names if available.

Chapter 4:

Discussion and Future Perspectives

Discussion and Future Perspectives

Our research has provided new insights into the molecular basis behind *S.* Typhimurium-induced cholesterol accumulation and the evasion of autophagy. Our previous work detailed that *S*. Typhimurium induces cholesterol accumulation through FAK/Akt-mediated downregulation of the cholesterol exporter *Abca1* (Greene et al., 2021). The presence and catalytic activity of SseJ, a SPI-2 effector, is important for activation of FAK and Akt during infection, and leads to the decrease in *Abca1* transcription, resulting in cholesterol accumulation (Greene et al., 2021). While cholesterol accumulation was protective to *S.* Typhimurium survival, the means through which excess cholesterol enhances bacterial survival remained unknown. Meanwhile, other work has demonstrated that high cholesterol levels in lysosome can lead to hyper-activation of mTORC1 and the suppression of autophagy (Lim et al., 2019). Here, we confirm that in immortalized murine macrophages, *S.* Typhimurium induces massive cholesterol accumulation, using a newly-discovered fluorescent probe to visualize endogenous cholesterol levels (Figure 2-1). We then determined that mTOR was recruited to SCVs during infection in a cholesterol-dependent manner (Figure 2-2). mTOR localization to the SCV was also dependent on the presence and catalytic activity of SseJ, further suggesting that cholesterol accumulation is necessary for mTOR recruitment to the SCV during *S*. Typhimurium infection. In line with the redistribution of mTORC1 from the cytosol to membranes, we observed increased mTORC1 activation in *S*. Typhimurium infected macrophages, which was also dependent on cholesterol accumulation and SseJ activity. Because activation of mTORC1 can lead to the suppression of autophagy, we next looked at processing and distribution of the autophagic adaptor LC3 during infection. We noted that LC3B staining significantly increases in *S.* Typhimurium-infected macrophages treated with T0901317, which blocks cholesterol accumulation, or in

macrophages infected with a strain of *S.* Typhimurium that lacks SseJ (Figure 2-3). Furthermore, the ratio of LC3B-II:LC3B-I was increased in these cells, indicating elevated formation of autophagosomes. Taken together, these results suggest that during *S*. Typhimurium infection, cholesterol accumulation plays an important role in recruiting and activating mTORC1 at the SCV, leading to the suppression of autophagy.

Previous work has demonstrated that OSBP, a cholesterol transport protein, is essential for mTORC1 activation at lysosomes (Lim et al., 2019). In agreement with this finding, we demonstrated that OSW1, a potent inhibitor of OSBP, blocks both mTOR recruitment to the SCV and mTORC1 activation during *S*. Typhimurium infection (Figure 2-4). OSW1 increases LC3B intensity and processing in *S*. Typhimurium-infected macrophages, demonstrating that *Salmonella* can manipulate OSBP lipid transfer activity to evade autophagy (Figure 2-5). Finally, we demonstrated that OSBP lipid transfer activity is important for *S.* Typhimurium survival, as OSW1 and 25-HC dramatically decrease survival rates (Figure 2-6). Both OSBP and cholesterol are closely complexed at the surface of SCVs, suggesting that OSBP delivers cholesterol from the ER to the SCV where it can recruit and activate mTORC1 to suppress autophagy. These results provide new perspectives on the mechanisms through which *Salmonella* can manipulate a hostile cell type such as the macrophage to promote its own survival. These findings also pose unanswered questions that provide new directions for our research.

<u>FAK activation and the role of SseJ:</u>

A lingering question remains for the role of SseJ in FAK activation, which is a key step to the downregulation of *Abca1* and cholesterol accumulation. Previous work from our lab

has demonstrated that FAK is readily recruited to the SCV during infection of primary peritoneal exudate macrophages and that the SPI-2 T3SS is necessary for this recruitment (Owen et al., 2014). Furthermore, catalytically-active SseJ is important for FAK activation during *S*. Typhimurium infection of BMDMs (Greene et al., 2021). These findings suggest that SseJ may play a role in recruiting FAK to the SCV membrane or modifying the SCV lipid environment in a manner that supports FAK recruitment.

Inactive FAK is dispersed in the cytosol, but when the FERM domain binds to integrins, conformational changes enable its autophosphorylation and activation (Schaller et al., 1994). This process can be enhanced by binding of the FERM domain to $PI(4,5)P_2$, which leads to FAK clustering and efficient autophosphorylation (Goñi et al., 2014). Given the importance of SseJ acyltransferase activity in FAK activation, it is plausible that SseJ modifies the lipid membranes of SCVs in order to promote $PI(4,5)P_2$ and FAK activation. While it is unlikely that SseJ generates $PI(4,5)P_2$ itself, the modification of other lipids in the SCV membrane may alter the lipid composition of the SCV to enable FAK recruitment. It is also possible that another SPI-2 effector with unknown functions may directly bind or influence the recruitment of FAK. A recent interactome of *Salmonella* effectors in RAW264.7 macrophages did not identify any direct binding partners of FAK, nor did it report an interaction between SseJ and FAK (Walch et al., 2020). Our own preliminary experiments with HeLa cells failed to co-precipitate FAK, talin, or Akt with ectopically expressed GFP-SseJ (Figure 4-1A-C). However, an older survey of host protein-effector interactions notes that SseL binds to Talin when ectopically expressed in HEK293 cells (Auweter et al., 2011). Talin is recruited to nascent focal adhesions by FAK where it binds and activates integrins (Lawson et al., 2012). It is possible that recycled

integrins, which remain active and bound to FAK and talin in the endosomal system, become accessible to SseL and SCVs (Nader et al., 2016).

Cholesterol homeostasis during *Salmonella* infection

The ER senses cholesterol levels to control cholesterol biosynthesis through SREBP2 (Hua et al., 1993. However, in *Salmonella* infected cells, expression of *hmgcr*, the rate-limiting enzyme in the cholesterol synthesis pathway, is unaffected (Figure 2-SC2), suggesting that SREBP2 is not retained in the ER and that cholesterol sufficiency is not signaled. In this scenario, cholesterol could either be diverted from the ER prior to delivery or transported away from the ER rapidly enough to prevent its binding to SCAP/Insig. While the discovery of OSBP at the SCV suggests an importance for cholesterol delivery, it is likely that this is not the sole transporter of cholesterol at SCV MCSs. Indeed, research into lipid transporters has revealed several families of lipid transfer proteins that may provide redundant or parallel functions and may be similarly manipulated by *Salmonella*.

The GRAMD family of lipid transporters are ER-resident proteins that mediate sterol transport between the PM and the ER via MCSs. The GRAMD proteins consist of an N-terminal GRAM domain, which possess similarity to the PH domain, a StART-like domain that can bind and transport cholesterol, and a C-terminal transmembrane domain for ER anchoring (Tong et al., 2018; Naito et al., 2021). Notably, GRAMD1 proteins bind to accessible cholesterol in the PM, and provide an important route for cholesterol delivery from the PM to the ER. When sphingomyelin is hydrolyzed in the

PM, leading to an increase in the pool of accessible cholesterol, GRAMD1 proteins rapidly form MCSs between the PM and the ER, leading to cholesterol transfer to the ER and suppression of SREBP-2 cleavage (Naito et al., 2021). The SCV has been described to make frequent interactions with multiple organelles, including the ER, and our own preliminary work in HeLa cells has shown similar results, with tubules of GRAMD1a and GRAMD1b positive ER wrapping around bacteria (Santos et al., 2015; Figure 4-2A). The strong interactions between SseJ, SseL, and OSBP also support the hypothesis that the SCV can form MCSs with the ER (Kolodziejek et al., 2019). It is possible to imagine that *Salmonella* may hijack the GRAMD1-mediated flow of cholesterol from the PM to the ER in order to enrich its own membrane. Further research will be required to determine if the GRAMD1 proteins are truly recruited to the SCV and if they interact with *Salmonella* effectors.

Excess cholesterol in the ER could also be shunted into cholesterol ester formation. As our lipidomics demonstrated, *Salmonella* infected macrophages accumulate large amounts of short-chain cholesterol esters (Figure 3-1F). The function of SseJ is homologous to the host protein ACAT, which esterifies cholesterol at the ER (Suckling and Stange, 1985). Increased cholesterol levels promote ACAT activity, providing an outlet for excess sterols and forming cholesterol esters that can be stored in lipid droplets (Zhang et al., 2003). Intriguingly, lipid droplet biogenesis has been noted in *Salmonella*-infected macrophages, with lipid droplets accumulating as early as one hour post-infection and reaching maximum levels at 24 hours post-infection (Kiarely-Souza et al., 2021). It is tempting to consider that SseJ contributes a large portion of these esters, however our lipid mass spectrometry results indicated that even in SseJ-deficient infected macrophages, cholesterol esters remain elevated above the level of uninfected

macrophages, albeit not as high as macrophages infected with WT *S.* Typhimurium (Figure 3-1). Thus, it is plausible that other effectors, potentially from the SPI-1 T3SS, are at work here, promoting the formation of cholesterol esters and lipid droplets. Alternatively, this rapid onset of lipid droplets could be an innate immune response to intracellular infection. In *M. tuberculosis* infection of macrophages, IFNγ induction led to lipid droplet formation, thus lipid droplet accumulation at later timepoints could represent an immune response (Knight et al., 2018). As for the importance of cholesterol esters and lipid droplets, it is still unclear what role they play in *Salmonella* survival, but cholesterol esters do seem to provide a protective effect to *Salmonella*, as blocking lipid droplet formation negatively impacted *Salmonella* survival (Kiearely-Souza et al., 2021). Perplexingly, SseL, known to bind SseJ, confers an opposite function in relation to lipid droplets. In *Salmonella*-infected mouse gallbladders, deleting *sseL* resulting in massive accumulation of lipid droplets and a decrease in fatty acids compared to WT infected mice (Arena et al., 2011). SseL is a deubiquitinase that can hydrolyze mono- and polyubiquitinated substrates and functions as an active deubiquitinase in infected cells (Rytkonen et al., 2007). Intriguingly, the deubiquitinase activity of SseL was necessary to prevent lipid droplet accumulation in infected cells (Arena et al., 2011). As our research demonstrates, SseL is not necessary for the cholesterol accumulation that occurs during *S.* Typhimurium infection (Figure 2-7B), thus its deubiquitinase activity may be functionally separate from its ability to complex with SseJ and OSBP. Whether SseL serves as a balance to the esterification activity of SseJ or if this control of lipid droplets serves another purpose for survival remains to be studied. A recent study adds a further layer of complexity, reporting that when lipid droplet-loaded macrophages were infected with *Salmonella*, the lipid droplets did not come in close contact with the bacteria (Bosch et al., 2020). The presence of lipid droplets during *Salmonella* infection suggests an intricate cross play between bacterial factors and the immune response and will require

further research to untangle a possible connection between lipid droplets and *Salmonella* survival.

Recruitment and sustainability of OSBP-mediated MCSs on the SCV

Our work has solidified that OSBP is necessary for both mTOR recruitment to the SCV and mTORC1 activation during *S.* Typhimurium infection. As the cholesterol transfer activity is essential for both of these functions, we propose that OSBP functions as a cholesterol transfer system, supplying the SCV with cholesterol to recruit and activate mTORC1. However, questions still remain surrounding the nature of this recruitment process and how the SCV sustains OSBP interactions.

The recruitment of OSBP to the SCV relies on interactions with SseJ and SseL. In the absence of SseJ, OSBP displays a cytoplasmic staining pattern and fails to localize to lysosomal compartments (Kolodziejek et al., 2019). Notably, this reliance on SseJ does not require its catalytic activity, as catalytically inactive SseJ expressed ectopically retains endosomal localization and colocalization with OSBP (LaRock et al., 2012, Kolodziejek et al., 2019). Instead, colocalization with OSBP depends on the ability of SseJ to bind RhoA, a small host GTPase that activates SseJ (LaRock et al., 2012; Kolodziejek et al., 2019). The deletion of both *sseJ* and *sseL* results in vacuolar instability and increased cytoplasmic bacteria in HeLa cells, indicating that the interaction between SseJ, SseL, and OSBP, as well as with the ER resident tethers VAPA/B, provides stability to the SCV (Kolodziejek et al., 2019). These findings suggest a model where MCSs between the ER and the SCV, mediated by OSBP, support SCV integrity through an unknown mechanism. It is possible that lipid exchange, occurring

through the ER-SCV MCSs, support the expansion of the SCV and SIFs, promoting vacuolar stability and bacterial survival. Alternatively, SseJ and SseL may coordinate their functions to protect the SCV. As SseJ induces cholesterol accumulation through the FAK/Akt mediated suppression of *Abca1*, SseL could remove ubiquitination signals on the SCV that would normally target it for autophagic clearance. Future studies will have to focus on dissecting the roles and functions of these effectors to better understand their function in both OSBP recruitment and bacterial survival.

To form an MCS, OSBP must bind VAPA/B in the ER through its FFAT motif and PI4P in the target membrane through its PH domain (Peretti et al., 2008; Wyles et al., 2002). Once formed, transfer of sterols between membranes occurs rapidly (2 seconds) and consumes over half of the PI4P present in the cell (Mesmin et al., 2017). In the canonical OSBP MCS between the ER and the Golgi, the PI4P gradient between the two organelles encourages the flow of lipids. PI4-kinases reside in the TGN and generate PI4P, but Sac1, an ER resident phosphatase, hydrolyzes PI4P to PI and maintains a sharp gradient between the organelles (Mesmin et al., 2013). The forward transfer of cholesterol is sustained preferentially by PI4KIIIβ, which colocalizes on the TGN with OSBP (Mesmin et al., 2017). If PI4P is scarce or PI4KIIIβ is inhibited, OSBP can “chase” the PI4KIIα kinase along the TGN membrane. When local PI4P levels are too low to sustain transfer, the OSBP MCSs move along the membrane, following the PI4P formed by PI4KIIα (Mesmin et al., 2017). Intriguingly, SseL was found to interact with PI4KIIα in a recent interactome of *Salmonella* infected macrophages (Walch et al., 2021). If this interaction is valid, it could be possible that *Salmonella* manipulates PI4P production via PI4KIIα to initiate and support OSBP MCSs with the ER. An alternative pathway could also exist through subversion of the host lysosomal repair pathways. When lysosomes

are damaged, PI4KIIα rapidly accumulates on the damaged membrane, producing large amounts of PI4P that can recruit OSBP, along with the related proteins ORP9/10/11, through the phosphoinositide-initiated membrane tethering and lipid transport (PITT) pathway (Tan and Finkel, 2022). These proteins form extensive MCSs between the damaged lysosome and the ER, stimulating the transfer of cholesterol and phosphatidylserine to support membrane repair. SseL, which has already been implicated in vacuolar stability, could potentially bind PI4KIIα to stimulate membrane repair by hijacking the PITT pathway. Future studies should focus on the presence of additional ORP family members on the SCV and how they may impact *Salmonella* survival.

The phosphoinositide composition of the SCV also remains an important subject for research. Early reports found that PI(4,5)P2 and PI(3,4,5)P3 are locally enriched in *Salmonella*-induced membrane ruffles during invasion (Terebiznik et al., 2002). PI3P has also been transiently found on membrane ruffles and SCVs in *Salmonella*-infected epithelial cells (Scott et al., 2002). Intriguingly, PI3P associates with the early SCV even in the presence of PI3K inhibitor Wortmannin, suggesting that *Salmonella* can activate a host PI3K that is resistant to Wortmannin, or that *Salmonella* translocates a PI3K of its own (Pattni et al., 2001). With the advent of highly specific, fluorescent phosphoinositide biosensors and super-resolution microscopy, the phosphoinositide composition of the SCV could be tracked. Alternatively, interaction of phosphoinositides with individual proteins, particularly *Salmonella* effectors, could be measured using lipid-protein interaction assays (PIP strips). Targeted phosphoinositide analysis is also possible using reversed-phase liquid chromatography coupled with tandem mass spectrometry, opening the door for quantification of phosphoinositides on isolated SCVs. In all, the

rapidly expanding molecular tools for studying phosphoinositide levels and localization within cells present exciting new opportunities for understanding how these molecules contribute to *Salmonella* infection.

Manipulation of cellular autophagy by *Salmonella*

Salmonella is well-understood to both trigger and evade autophagy during cellular infection. During the first hours of infection, the SPI-1 needle can damage the PM and SCV membrane, resulting in amino-acid starvation induced autophagy and recognition of bacterial components by galectins (Tattoli et al., 2012b). However, this induction is short-lived, declining 3 hours post-infection in coincidence with the down-regulation of the SPI-1 T3SS. To offset autophagy during early infection, SPI-1 effector SopF inhibits autophagy through ADP-ribosylation of vATPase (Xu et al., 2019). Such methods of evading autophagy have been described during early-mid infection (1-5 hours post infection); however, few studies have examined how *Salmonella* avoids autophagic clearance at later timepoints.

Our work demonstrates that at 18 hours post infection, which is the point at which cholesterol accumulation reaches a maximum, cholesterol is important for mTORC1 activation and the suppression of autophagy. These results demonstrate that *Salmonella* can manipulate multiple aspects of the host cell to escape autophagy. The reliance of *Salmonella* on a given effector or autophagy evasion method may depend significantly on the cell type in question or the timepoint of infection. SopF, for instance, may provide sufficient control of autophagy during early infection, but the downregulation of SPI-1 after 5 hours of infection would suggest that other mechanisms are necessary to provide

continual evasion of autophagy. Additionally, *Salmonella* most likely possesses redundant mechanisms to escape autophagy at late timepoints. A recent study demonstrated that when the SPI-2 effectors SseF and SseG are ectopically expressed in HeLa cells, they bind to Rab1A, thereby inhibiting its activation of ULK1 and autophagy (Feng et al., 2018). This process has been demonstrated to reduce autophagic clearance of *Salmonella* at 12 hours post infection, providing another outlet for evasion of autophagy. Meanwhile, the SPI-2 deubiquitinase SseL, in addition to its role in recruiting OSBP to the SCV, can deubiquitinate aggresome-like structures that are induced by *Salmonella* infection, lowering autophagic flux and promoting survival (Mesquita et al., 2012).

Clearly, *Salmonella* and its effectors possess diverse and flexible options to modulate autophagy in the host cells and promote bacterial survival. This form of pathway redundancy ensures that *Salmonella* can achieve intracellular survival even in the face of immune restriction or nutrient limitation. It is also possible that these pathways may synergize to enhance autophagy evasion. While SseL provides a deubiquitinase activity at the SCV, it also is important for the recruitment of OSBP, resulting in cholesterol transfer and mTORC1 activation. These dual mechanisms of SseL could provide *Salmonella* with vacuolar stability as well as evasion from autophagy. Similarly, the flow of cholesterol to the SCV via OSBP provides activation for mTORC1 but may also provide lipids for stabilization and expansion of the SCV and SIF network as the bacteria replicate. Notably, several of these pathways converge with negative regulation of ULK1, which is key to autophagosome formation. Possessing multiple avenues for inhibiting ULK1 may ensure that *Salmonella* is able to control autophagy at later time points. Overall, *Salmonella* exhibits diverse and flexible pathway redundancy during intracellular

infection, providing multiple outlets for autophagy evasion and bacterial survival (Figure 4-3).

The changing lipidome of *Salmonella* infected macrophages

Our results have detailed extensive changes in the lipid contents of *S.* Typhimurium infected macrophages, indicating that *Salmonella* can influence broad changes that impact the function and metabolic processing of the host cell. Among those changes are significant increases in LPC and cholesterol esters, as well as a marked decrease in triglyceride species (Figure 3-1F-G; Figure 3-2C). These results provide ample insights into the metabolic status of infected macrophages, but also leave many questions to be further explored.

The metabolism of macrophages is often used to categorize their function. Pro-inflammatory macrophages heavily invest in glycolysis, while anti-inflammatory macrophages prefer fatty acid oxidation. These polarization states are reflected in our results where we see decreased triglyceride synthesis and increased ether lipids. However, further research into the metabolic signature of *Salmonella* infected macrophages is required. Of particular interest is the increase in ether lipids and plasmalogens found in *Salmonella* infected iBMDMs. As these ether lipids can serve as ligands for PPARγ, which promotes M2 polarization, it is tempting to connect the presence of these lipids to the polarization of *Salmonella* infected macrophages into a more favorable replicative niche. Furthermore, lipid mass spectrometry of M1 and M2 macrophages has revealed that M2 macrophages contain higher levels of glycerophospholipids and ether lipids than their M1 counterparts (Morgan et al., 2021).

M1 macrophages produce high levels of ROS and pro-inflammatory cytokines and are largely non-permissive to *Salmonella* replication, thus *Salmonella* faces pressure to influence macrophages into a more favorable niche (Saliba et al., 2016). One mode of influence is through the SPI-2 effector SteE, which counteracts TNFα signaling to promote M2 polarization in granuloma macrophages (Pham et al., 2020). A study using larval zebrafish demonstrated that during early infection, neutrophils and macrophages converge on the site of infection and invoke a strong M1 phenotype (Leiba et al., 2024). As infection progressed to later stages, however, *Salmonella* persisted and replicated in non-inflammatory, M2 macrophages (Leiba et al., 2024). These results suggest that *Salmonella* can play an active role in modulating macrophage polarization to promote survival and long-term persistence. However, it is still unclear if the lipidomic changes in *Salmonella* infected macrophages are the result of direct action of bacterial effectors or the outcome of M2 polarization. Further research should dive deeper into the changes that occur during Salmonella infection, focusing on what metabolites influence macrophage polarization.

A lingering question remains related to the presence of short-chain cholesterol esters (ChE 2:0). While the LPC species found generated during *Salmonella* infection have longer acyl chains, the short chains found on *Salmonella*-induced cholesterol esters suggest that further modification is occurring either before or after acyl chain transfer. Research has suggested that ChE 2:0 (cholesteryl acetate) can form monolayers that are almost indistinguishable from cholesterol (Adam and Jessop, 1928; Kwong et al., 1971; Sarkar and Suresh, 2017), thus this modification of cholesterol esters may act as a method to alter long chain esters into forms that are more easily packaged in membranes or lipid droplets. It is unclear if *Salmonella* influences the creation or

modification of these short chain esters through bacterial effectors or through manipulation of host processes. Taken together, our work has provided new insights into the lipidome of *Salmonella* infected macrophages, hopefully sparking new interest and research into how *Salmonella* influences these lipidomic changes.

Summary

Previous research has established that *S.* Typhimurium induces cholesterol accumulation in both epithelial and macrophage cells, with cholesterol levels peaking at 18-20 hours post infection (Catron et al., 2002; Brumell et al., 2001). Our lab has recently described a mechanism through which *S.* Typhimurium promotes cholesterol accumulation via the SPI-2 effector SseJ (Greene et al., 2021). SseJ is a cholesterol acyltransferase that is important for the activation of host kinases FAK and Akt during infection (Greene et al., 2021). Through activation of FAK/Akt, a signaling cascade leads to the downregulation of the cholesterol exporter *Abca1*, resulting in cholesterol accumulation within the macrophage (Greene et al., 2021). This mechanism provided new insight in how *S.* Typhimurium can influence cholesterol homeostasis, but how cholesterol benefits bacterial survival remained unknown. The work in this thesis fills this gap in knowledge, presenting evidence that *S*. Typhimurium induces cholesterol accumulation in order to activate mTORC1 and suppress the host autophagic machinery. We found that the catalytic activity of SseJ and downstream cholesterol accumulation are necessary for mTOR recruitment to the surface of the SCV, mTORC1 activation, and the suppression of autophagosome formation. Importantly, if cholesterol accumulation is blocked through pharmacological stimulation of *Abca1*, deletion of *sseJ*, or mutation of SseJ catalytic activity, autophagosome formation increases and bacterial survival

decreases (Greene et al., 2021). Together, these results provide new understanding into how *Salmonella* can manipulate host cholesterol levels to promote its own survival.

Prior work has shown that the *Salmonella* effectors SseJ and SseL are important for the recruitment of host cholesterol transporter OSBP to the SCV (Kolodziejek et al., 2019). This work implicated OSBP in promoting stability of the vacuole, but the well-established role of OSBP in sterol transport has not been explored in the context of *Salmonella* infection. We demonstrate here that OSBP is readily recruited to the surface of SCVs, in close association with cholesterol. Further, the cholesterol transfer activity of OSBP is important for *Salmonella* survival. If OSBP is inhibited, the recruitment and activation of mTORC1 is impaired, leading to increased autophagosome formation. OSBP inhibition also impacts bacterial survival, with a 70% decrease in *Salmonella* survival when treated with OSW1. These results demonstrate that the role of OSBP in delivering cholesterol to the SCV is important for mTOR recruitment and activation, ultimately impacting autophagy and bacterial survival.

Finally, we have compiled the first known lipidome of *Salmonella* infected macrophages. This information will be key in future studies of how *Salmonella* impacts the metabolic environment of infected cells. We found that *S.* Typhimurium infection leads to an increase in cholesterol esters, lysophosphatidylcholine, and ether lipids, while decreasing triglycerides. These results align with previous reports that *Salmonella* prefers M2 macrophages for long-term replication and persistence. We also provided new evidence into the catalytic activity of SseJ, with our results suggesting that SseJ prefers to target phosphatidylcholine with its acyltransferase activity. Together, our

results highlight the importance of cholesterol in *Salmonella* survival and how the bacteria can manipulate host processes to benefit itself. We hope that the work accomplished here will provide new insights and ideas to the field and help identify new approaches to developing treatments and strategies for *Salmonella* infection.

Figure 4-1

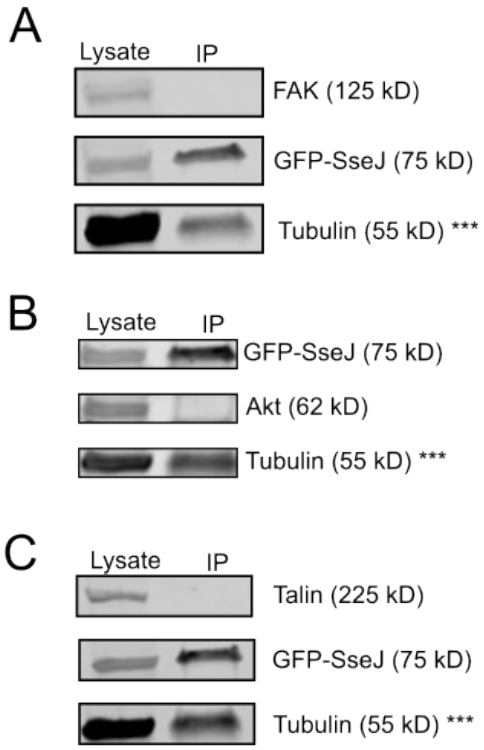

Figure 4-1. GFP-SseJ does not co-precipitate FAK, Akt, or talin when expressed ectopically in HeLa cells. (A) HeLa cells were transiently transfected with GFP-SseJ and lysates were collected. Lysates were incubated with anti-GFP antibody (CST) and immunoprecipitated with Protein A/G Sepharose beads. Total lysate and pull-downs were loaded on 4-20% SDS-polyacrylamide gels, transferred onto PVDF membranes, and probed using the following antibodies: mouse anti-FAK (Santa Cruz); rabbit anti-Akt (CST); rabbit anti-GFP (CST); and mouse anti β-tubulin. *** indicates that in the IP lane, the band at ~50 kD is presumably the heavy chain of IgG.

Figure 4-2

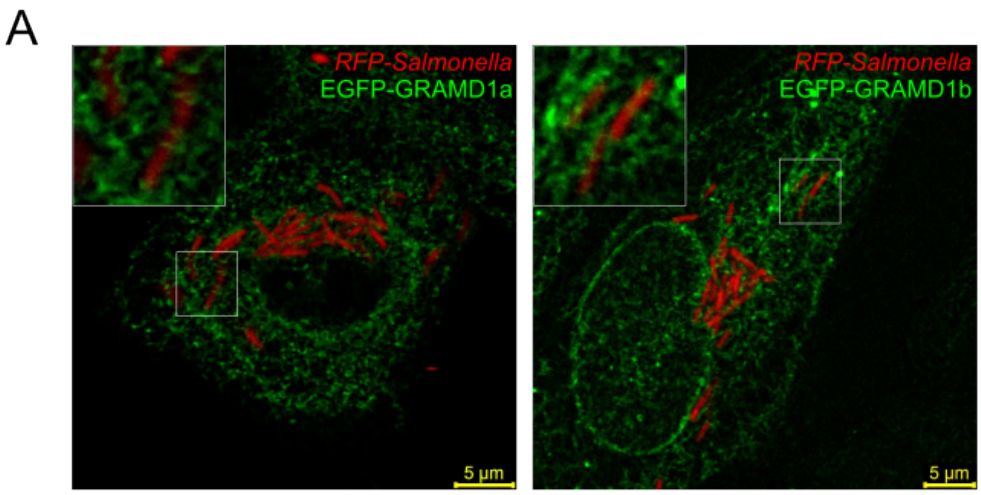

Figure 4-2. Localization of GRAMD1a and GRAMD1b with *Salmonella*. (A) HeLa cells were transiently transfected with plasmids containing EGFP-GRAMD1a or EGFP-GRAMD1b, then infected with RFP-SL1344 for 18 hours prior to imaging. Cells were imaged live using Leica Stellaris TauSTED. Inset represents 2.5X zoom. Scale bar represents 5 uM.

Figure 4-3

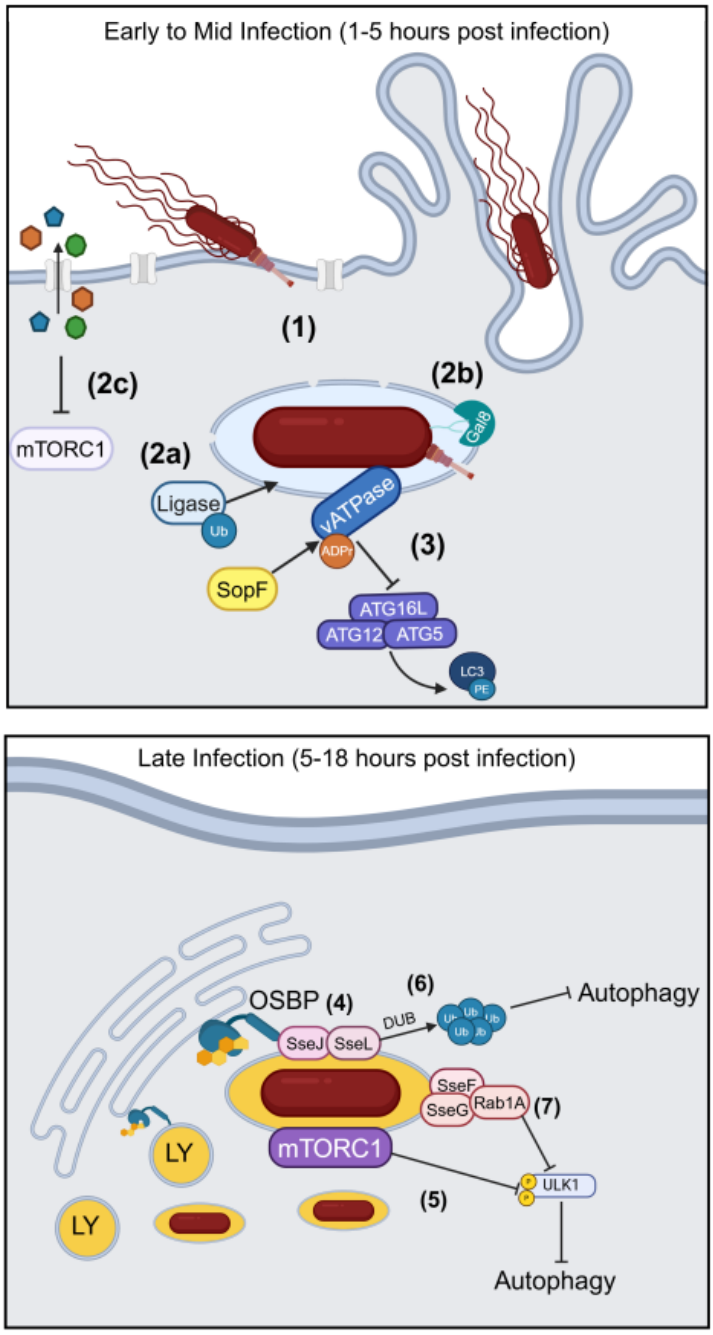

Figure 4-3. Summary of known *Salmonella* mechanisms to evade autophagy.

During early infection (1-5 hours post infection), the SPI-1 T3SS pokes holes in the PM and SCV membrane (1). This results in the recognition of *Salmonella* by ubiquitin ligases (2a) and galectin-8 (2b), triggering autophagy. Simultaneously, leakage of amino acids

from pores in the PM results in the deactivation of mTORC1 (2c), compounding the induction of autophagy. *Salmonella* mitigates autophagy through the SPI-1 effector SopF, which will ADP-ribosylate vATPase (3), preventing its association with ATG16L and blocking the lipidation of LC3 through the ATG16L-12-5 complex. At later timepoints (5-18 hours post infection), *Salmonella* displays pathway redundancy, with multiple effectors converging on inhibition of autophagy. Our research describes a novel mechanism through which *Salmonella*-induces cholesterol accumulation to inhibit autophagy. Cholesterol is transferred to the SCV via OSBP, which is recruited to the SCV by SPI-2 effectors SseJ and SseL (4), leading to the activation of mTORC1 on the surface of the SCV, suppressing autophagy through inhibitory phosphorylation of ULK1 (5). Concurrently, SseL can deubiquitinate aggresome-like induced structures that accumulate during *Salmonella* infection. Through this deubiquitinase activity, SseL reduces autophagic flux. Finally, the SPI-2 effectors SseF and SseG are also described to localize to the SCV, where they bind Rab1A, preventing its activation of ULK1 (7).

References

Abshire, CF, Dragoi, A-M, Roy, CR, and Ivanov, SS (2016). MTOR-Driven Metabolic Reprogramming Regulates Legionella pneumophila Intracellular Niche Homeostasis. PLoS Pathog 12, e1006088.

Adam., N.K. and Jessop, G. (1928). The structure of thin films. Cholesterol and its effect in admixture with other substances. Proc. Roy. Soc. London, 126, 366-372.

Ailte, I, Lingelem, ABD, Kavaliauskiene, S, Bergan, J, Kvalvaag, AS, Myrann, A-G, Skotland, T, and Sandvig, K (2016). Addition of lysophospholipids with large head groups to cells inhibits Shiga toxin binding. Sci Rep 6, 30336.

Alessi, DR, James, SR, Downes, CP, Holmes, AB, Gaffney, PR, Reese, CB, and Cohen, P (1997). Characterization of a 3-phosphoinositide-dependent protein kinase which phosphorylates and activates protein kinase Balpha. Curr Biol 7, 261–269.

Anderson, RA, Joyce, C, Davis, M, Reagan, JW, Clark, M, Shelness, GS, and Rudel, LL (1998). Identification of a form of acyl-CoA:cholesterol acyltransferase specific to liver and intestine in nonhuman primates. J Biol Chem 273, 26747–26754.

Ao, TT, Feasey, NA, Gordon, MA, Keddy, KH, Angulo, FJ, and Crump, JA (2015). Global burden of invasive nontyphoidal Salmonella disease, 2010. Emerging Infect Dis 21.

Arena, ET et al. (2011). The deubiquitinase activity of the Salmonella pathogenicity island 2 effector, SseL, prevents accumulation of cellular lipid droplets. Infect Immun 79, 4392–4400.

Auweter, SD et al. (2011). Quantitative mass spectrometry catalogues Salmonella pathogenicity island-2 effectors and identifies their cognate host binding partners. J Biol Chem 286, 24023–24035.

Bajaj, V, Lucas, RL, Hwang, C, and Lee, CA (1996). Co-ordinate regulation of Salmonella typhimurium invasion genes by environmental and regulatory factors is mediated by control of hilA expression. Mol Microbiol 22, 703–714.

Bakowski, MA, Braun, V, Lam, GY, Yeung, T, Heo, WD, Meyer, T, Finlay, BB, Grinstein, S, and Brumell, JH (2010). The phosphoinositide phosphatase SopB manipulates membrane surface charge and trafficking of the Salmonella-containing vacuole. Cell Host Microbe 7, 453–462.

Balla, A, Tuymetova, G, Tsiomenko, A, Várnai, P, and Balla, T (2005). A plasma membrane pool of phosphatidylinositol 4-phosphate is generated by phosphatidylinositol 4-kinase type-III alpha: studies with the PH domains of the oxysterol binding protein and FAPP1. Mol Biol Cell 16, 1282–1295.

Batool, R, Qamar, ZH, Salam, RA, Yousafzai, MT, Ashorn, P, and Qamar, FN (2024). Efficacy of typhoid vaccines against culture-confirmed Salmonella Typhi in typhoid endemic countries: a systematic review and meta-analysis. Lancet Glob Health 12, e589–e598.

Birmingham, CL, Smith, AC, Bakowski, MA, Yoshimori, T, and Brumell, JH (2006). Autophagy controls Salmonella infection in response to damage to the Salmonella-containing vacuole. J Biol Chem 281, 11374–11383.

Blanc, M et al. (2011). Host defense against viral infection involves interferon mediated down-regulation of sterol biosynthesis. PLoS Biol 9, e1000598.

Blanc, M et al. (2013). The transcription factor STAT-1 couples macrophage synthesis of 25-hydroxycholesterol to the interferon antiviral response. Immunity 38, 106–118.

Bligh, EG, and Dyer, WJ (1959). A rapid method of total lipid extraction and purification. Can J Biochem Physiol 37, 911–917.

Boddy, KC et al. (2021). Salmonella effector SopD promotes plasma membrane scission by inhibiting Rab10. Nat Commun 12, 4707.

Bouhlel, MA et al. (2007). PPARgamma activation primes human monocytes into alternative M2 macrophages with anti-inflammatory properties. Cell Metab 6, 137–143.

Bosch, M et al. (2020). Mammalian lipid droplets are innate immune hubs integrating cell metabolism and host defense. Science 370.

Braverman, NE, and Moser, AB (2012). Functions of plasmalogen lipids in health and disease. Biochim Biophys Acta 1822, 1442–1452.

Brent, AJ, Oundo, JO, Mwangi, I, Ochola, L, Lowe, B, and Berkley, JA (2006). Salmonella bacteremia in Kenyan children. Pediatr Infect Dis J 25, 230–236.

Brown, MS, and Goldstein, JL (1979). Receptor-mediated endocytosis: insights from the lipoprotein receptor system. Proc Natl Acad Sci USA 76, 3330–3337.

Brumell, JH, Tang, P, Mills, SD, and Finlay, BB (2001). Characterization of Salmonella-induced filaments (Sifs) reveals a delayed interaction between Salmonella-containing vacuoles and late endocytic compartments. Traffic 2, 643–653.

Burgett, AWG et al. (2011). Natural products reveal cancer cell dependence on oxysterol-binding proteins. Nat Chem Biol 7, 639–647.

Casanova, JE (2017). Bacterial Autophagy: Offense and Defense at the Host-Pathogen Interface. Cell Mol Gastroenterol Hepatol 4, 237–243.

Castellano, BM et al. (2017). Lysosomal cholesterol activates mTORC1 via an SLC38A9-Niemann-Pick C1 signaling complex. Science 355, 1306–1311.

Castoldi, A et al. (2020). Triacylglycerol synthesis enhances macrophage inflammatory function. Nat Commun 11, 4107.

Catron, DM, Lange, Y, Borensztajn, J, Sylvester, MD, Jones, BD, and Haldar, K (2004). Salmonella enterica serovar Typhimurium requires nonsterol precursors of the cholesterol biosynthetic pathway for intracellular proliferation. Infect Immun 72, 1036–1042.

Catron, DM, Sylvester, MD, Lange, Y, Kadekoppala, M, Jones, BD, Monack, DM, Falkow, S, and Haldar, K (2002). The Salmonella-containing vacuole is a major site of intracellular cholesterol accumulation and recruits the GPI-anchored protein CD55. Cell Microbiol 4, 315–328.

Centre for Desease Control (2019). Antibiotic Resistance Threats in the United States (2019 AR Threats Report), U.S. Department of Health and Human Services, CDC.

Chatterjee, R, Chaudhuri, D, Setty, SRG, and Chakravortty, D (2023). Deceiving the big eaters: Salmonella Typhimurium SopB subverts host cell xenophagy in macrophages via dual mechanisms. Microbes Infect 25, 105128.

Chen, S, Saeed, AFUH, Liu, Q, Jiang, Q, Xu, H, Xiao, GG, Rao, L, and Duo, Y (2023). Macrophages in immunoregulation and therapeutics. Signal Transduct Target Ther 8, 207.

Chen, Z, Kong, X, Ma, Q, Chen, J, Zeng, Y, Liu, H, Wang, X, and Lu, S (2024). The impact of Mycobacterium tuberculosis on the macrophage cholesterol metabolism pathway. Front Immunol 15.

Chilcott, GS, and Hughes, KT (2000). Coupling of flagellar gene expression to flagellar assembly in Salmonella enterica serovar typhimurium and Escherichia coli. Microbiol Mol Biol Rev 64, 694–708.

Christen, M, Coye, LH, Hontz, JS, LaRock, DL, Pfuetzner, RA, Megha, and Miller, SI (2009). Activation of a bacterial virulence protein by the GTPase RhoA. Sci Signal 2, ra71.

Cirillo, DM, Valdivia, RH, Monack, DM, and Falkow, S (1998). Macrophage-dependent induction of the Salmonella pathogenicity island 2 type III secretion system and its role in intracellular survival. Mol Microbiol 30, 175–188.

Collins, FM (1972). Salmonellosis in orally infected specific pathogen-free C57B1 mice. Infect Immun 5, 191–198.

Darwin, KH, and Miller, VL (1999). Molecular basis of the interaction of Salmonella with the intestinal mucosa. Clin Microbiol Rev 12, 405–428.

Das, A, Brown, MS, Anderson, DD, Goldstein, JL, and Radhakrishnan, A (2014). Three pools of plasma membrane cholesterol and their relation to cholesterol homeostasis. ELife 3.

Davies, SS et al. (2001). Oxidized alkyl phospholipids are specific, high affinity peroxisome proliferator-activated receptor gamma ligands and agonists. J Biol Chem 276, 16015–16023.

Diercks, AH et al. (2024). Oxysterol binding protein regulates the resolution of TLR-induced cytokine production in macrophages. Proc Natl Acad Sci USA 121, e2406492121.

Dong, R, Saheki, Y, Swarup, S, Lucast, L, Harper, JW, and De Camilli, P (2016). Endosome-ER Contacts Control Actin Nucleation and Retromer Function through VAP-Dependent Regulation of PI4P. Cell 166, 408–423.

Dooley, HC, Razi, M, Polson, HEJ, Girardin, SE, Wilson, MI, and Tooze, SA (2014). WIPI2 links LC3 conjugation with PI3P, autophagosome formation, and pathogen clearance by recruiting Atg12-5-16L1. Mol Cell 55, 238–252.

Drecktrah, D, Levine-Wilkinson, S, Dam, T, Winfree, S, Knodler, LA, Schroer, TA, and Steele-Mortimer, O (2008). Dynamic behavior of Salmonella-induced membrane tubules in epithelial cells. Traffic 9, 2117–2129.

Eden, S, Rohatgi, R, Podtelejnikov, AV, Mann, M, and Kirschner, MW (2002). Mechanism of regulation of WAVE1-induced actin nucleation by Rac1 and Nck. Nature 418, 790–793.

Eisele, NA, Ruby, T, Jacobson, A, Manzanillo, PS, Cox, JS, Lam, L, Mukundan, L, Chawla, A, and Monack, DM (2013). Salmonella require the fatty acid regulator PPARδ for the establishment of a metabolic environment essential for long-term persistence. Cell Host Microbe 14, 171–182.

Espenshade, PJ, Li, W-P, and Yabe, D (2002). Sterols block binding of COPII proteins to SCAP, thereby controlling SCAP sorting in ER. Proc Natl Acad Sci USA 99, 11694–11699.

Everest, P, Wain, J, Roberts, M, Rook, G, and Dougan, G (2001). The molecular mechanisms of severe typhoid fever. Trends Microbiol 9, 316–320.

Feasey, NA, Dougan, G, Kingsley, RA, Heyderman, RS, and Gordon, MA (2012). Invasive non-typhoidal salmonella disease: an emerging and neglected tropical disease in Africa. Lancet 379, 2489–2499.

Figueira, R, and Holden, DW (2012). Functions of the Salmonella pathogenicity island 2 (SPI-2) type III secretion system effectors. Microbiology (Reading, Engl) 158, 1147–1161.

Frechin, M, Stoeger, T, Daetwyler, S, Gehin, C, Battich, N, Damm, E-M, Stergiou, L, Riezman, H, and Pelkmans, L (2015). Cell-intrinsic adaptation of lipid composition to local crowding drives social behaviour. Nature 523, 88–91.

Freeman, JA, Ohl, ME, and Miller, SI (2003). The Salmonella enterica serovar typhimurium translocated effectors SseJ and SifB are targeted to the Salmonella-containing vacuole. Infect Immun 71, 418–427.

Frey, A, Giannasca, KT, Weltzin, R, Giannasca, PJ, Reggio, H, Lencer, WI, and Neutra, MR (1996). Role of the glycocalyx in regulating access of microparticles to apical plasma membranes of intestinal epithelial cells: implications for microbial attachment and oral vaccine targeting. J Exp Med 184, 1045–1059.

Friebel, A, Ilchmann, H, Aepfelbacher, M, Ehrbar, K, Machleidt, W, and Hardt, WD (2001). SopE and SopE2 from Salmonella typhimurium activate different sets of RhoGTPases of the host cell. J Biol Chem 276, 34035–34040.

Furter, M, Sellin, ME, Hansson, GC, and Hardt, W-D (2019). Mucus Architecture and Near-Surface Swimming Affect Distinct Salmonella Typhimurium Infection Patterns along the Murine Intestinal Tract. Cell Rep 27, 2665-2678.e3.

Gal-Mor, O, Boyle, EC, and Grassl, GA (2014). Same species, different diseases: how and why typhoidal and non-typhoidal Salmonella enterica serovars differ. Front Microbiol 5, 391.

Garcia-del Portillo, F, and Finlay, BB (1995). Targeting of Salmonella typhimurium to vesicles containing lysosomal membrane glycoproteins bypasses compartments with mannose 6-phosphate receptors. J Cell Biol 129, 81–97.

Gelissen, IC, Harris, M, Rye, K-A, Quinn, C, Brown, AJ, Kockx, M, Cartland, S, Packianathan, M, Kritharides, L, and Jessup, W (2006). ABCA1 and ABCG1 synergize to mediate cholesterol export to apoA-I. Arterioscler Thromb Vasc Biol 26, 534–540.

Gilk, SD, Cockrell, DC, Luterbach, C, Hansen, B, Knodler, LA, Ibarra, JA, Steele-Mortimer, O, and Heinzen, RA (2013). Bacterial colonization of host cells in the absence of cholesterol. PLoS Pathog 9, e1003107.

Gill, S, Stevenson, J, Kristiana, I, and Brown, AJ (2011). Cholesterol-dependent degradation of squalene monooxygenase, a control point in cholesterol synthesis beyond HMG-CoA reductase. Cell Metab 13, 260–273.

Goldberg, MF, Roeske, EK, Ward, LN, Pengo, T, Dileepan, T, Kotov, DI, and Jenkins, MK (2018). Salmonella Persist in Activated Macrophages in T Cell-Sparse Granulomas but Are Contained by Surrounding CXCR3 Ligand-Positioned Th1 Cells. Immunity 49, 1090-1102.e7.

Goldstein, JL, Dana, SE, Faust, JR, Beaudet, AL, and Brown, MS (1975). Role of lysosomal acid lipase in the metabolism of plasma low density lipoprotein. Observations in cultured fibroblasts from a patient with cholesteryl ester storage disease. J Biol Chem 250, 8487–8495.

Gómez-Sánchez, R et al. (2018). Atg9 establishes Atg2-dependent contact sites between the endoplasmic reticulum and phagophores. J Cell Biol 217, 2743–2763.

Gong, Y, Lee, JN, Lee, PCW, Goldstein, JL, Brown, MS, and Ye, J (2006). Sterol-regulated ubiquitination and degradation of Insig-1 creates a convergent mechanism for feedback control of cholesterol synthesis and uptake. Cell Metab 3, 15–24.

Goñi, GM et al. (2014). Phosphatidylinositol 4,5-bisphosphate triggers activation of focal adhesion kinase by inducing clustering and conformational changes. Proc Natl Acad Sci USA 111, E3177-86.

Gordon, MA, Banda, HT, Gondwe, M, Gordon, SB, Boeree, MJ, Walsh, AL, Corkill, JE, Hart, CA, Gilks, CF, and Molyneux, ME (2002). Non-typhoidal salmonella bacteraemia among HIV-infected Malawian adults: high mortality and frequent recrudescence. AIDS 16, 1633–1641.

Greene, AR, Owen, KA, and Casanova, JE (2021). Salmonella Typhimurium manipulates macrophage cholesterol homeostasis through the SseJ-mediated suppression of the host cholesterol transport protein ABCA1. Cell Microbiol 23, e13329.

Gunn, JS, Marshall, JM, Baker, S, Dongol, S, Charles, RC, and Ryan, ET (2014). Salmonella chronic carriage: epidemiology, diagnosis, and gallbladder persistence. Trends Microbiol 22, 648–655.

Guzman, CA, Borsutzky, S, Griot-Wenk, M, Metcalfe, IC, Pearman, J, Collioud, A, Favre, D, and Dietrich, G (2006). Vaccines against typhoid fever. Vaccine 24, 3804–3811.

Hardt, WD, Chen, LM, Schuebel, KE, Bustelo, XR, and Galán, JE (1998). S. typhimurium encodes an activator of Rho GTPases that induces membrane ruffling and nuclear responses in host cells. Cell 93, 815–826.

Hay, N, and Sonenberg, N (2004). Upstream and downstream of mTOR. Genes Dev 18, 1926–1945.

Hensel, M, Shea, JE, Gleeson, C, Jones, MD, Dalton, E, and Holden, DW (1995). Simultaneous identification of bacterial virulence genes by negative selection. Science 269, 400–403.

Hersh, D, Monack, DM, Smith, MR, Ghori, N, Falkow, S, and Zychlinsky, A (1999). The Salmonella invasin SipB induces macrophage apoptosis by binding to caspase-1. Proc Natl Acad Sci USA 96, 2396–2401.

Hollenstein, DM, and Kraft, C (2020). Autophagosomes are formed at a distinct cellular structure. Curr Opin Cell Biol 65, 50–57.

Horton, JD, Goldstein, JL, and Brown, MS (2002). SREBPs: activators of the complete program of cholesterol and fatty acid synthesis in the liver. J Clin Invest 109, 1125–1131.

Hosokawa, N et al. (2009). Nutrient-dependent mTORC1 association with the ULK1-Atg13-FIP200 complex required for autophagy. Mol Biol Cell 20, 1981–1991.

Hua, X, Yokoyama, C, Wu, J, Briggs, MR, Brown, MS, Goldstein, JL, and Wang, X (1993). SREBP-2, a second basic-helix-loop-helix-leucine zipper protein that stimulates transcription by binding to a sterol regulatory element. Proc Natl Acad Sci USA 90, 11603–11607.

Huang, J, and Manning, BD (2009). A complex interplay between Akt, TSC2 and the two mTOR complexes. Biochem Soc Trans 37, 217–222.

Huang, SC-C et al. (2014). Cell-intrinsic lysosomal lipolysis is essential for alternative activation of macrophages. Nat Immunol 15, 846–855.

Humphreys, D, Davidson, A, Hume, PJ, and Koronakis, V (2012). Salmonella virulence effector SopE and Host GEF ARNO cooperate to recruit and activate WAVE to trigger bacterial invasion. Cell Host Microbe 11, 129–139.

Ibarra, JA, and Steele-Mortimer, O (2009). *Salmonella*-the ultimate insider. *Salmonella* virulence factors that modulate intracellular survival. Cell Microbiol 11, 1579–1586.

Ichimura, Y et al. (2000). A ubiquitin-like system mediates protein lipidation. Nature 408, 488–492.

Infante, RE, Wang, ML, Radhakrishnan, A, Kwon, HJ, Brown, MS, and Goldstein, JL (2008). NPC2 facilitates bidirectional transfer of cholesterol between NPC1 and lipid bilayers, a step in cholesterol egress from lysosomes. Proc Natl Acad Sci USA 105, 15287–15292.

Jepson, MA, and Clark, MA (2001). The role of M cells in Salmonella infection. Microbes Infect 3, 1183–1190.

Jha, AK et al. (2015). Network integration of parallel metabolic and transcriptional data reveals metabolic modules that regulate macrophage polarization. Immunity 42, 419–430.

Jones, BD, Ghori, N, and Falkow, S (1994). Salmonella typhimurium initiates murine infection by penetrating and destroying the specialized epithelial M cells of the Peyer's patches. J Exp Med 180, 15–23.

Kabeya, Y, Mizushima, N, Ueno, T, Yamamoto, A, Kirisako, T, Noda, T, Kominami, E, Ohsumi, Y, and Yoshimori, T (2000). LC3, a mammalian homologue of yeast Apg8p, is localized in autophagosome membranes after processing. EMBO J 19, 5720–5728.

Kernéis, S, Bogdanova, A, Kraehenbuhl, JP, and Pringault, E (1997). Conversion by Peyer's patch lymphocytes of human enterocytes into M cells that transport bacteria. Science 277, 949–952.

Kiarely-Souza, E et al. (2022). Lipid droplet accumulation occurs early following Salmonella infection and contributes to intracellular bacterial survival and replication. Mol Microbiol 117, 293–306.

Kim, J, Kundu, M, Viollet, B, and Guan, K-L (2011). AMPK and mTOR regulate autophagy through direct phosphorylation of Ulk1. Nat Cell Biol 13, 132–141.

Kirkegaard, K, Taylor, MP, and Jackson, WT (2004). Cellular autophagy: surrender, avoidance and subversion by microorganisms. Nat Rev Microbiol 2, 301–314.

Knight, M, Braverman, J, Asfaha, K, Gronert, K, and Stanley, S (2018). Lipid droplet formation in Mycobacterium tuberculosis infected macrophages requires IFN-γ/HIF-1α signaling and supports host defense. PLoS Pathog 14, e1006874.

Knodler, LA, Vallance, BA, Celli, J, Winfree, S, Hansen, B, Montero, M, and Steele-Mortimer, O (2010). Dissemination of invasive Salmonella via bacterial-induced extrusion of mucosal epithelia. Proc Natl Acad Sci USA 107, 17733–17738.

Knuff, K, and Finlay, BB (2017). What the SIF Is Happening-The Role of Intracellular Salmonella-Induced Filaments. Front Cell Infect Microbiol 7, 335.

Knuff-Janzen, K, Tupin, A, Yurist-Doutsch, S, Rowland, JL, and Finlay, BB (2020). Multiple Salmonella-pathogenicity island 2 effectors are required to facilitate bacterial establishment of its intracellular niche and virulence. PLoS ONE 15, e0235020.

Kolodziejek, AM, Altura, MA, Fan, J, Petersen, EM, Cook, M, Brzovic, PS, and Miller, SI (2019). Salmonella translocated effectors recruit OSBP1 to the phagosome to promote vacuolar membrane integrity. Cell Rep 27, 2147-2156.e5.

Koronakis, V, Hume, PJ, Humphreys, D, Liu, T, Hørning, O, Jensen, ON, and McGhie, EJ (2011). WAVE regulatory complex activation by cooperating GTPases Arf and Rac1. Proc Natl Acad Sci USA 108, 14449–14454.

Kreibich, S, Emmenlauer, M, Fredlund, J, Rämö, P, Münz, C, Dehio, C, Enninga, J, and Hardt, W-D (2015). Autophagy proteins promote repair of endosomal membranes damaged by the salmonella type three secretion system 1. Cell Host Microbe 18, 527–537.

Kurtz, JR, Goggins, JA, and McLachlan, JB (2017). Salmonella infection: Interplay between the bacteria and host immune system. Immunol Lett 190, 42–50.

Kwong, CN, Heikkila, RE, and Cornwell, DG (1971). Properties of cholesteryl esters in pure and mixed monolayers. J Lipid Res 12, 31–35.

Lange, Y (1991). Disposition of intracellular cholesterol in human fibroblasts. J Lipid Res 32, 329–339.

LaRock, DL, Brzovic, PS, Levin, I, Blanc, M-P, and Miller, SI (2012). A Salmonella typhimurium-translocated glycerophospholipid:cholesterol acyltransferase promotes virulence by binding to the RhoA protein switch regions. J Biol Chem 287, 29654–29663.

Lau, N, Haeberle, AL, O'Keeffe, BJ, Latomanski, EA, Celli, J, Newton, HJ, and Knodler, LA (2019). SopF, a phosphoinositide binding effector, promotes the stability of the nascent Salmonella-containing vacuole. PLoS Pathog 15, e1007959.

Lawson, C, Lim, S-T, Uryu, S, Chen, XL, Calderwood, DA, and Schlaepfer, DD (2012). FAK promotes recruitment of talin to nascent adhesions to control cell motility. J Cell Biol 196, 223–232.

Leiba, J et al. (2024). Dynamics of macrophage polarization support Salmonella persistence in a whole living organism. ELife 13.

Li, X, Bleumink-Pluym, NMC, Luijkx, YMCA, Wubbolts, RW, van Putten, JPM, and Strijbis, K (2019a). MUC1 is a receptor for the Salmonella SiiE adhesin that enables apical invasion into enterocytes. PLoS Pathog 15, e1007566.

Li, Z, Liu, Y, Fu, J, Zhang, B, Cheng, S, Wu, M, Wang, Z, Jiang, J, Chang, C, and Liu, X (2019b). Salmonella Proteomic Profiling during Infection Distinguishes the Intracellular Environment of Host Cells. MSystems 4.

Lietha, D, Cai, X, Ceccarelli, DFJ, Li, Y, Schaller, MD, and Eck, MJ (2007). Structural basis for the autoinhibition of focal adhesion kinase. Cell 129, 1177–1187.

Lim, C-Y, Davis, OB, Shin, HR, Zhang, J, Berdan, CA, Jiang, X, Counihan, JL, Ory, DS, Nomura, DK, and Zoncu, R (2019). ER-lysosome contacts enable cholesterol sensing by mTORC1 and drive aberrant growth signalling in Niemann-Pick type C. Nat Cell Biol 21, 1206–1218.

Lin, FY et al. (2001). The efficacy of a Salmonella typhi Vi conjugate vaccine in two-to-five-year-old children. N Engl J Med 344, 1263–1269.

Lin, MG, and Hurley, JH (2016). Structure and function of the ULK1 complex in autophagy. Curr Opin Cell Biol 39, 61–68.

Long, X, Lin, Y, Ortiz-Vega, S, Yonezawa, K, and Avruch, J (2005). Rheb binds and regulates the mTOR kinase. Curr Biol 15, 702–713.

Lu, A, Hsieh, F, Sharma, BR, Vaughn, SR, Enrich, C, and Pfeffer, SR (2022). CRISPR screens for lipid regulators reveal a role for ER-bound SNX13 in lysosomal cholesterol export. J Cell Biol 221.

Ma, XM, and Blenis, J (2009). Molecular mechanisms of mTOR-mediated translational control. Nat Rev Mol Cell Biol 10, 307–318.

Maekawa, M (2017). Domain 4 (D4) of Perfringolysin O to Visualize Cholesterol in Cellular Membranes-The Update. Sensors 17.

Mallo, GV, Espina, M, Smith, AC, Terebiznik, MR, Alemán, A, Finlay, BB, Rameh, LE, Grinstein, S, and Brumell, JH (2008). SopB promotes phosphatidylinositol 3-phosphate formation on Salmonella vacuoles by recruiting Rab5 and Vps34. J Cell Biol 182, 741–752.

Marchello, CS, Carr, SD, and Crump, JA (2020). A Systematic Review on Antimicrobial Resistance among Salmonella Typhi Worldwide. Am J Trop Med Hyg 103, 2518–2527.

McGourty, K, Thurston, TL, Matthews, SA, Pinaud, L, Mota, LJ, and Holden, DW (2012). Salmonella inhibits retrograde trafficking of mannose-6-phosphate receptors and lysosome function. Science 338, 963–967.

Mesmin, B, Bigay, J, Moser von Filseck, J, Lacas-Gervais, S, Drin, G, and Antonny, B (2013). A four-step cycle driven by PI(4)P hydrolysis directs sterol/PI(4)P exchange by the ER-Golgi tether OSBP. Cell 155, 830–843.

Mesmin, B, Bigay, J, Polidori, J, Jamecna, D, Lacas-Gervais, S, and Antonny, B (2017). Sterol transfer, PI4P consumption, and control of membrane lipid order by endogenous OSBP. EMBO J 36, 3156–3174.

Michelucci, A et al. (2013). Immune-responsive gene 1 protein links metabolism to immunity by catalyzing itaconic acid production. Proc Natl Acad Sci USA 110, 7820–7825.

Moest, TP, and Méresse, S (2013). Salmonella T3SSs: successful mission of the secret(ion) agents. Curr Opin Microbiol 16, 38–44.

Moon, J-S et al. (2015). UCP2-induced fatty acid synthase promotes NLRP3 inflammasome activation during sepsis. J Clin Invest 125, 665–680.

Morgan, PK, Huynh, K, Pernes, G, Miotto, PM, Mellett, NA, Giles, C, Meikle, PJ, Murphy, AJ, and Lancaster, GI (2021). Macrophage polarization state affects lipid composition and the channeling of exogenous fatty acids into endogenous lipid pools. J Biol Chem 297, 101341.

Morpeth, SC, Ramadhani, HO, and Crump, JA (2009). Invasive non-Typhi Salmonella disease in Africa. Clin Infect Dis 49, 606–611.

Müller, AJ et al. (2012). Salmonella gut invasion involves TTSS-2-dependent epithelial traversal, basolateral exit, and uptake by epithelium-sampling lamina propria phagocytes. Cell Host Microbe 11, 19–32.

Nader, GPF, Ezratty, EJ, and Gundersen, GG (2016). FAK, talin and PIPKIγ regulate endocytosed integrin activation to polarize focal adhesion assembly. Nat Cell Biol 18, 491–503.

Nagan, N, Hajra, AK, Das, AK, Moser, HW, Moser, A, Lazarow, P, Purdue, PE, and Zoeller, RA (1997). A fibroblast cell line defective in alkyl-dihydroxyacetone phosphate synthase: a novel defect in plasmalogen biosynthesis. Proc Natl Acad Sci USA 94, 4475–4480.

Nagy, C, and Haschemi, A (2015). Time and demand are two critical dimensions of immunometabolism: the process of macrophage activation and the pentose phosphate pathway. Front Immunol 6, 164.

Naito, T, Ercan, B, Krshnan, L, Triebl, A, Koh, DHZ, Wei, F-Y, Tomizawa, K, Torta, FT, Wenk, MR, and Saheki, Y (2019). Movement of accessible plasma membrane cholesterol by the GRAMD1 lipid transfer protein complex. ELife 8.

Naito, T, and Saheki, Y (2021). GRAMD1-mediated accessible cholesterol sensing and transport. Biochim Biophys Acta Mol Cell Biol Lipids 1866, 158957.

Nawabi, P, Catron, DM, and Haldar, K (2008). Esterification of cholesterol by a type III secretion effector during intracellular Salmonella infection. Mol Microbiol 68, 173–185.

Niess, JH, and Reinecker, H-C (2006). Dendritic cells in the recognition of intestinal microbiota. Cell Microbiol 8, 558–564.

Ogawa, M, Satoh, M, Kataoka, M, Ando, S, and Saijo, M (2017). Nitric oxide enhanced the growth of an obligated intracellular bacterium Orientia tsutsugamushi in murine macrophages. Microb Pathog 107, 335–340.

Ohlson, MB, Fluhr, K, Birmingham, CL, Brumell, JH, and Miller, SI (2005). SseJ deacylase activity by Salmonella enterica serovar Typhimurium promotes virulence in mice. Infect Immun 73, 6249–6259.

Ondari, E, Wilkins, A, Latimer, B, Dragoi, A-M, and Ivanov, SS (2023). Cellular cholesterol licenses Legionella pneumophila intracellular replication in macrophages. Microb Cell 10, 1–17.

O'Neill, LAJ, and Pearce, EJ (2016). Immunometabolism governs dendritic cell and macrophage function. J Exp Med 213, 15–23.

Oram, JF, and Heinecke, JW (2005). ATP-binding cassette transporter A1: a cell cholesterol exporter that protects against cardiovascular disease. Physiol Rev 85, 1343–1372.

Orecchioni, M, Ghosheh, Y, Pramod, AB, and Ley, K (2019). Macrophage Polarization: Different Gene Signatures in M1(LPS+) vs. Classically and M2(LPS-) vs. Alternatively Activated Macrophages. Front Immunol 10, 1084.

Owen, KA, Meyer, CB, Bouton, AH, and Casanova, JE (2014). Activation of focal adhesion kinase by Salmonella suppresses autophagy via an Akt/mTOR signaling pathway and promotes bacterial survival in macrophages. PLoS Pathog 10, e1004159.

Panagi, I et al. (2020). Salmonella Effector SteE Converts the Mammalian Serine/Threonine Kinase GSK3 into a Tyrosine Kinase to Direct Macrophage Polarization. Cell Host Microbe 27, 41-53.e6.

Pandey, AK, and Sassetti, CM (2008). Mycobacterial persistence requires the utilization of host cholesterol. Proc Natl Acad Sci USA 105, 4376–4380.

Parry, CM, Hien, TT, Dougan, G, White, NJ, and Farrar, JJ (2002). Typhoid fever. N Engl J Med 347, 1770–1782.

Parsons, JT (2003). Focal adhesion kinase: the first ten years. J Cell Sci 116, 1409–1416.

Parveen, N, Varman, R, Nair, S, Das, G, Ghosh, S, and Mukhopadhyay, S (2013). Endocytosis of Mycobacterium tuberculosis heat shock protein 60 is required to induce interleukin-10 production in macrophages. J Biol Chem 288, 24956–24971.

Peretti, D, Dahan, N, Shimoni, E, Hirschberg, K, and Lev, S (2008). Coordinated lipid transfer between the endoplasmic reticulum and the Golgi complex requires the VAP proteins and is essential for Golgi-mediated transport. Mol Biol Cell 19, 3871–3884.

Pham, THM et al. (2020). Salmonella-Driven Polarization of Granuloma Macrophages Antagonizes TNF-Mediated Pathogen Restriction during Persistent Infection. Cell Host Microbe 27, 54-67.e5.

Raffatellu, M, Wilson, RP, Chessa, D, Andrews-Polymenis, H, Tran, QT, Lawhon, S, Khare, S, Adams, LG, and Bäumler, AJ (2005). SipA, SopA, SopB, SopD, and SopE2 contribute to Salmonella enterica serotype typhimurium invasion of epithelial cells. Infect Immun 73, 146–154.

Rathman, M, Barker, LP, and Falkow, S (1997). The unique trafficking pattern of Salmonella typhimurium-containing phagosomes in murine macrophages is independent of the mechanism of bacterial entry. Infect Immun 65, 1475–1485.

Reinfeld, BI et al. (2021). Cell-programmed nutrient partitioning in the tumour microenvironment. Nature 593, 282–288.

Reiske, HR, Kao, SC, Cary, LA, Guan, JL, Lai, JF, and Chen, HC (1999). Requirement of phosphatidylinositol 3-kinase in focal adhesion kinase-promoted cell migration. J Biol Chem 274, 12361–12366.

Repa, JJ, Turley, SD, Lobaccaro, JA, Medina, J, Li, L, Lustig, K, Shan, B, Heyman, RA, Dietschy, JM, and Mangelsdorf, DJ (2000). Regulation of absorption and ABC1-mediated efflux of cholesterol by RXR heterodimers. Science 289, 1524–1529.

Richter-Dahlfors, A, Buchan, AM, and Finlay, BB (1997). Murine salmonellosis studied by confocal microscopy: Salmonella typhimurium resides intracellularly inside macrophages and exerts a cytotoxic effect on phagocytes in vivo. J Exp Med 186, 569–580.

Ridgway, ND (2000). Interactions between metabolism and intracellular distribution of cholesterol and sphingomyelin. Biochim Biophys Acta 1484, 129–141.

Ridgway, ND, Dawson, PA, Ho, YK, Brown, MS, and Goldstein, JL (1992). Translocation of oxysterol binding protein to Golgi apparatus triggered by ligand binding. J Cell Biol 116, 307–319.

Robinet, P, Wang, Z, Hazen, SL, and Smith, JD (2010). A simple and sensitive enzymatic method for cholesterol quantification in macrophages and foam cells. J Lipid Res 51, 3364–3369.

Russell, RC, Tian, Y, Yuan, H, Park, HW, Chang, Y-Y, Kim, J, Kim, H, Neufeld, TP, Dillin, A, and Guan, K-L (2013). ULK1 induces autophagy by phosphorylating Beclin-1 and activating VPS34 lipid kinase. Nat Cell Biol 15, 741–750.

Sancak, Y, Bar-Peled, L, Zoncu, R, Markhard, AL, Nada, S, and Sabatini, DM (2010). Ragulator-Rag complex targets mTORC1 to the lysosomal surface and is necessary for its activation by amino acids. Cell 141, 290–303.

Sancak, Y, Peterson, TR, Shaul, YD, Lindquist, RA, Thoreen, CC, Bar-Peled, L, and Sabatini, DM (2008). The Rag GTPases bind raptor and mediate amino acid signaling to mTORC1. Science 320, 1496–1501.

Sanowar, S et al. (2010). Interactions of the transmembrane polymeric rings of the Salmonella enterica serovar Typhimurium type III secretion system. MBio 1.

Santos, JC, Duchateau, M, Fredlund, J, Weiner, A, Mallet, A, Schmitt, C, Matondo, M, Hourdel, V, Chamot-Rooke, J, and Enninga, J (2015). The COPII complex and lysosomal VAMP7 determine intracellular Salmonella localization and growth. Cell Microbiol 17, 1699–1720.

Sarkar, A, and Suresh, KA (2017). Self-assembly and molecular packing in cholesteryl esters at interfaces. J Chem Phys 146, 214702.

Schaller, MD, Hildebrand, JD, Shannon, JD, Fox, JW, Vines, RR, and Parsons, JT (1994). Autophosphorylation of the focal adhesion kinase, pp125FAK, directs SH2-dependent binding of pp60src. Mol Cell Biol 14, 1680–1688.

Schuster, E-M et al. (2022). TFEB induces mitochondrial itaconate synthesis to suppress bacterial growth in macrophages. Nat Metab 4, 856–866.

Shi, J, Scita, G, and Casanova, JE (2005). WAVE2 signaling mediates invasion of polarized epithelial cells by Salmonella typhimurium. J Biol Chem 280, 29849–29855.

Simons, K, and Ikonen, E (1997). Functional rafts in cell membranes. Nature 387, 569–572.

Siperstein, MD, and Guest, MJ (1960). Studies on the site of the feedback control of cholesterol synthesis. J Clin Invest 39, 642–652.

Steele-Mortimer, O (2008). The Salmonella-containing vacuole: moving with the times. Curr Opin Microbiol 11, 38–45.

Subra, M, Antonny, B, and Mesmin, B (2023). New insights into the OSBP–VAP cycle. Curr Opin Cell Biol 82, 102172.

Subramanian, K, and Balch, WE (2008). NPC1/NPC2 function as a tag team duo to mobilize cholesterol. Proc Natl Acad Sci USA 105, 15223–15224.

Suckling, KE, and Stange, EF (1985). Role of acyl-CoA: cholesterol acyltransferase in cellular cholesterol metabolism. J Lipid Res 26, 647–671.

Szeto, J, Namolovan, A, Osborne, SE, Coombes, BK, and Brumell, JH (2009). Salmonella-containing vacuoles display centrifugal movement associated with cell-to-cell transfer in epithelial cells. Infect Immun 77, 996–1007.

Tan, JX, and Finkel, T (2022). A phosphoinositide signalling pathway mediates rapid lysosomal repair. Nature 609, 815–821.

Tan, Z, Xie, N, Cui, H, Moellering, DR, Abraham, E, Thannickal, VJ, and Liu, G (2015). Pyruvate dehydrogenase kinase 1 participates in macrophage polarization via regulating glucose metabolism. J Immunol 194, 6082–6089.

Tannahill, GM et al. (2013). Succinate is an inflammatory signal that induces IL-1β through HIF-1α. Nature 496, 238–242.

Tantibhedhyangkul, W, Ben Amara, A, Textoris, J, Gorvel, L, Ghigo, E, Capo, C, and Mege, J-L (2013). Orientia tsutsugamushi, the causative agent of scrub typhus, induces an inflammatory program in human macrophages. Microb Pathog 55, 55–63.

Tarling, EJ, and Edwards, PA (2011). ATP binding cassette transporter G1 (ABCG1) is an intracellular sterol transporter. Proc Natl Acad Sci USA 108, 19719–19724.

Tattoli, I, Philpott, DJ, and Girardin, SE (2012a). The bacterial and cellular determinants controlling the recruitment of mTOR to the Salmonella-containing vacuole. Biol Open 1, 1215–1225.

Tattoli, I, Sorbara, MT, Vuckovic, D, Ling, A, Soares, F, Carneiro, LAM, Yang, C, Emili, A, Philpott, DJ, and Girardin, SE (2012b). Amino acid starvation induced by invasive

bacterial pathogens triggers an innate host defense program. Cell Host Microbe 11, 563–575.

Tong, J, Manik, MK, and Im, YJ (2018). Structural basis of sterol recognition and nonvesicular transport by lipid transfer proteins anchored at membrane contact sites. Proc Natl Acad Sci USA 115, E856–E865.

Tontonoz, P, and Mangelsdorf, DJ (2003). Liver X receptor signaling pathways in cardiovascular disease. Mol Endocrinol 17, 985–993.

Tremel, S et al. (2021). Structural basis for VPS34 kinase activation by Rab1 and Rab5 on membranes. Nat Commun 12, 1564.

Van Puyvelde, S et al. (2023). A genomic appraisal of invasive Salmonella Typhimurium and associated antibiotic resistance in sub-Saharan Africa. Nat Commun 14, 6392.

Vidal, S, Tremblay, ML, Govoni, G, Gauthier, S, Sebastiani, G, Malo, D, Skamene, E, Olivier, M, Jothy, S, and Gros, P (1995). The Ity/Lsh/Bcg locus: natural resistance to infection with intracellular parasites is abrogated by disruption of the Nramp1 gene. J Exp Med 182, 655–666.

Walch, P et al. (2021). Global mapping of Salmonella enterica-host protein-protein interactions during infection. Cell Host Microbe 29, 1316-1332.e12.

Wang, C, JeBailey, L, and Ridgway, ND (2002). Oxysterol-binding-protein (OSBP)-related protein 4 binds 25-hydroxycholesterol and interacts with vimentin intermediate filaments. Biochem J 361, 461–472.

Wangdi, T, Lee, C-Y, Spees, AM, Yu, C, Kingsbury, DD, Winter, SE, Hastey, CJ, Wilson, RP, Heinrich, V, and Bäumler, AJ (2014). The Vi capsular polysaccharide enables

Salmonella enterica serovar typhi to evade microbe-guided neutrophil chemotaxis. PLoS Pathog 10, e1004306.

Wilson, RP, Winter, SE, Spees, AM, Winter, MG, Nishimori, JH, Sanchez, JF, Nuccio, S-P, Crawford, RW, Tükel, Ç, and Bäumler, AJ (2011). The Vi capsular polysaccharide prevents complement receptor 3-mediated clearance of Salmonella enterica serotype Typhi. Infect Immun 79, 830–837.

World Health Organization (2019). Typhoid vaccines: WHO position paper, March 2018 - Recommendations. Vaccine 37, 214–216.

Xie, Z, Nair, U, and Klionsky, DJ (2008). Atg8 controls phagophore expansion during autophagosome formation. Mol Biol Cell 19, 3290–3298.

Xu, Y et al. (2019). A Bacterial Effector Reveals the V-ATPase-ATG16L1 Axis that Initiates Xenophagy. Cell 178, 552-566.e20.

Xu, Y, Cheng, S, Zeng, H, Zhou, P, Ma, Y, Li, L, Liu, X, Shao, F, and Ding, J (2022). ARF GTPases activate Salmonella effector SopF to ADP-ribosylate host V-ATPase and inhibit endomembrane damage-induced autophagy. Nat Struct Mol Biol 29, 67–77.

Yabe, D, Brown, MS, and Goldstein, JL (2002). Insig-2, a second endoplasmic reticulum protein that binds SCAP and blocks export of sterol regulatory element-binding proteins. Proc Natl Acad Sci USA 99, 12753–12758.

Yamamoto, H, Kakuta, S, Watanabe, TM, Kitamura, A, Sekito, T, Kondo-Kakuta, C, Ichikawa, R, Kinjo, M, and Ohsumi, Y (2012). Atg9 vesicles are an important membrane source during early steps of autophagosome formation. J Cell Biol 198, 219–233.

Zhang, Y, Yu, C, Liu, J, Spencer, TA, Chang, CCY, and Chang, T-Y (2003). Cholesterol is superior to 7-ketocholesterol or 7 alpha-hydroxycholesterol as an allosteric activator for acyl-coenzyme A:cholesterol acyltransferase 1. J Biol Chem 278, 11642–11647.

Zhou, F et al. (2019). Rab5-dependent autophagosome closure by ESCRT. J Cell Biol 218, 1908–1927.

Zoncu, R, Bar-Peled, L, Efeyan, A, Wang, S, Sancak, Y, and Sabatini, DM (2011). mTORC1 senses lysosomal amino acids through an inside-out mechanism that requires the vacuolar H(+)-ATPase. Science 334, 678–683.